Fractional Order Control and Its Applications in Motion Control

(非整数次制御およびモーションコントロールへの応用)

A Doctoral Dissertation Submitted to
The Department of Electrical Engineering
for the Degree
Doctor of Philosophy

by

Chengbin Ma
(馬　澄斌)

Supervisor
Professor Yoichi Hori

Department of Electrical Engineering
The University of Tokyo

June 2004

内容概要

本博士学位論文では非整数次制御（Fractional Order Control）の理論及びモーションコントロールへの応用について論じた。非整数次制御とは非整数次微積分方程式を用い、制御対象のモデリングと制御器の構築を行う研究である。

非整数次制御は長い歴史を持つ “新しい”研究といえる。非整数次微積分は、整数次微積分とほぼ同時に Leibniz によって言及された概念である（1695 年）。Tustin 教授は 1958 年に発表した論文の中で出力トルクの飽和を含む一慣性系の位置制御に非整数次の微分制御器 D^α を適用した。その提案手法によって、微分制御器次数 α を連続的に調整し、critical point 付近の広い周波数範囲で十分な位相余裕を容易に確保できると結論付けている。しかし、当時非整数次微積分は一般の工学者に馴染みのない研究分野であった上に、実際の応用が少なく、計算機の演算能力では非整数次制御系の実現が困難であったため、過去の半世紀で、制御の研究者に注目されることはほとんどなかった。

近年では様々な制御対象に対し、非整数次微積分方程式が従来の整数次微積分方程式よりもよい精度でモデリングできることが実証されている。非整数次微積分方程式は複雑系のダイナミックスを簡潔に表現できる有効なツールである。また、非整数次微積分モデルで表現された制御対象には非整数次制御器の導入が必要になってくる。さらに、計算技術の発達に伴い、非整数次制御系をシミュレーションする事や実現する事は以前よりも容易になった。以上の進歩のおかげで、非整数次微積分理論は多数の研究分野でその重要性が再認識され始めている。特に、非整数次制御は非整数次微積分理論の制御への応用として現在国際研究コミューニティから大きな注目を浴びている。非整数次制御専門のシンポジウムや会議は ASME、IFAC をはじめとする国際的な学術団体でも開催されている。

本学位論文は非整数次制御のシステマティックな紹介を行った上で筆者のオリジナルな研究に基づいた非整数次制御の設計から実現まで全面的な知識を述べた。筆者は非整数次制御の理論的な研究が重要だと認識しているが、同時に応用面の研究にも注力すべきだと考えている。ほかの研究と同様に、非整数次制御の研究にも同じ分野の研究者の協力が不可欠であるので、良好な応用結果によって、有志の研究者を非整数次制御の研究に吸収し、新しい研究

成果を生み出すことを期待している。非整数次制御の研究はまだ初期段階であり、特にモーションコントロールの領域ではほぼ空白の状態と言っても過言ではない。非整数次制御のモーションコントロールへの応用の “先駆者” として、筆者は強く責任感を感じ、後の研究者のために、良い起点を築きたいと思っている。

以上の考えに基づき、本論文ではできる限り非整数次制御のあらゆる側面、必要な数学的基礎知識、非整数次モデリングと同定、非整数次制御の理論及び実現法、制御系の設計と実際の応用を紹介した。第一章では、非整数次制御の歴史、現状に触れる。第二章は非整数次制御を理解するための必要な数学知識を紹介する。第三章では、非整数次制御の基礎知識、例えば数学の表現、非整数次制御系の線形性、モデリング及び同定について述べる。第四章は非整数次制御の導入によって、従来の整数次制御理論への影響を討論する。制御系のタイプ、安定性の判定、周波数特性、ロバスト性及び筆者が提案した二段階の非整数次制御設計法を言及する。第五章は離散的非整数次制御系のサンプリングタイムスケーリング特性を提案する。この特性を活かし、非整数次制御が時間領域において、過去のサンプリング入力に重み関数付きで記憶し、新しい出力を算出するという解釈を提案する。第六章では複数の非整数次制御器の実現法（周波数の折れ線近似法と他の直接離散法）を時間領域と周波数領域で評価する。第七、八、九章は非整数次制御の応用および実験的検証を行う。従来の PID 制御器、ローパスフィルター及び外乱オブザーバーを非整数次制御に拡張し、軸捻れ装置を使い、制御効果を検証する。制御器設計の明快さと良好な実験結果によって、非整数次制御の有効性を実証する。最後に、第十章では結論及び今後の研究課題を詳しく述べる。

約三年間の非整数次制御の調査及び研究に従事した上で、非整数次制御の優位性が以下の三点であると筆者は強く主張する：

- 制御対象のより正確なモデリング
- 明快かつ効果的なロバスト制御系設計
- 良い近似的な実現

モーションコントロールの問題に本質的に含まれている非線形要素、ロバスト性と他の制御性能への要求などを考え、非整数次制御は一般的な手法であり、従来の整数次制御系の中間的な性質をもつ制御系を容易に設計できる。筆者は非整数次制御の導入によって、我々が多くの斬新な発見をできると確信している。

SUMMARY

This dissertation deals with Fractional Order Control (FOC) and its applications in motion control. The concept of FOC means controlled systems and/or controllers are described by fractional order differential equations.

FOC is a "new" research with quite "old" history. The notation of fractional order calculus was mentioned by Leibniz in 1695 as soon as the ideas of conventional calculus were known. Prof. Tustin discussed using fractional order D controllers, s^α, for the position control of massive objects in 1958, where actuator saturation requires sufficient phase margin around and below the critical point. However, due to the unfamiliar idea of taking fractional order, so few physical applications and limited computational power available at that time, fractional order calculus was not widely incorporated into control engineering in past half century.

In recent years, researchers reported that fractional order differential equations could model various materials more adequately than integer order ones and provide an excellent tool for describing complex dynamic features. Obviously, the fractional order models need fractional order controllers for more effective control of the "real" systems. The rapid progress of available computational power also makes modeling and realization of fractional order systems much easier than before. Thanks to these developments, fractional calculus has begun to play a very important role in various fields. Especially, its application in control engineering, FOC, is becoming a more and more important issue for the international scientific community. Special international symposiums and workshops organized by ASME and IFAC were held to promote international exchange and cooperation in Fractional Derivatives and Their Applications (FDTA) research.

In this dissertation, a systematic introduction and the author's original works in applying FOC into motion control are mentioned in detail. The author thinks that parallel to the development in theoretical aspects of FOC, efforts to apply it in real control problems are

of same importance. Like all the other researches, the FOC research is also inevitably a team work. Superior application results will absorb excellent researchers into FOC field and produce more fruits in future FOC research. At the same time, FOC is still in a primitive stage, especially in motion control field. Few researchers in control engineering know this concept, at least in Japan. As a FOC "pioneer" (perhaps), the author feels a strong sense of responsibility to establish a good basis for future FOC researchers.

Based on above considerations, this dissertation tries to cover nearly all the aspects of FOC research, from mathematical preliminary, fractional order modeling and identification, theoretical issues to realization methods, control design and real applications.

In chapter 1, the history and present situation of FOC research are introduced. Chapter 2 describes necessary mathematic preliminary for understanding FOC research. Chapter 3 gives fundamental issues for FOC. For example, the mathematic representations, linearity of FOC systems, the modeling and identification issues. In chapter 4, the impacts of introducing FOC concept to control engineering are discussed. Control system type, stability determination, frequency responses and robustness for FOC systems are reviewed. A two-stage approach for design of FOC system is also proposed in this chapter. Chapter 5 explores the sampling time scaling property for discrete fractional order controllers. This time-domain explanation provides more insight into FOC as control with self-scaled memory. Chapter 6 mentions and compares different realization methods for fractional order controllers, frequency-band approximation and direct discretization methods. Chapter 7, 8 and 9 concern the application of FOC to various conventional control methods, PID control, low-pass filter and disturbance observer. The proposed FOC approaches are experimented using torsional system. The control design and experimental results clearly display the advantages of FOC both in control design and real applications. In chapter 10, the above chapters are concluded. The future works for FOC research are also mentioned in detail.

After three years of investigation and research in FOC, the author believes the advantages for introducing FOC to control engineering can be concluded in three points:

- Adequate modeling of control plant's dynamic features

- Effective and clear-cut robust control design
- Reasonable realization by approximation

Due to the non-linearities, demands for robustness and other control performances in motion control problems, FOC could be a natural, general and effective approach with "in-between" characteristics. With fractional order calculus and fractional order control, we may be able to extend a lot of new things ....

ACKNOWLEDGEMENTS

It is a pleasure to thank the many people who made this dissertation possible.

It is difficult to overstate my gratitude to my PH. D supervisor, Prof. Yoichi Hori, for his wisdom, friendship, understanding, and for teaching me how to be a (successful?) researcher. Three years ago, Prof. Hori gave me the opportunity to jump into this new field, Fractional Order Control (FOC), with a rare chance to do real research. He always offered my good advice and brought previously unrecognized aspects of each situation to my attention not only in my research but also in daily life. He encouraged me and gave me chances to attend domestic and international conferences and discuss my research with other researchers. Without his enthusiasm, his inspiration and many insightful conversations during the development of the ideas of this dissertation, this dissertation would not exist.

I owe a great deal to Prof. Yasumasa Fujii, my master supervisor in the same department of the University of Tokyo from Oct. 1999 to Sept. 2001. I can never forget that in order to improve my master thesis, Prof. Fujii took me to other energy engineering researchers in Kyoto and Nagaoka and let me present and discuss my researches with them. He respected my wish to continue my doctor research in control engineering and unselfishly recommended me to Prof. Hori. Thanks! Prof. Fujii. You and Prof. Hori make me proud of being your student and one of the graduates of the University of Tokyo.

I also extend my sincere gratitude to Prof. Shunji Manabe from Tokai University for many helpful discussions. His insightful comments and viewpoints stimulated me to focus my research on the essence of FOC and find new things such as the sampling time scaling property of discrete fractional order controllers. The Coefficient Diagram Method (CDM), an excellent design method proposed by Prof. Manabe, is the starting point for me to design controllers. I would also wish to thank Prof. Yangquan Chen from Utah State University for his encouragement and the intuitive talk about applying FOC concept to modern digital control theories During the ASME 2003 DETC Chicago conference.

I am grateful to all the former and present Hori laboratory members for providing a stimulating and fun environment in which to learn and grow. I especially thank Mr. Toshiyuki Uchida, the technical staff, and Ms. Hideko Sakiyama, the secretary, for helping Hori laboratory to run smoothly and for assisting me in many technical and office works. I wish to thank Dr. Shichirousai Oyobe, Dr. Okazu Seki, Sehoon Oh, Nobutaka Bando, Naoki Hata, Byunghoon Chang, Jiunde Wu, Kimihisa Furukawa, Ryo Fukui, Kenichiro Aoki, Shinya Kodama, Yoshifumi Aoki and all the other student colleagues, for the helpful discussions, support, comradeship, and entertainment.

Special thanks to all the members in the office (including COE office) of the electrical engineering department of the University of Tokyo for assisting me in scholarship and dormitory applications and many other different things. Ms. Yagyu, Ms. Ohno, Ms. Tanaka, Ms. Fukano and Ms. Shigihara deserve special mention.

I have been supported financially by the 21st century COE program in Electrical Engineering and Electronics of the University of Tokyo and Rotary Yoneyama Memorial Foundation. For this assistance, I am very grateful.

Finally, I am forever indebted to my family and friends for their understanding, endless patience and encouragement when it was most required. They are always supportive and the most important persons for me. To them I dedicate this dissertation.

Chengbin Ma

the University of Tokyo

June 2004

STRUCTURE OF DISSERTATION

Background Knowledge

I. Introduction

II. Mathematic Preliminary

Theoretical Aspects

III. Fundamental Issues

IV. Control Impacts

V. Sampling Time Scaling Property

Real Applications

VI. Realization Methods

VII. Fractional Order $PI^{\alpha}D^{\beta}$ Control

VIII. Fractional Order Filter

IX. Fractional Order Disturbance Observer

Conclusions

X. Conclusions and Future Works

TABLE OF CONTENTS

LIST OF TABLES

LIST OF FIGURES

NOTATIONS AND SYMBOLS

$\mathbf{A}$	matrix
$\mathbf{A}(\mathbf{s})$	transfer function Matrix
${}_aD_t^{\alpha}f(t)$	fractional α order derivative between a and t
$F_e\{f(t)\}$	Fourier transform of $f(t)$
$G(s)$	continuous transfer function
$\mathbf{I}$	identity matrix
iff	if and only if
$L\{f(t)\}$	Laplace transform of $f(t)$
$L^{-1}\{f(t)\}$	inverse Laplace transform of $f(t)$
Δ	unmodeled uncertainty or change
$:=$	defined as
$\\|\cdot\\|_\infty$	∞-norm
$Z\{f(t)\}$	z-transfer (discretization) of $f(t)$

LIST OF ACRONYMS

CDM	coefficient diagram method
DOB	disturbance observer
FDTA	fractional derivatives and their applications
FOC	fractional order control
IOC	integer order control
MIMO	multi-input multi-output
SISO	single-input single-output
SMP	short memory principle
STS	sampling time scaling
TDOF	two degree of freedom
TTE	Tustin taylor expansion
LIF	Lagrange interpolation function

CHAPTER I

INTRODUCTION

1.1 Review of History

The concept of Fractional Order Control (FOC) means controlled systems and/or controllers are described by fractional order differential equations. Expanding derivatives and integrals to fractional orders is by no means new and actually has a firm and long standing theoretical foundation. Interest in this subject was evident almost as soon as the ideas of the classical calculus were known.

Leibniz mentioned it in a letter to L'Hospital over three hundred years ago (1695). Leibniz raised the following question:

Can the meaning of derivatives with integer order $\frac{d^n y(x)}{dx^n}$ *be generalized to derivatives with non-integer orders?*

The story goes that L'Hospital was somewhat curious about that question and replied by another question to Leibniz:

What if the order will be 1/2?

Leibniz in a letter dated September 30, 1695 replied:

It will lead to a paradox, from which one day useful consequences will be drawn.

The earliest more or less systematic studies seem to have been made in the beginning and middle of the 19th century by Liouville, Holmgren and Riemann, although Eular, Lagrange, and others made contribution even earlier [1].

Parallel to these theoretical beginnings was the development of applying fractional calculus to various problems. The fractional order calculus is not a sterile exercise in pure mathematics. Many problems in physical sciences can be expressed and solved succinctly by recourse to the fractional calculus. In a sense, the first of these was the discovery by Abel in 1823 that the solution of the integral equation for the tautochrone could be accomplished via an integral transform, which benefits from being written as a 0.5 order derivative [1].

It was also found that the use of 0.5 order derivatives and integrals leads to a formulation of certain electro-chemical problems, which is more economical and useful than the conventional integer order approach [1].

As to fractional calculus' application in control engineering, FOC was introduced by Tustin for the position control of massive objects (see Fig. 1) half a century ago in 1958, where actuator saturation requires sufficient phase margin around and below the critical point [2].

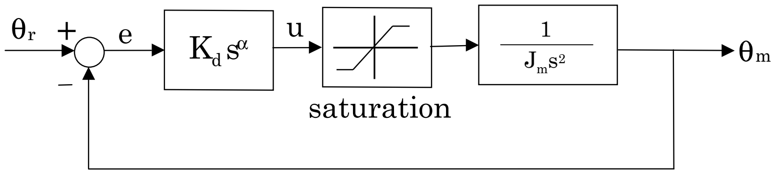

Figure 1: The position control loop with fractional order D^α controller

The characteristic equation of the above close-loop $1/s^\beta$ system with variable gain factor A is

$$1 + As^\beta = 0 \tag{1}$$

where $A = J_m/K_d$ in nominal case and $\beta = 2-\alpha$. For $1 < \beta < 2$, Equ. (1) has two complex-conjugate dominant poles in the main sheet of the Riemann surface, $-\pi < arg(s) < \pi$:

$$s_{1,2} = A^{-\frac{1}{\beta}} e^{\pm j\pi/\beta} \tag{2}$$

The relative damping ratio ζ is

$$\zeta = cos\left(\pi - \frac{\pi}{\beta}\right) = -cos\left(\frac{\pi}{\beta}\right) \tag{3}$$

This result shows that the relative damping ratio ζ is exclusively decided by order β and independent of the gain factor A.

In frequency domain, the characteristic equation is

$$1 + A(j\omega)^\beta = 0 \tag{4}$$

Equation. (4) can be rewritten in the form

$$(j\omega)^\beta = -\frac{1}{A} \tag{5}$$

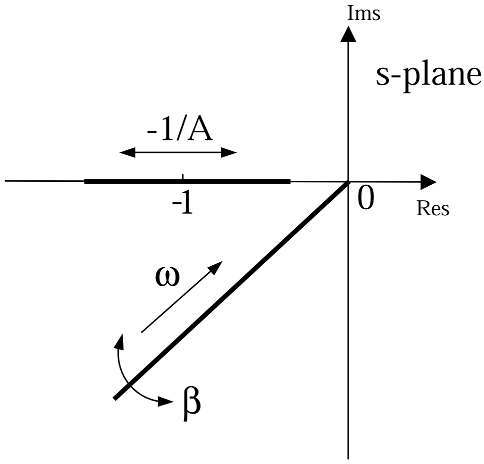

Figure 2: Nyquist plots of the fractional order $1/s^{\beta}$ system

The movement of $-1/A$ can be considered to be the locus of the critical point (see Fig. 2) when the gain variation occurs. For integer order system, when $\beta = 2$, the system will be oscillatory due to its zero phase margin. Taking $\beta = 1$ leads to poor robustness against saturation since pure D controller will be used. By letting β be fractional between 1 and 2, a better tradeoff between stability and robustness will be obtained. Namely, the fractional order D^{α} controller is naturally introduced whose order α should be chosen properly between 0 and 1. Therefore, necessary phase margin can be easily kept to any desired amount in wide range of frequencies below and in the neighborhood of the critical point. This characteristic highlights the hopeful aspect of applying FOC to control engineering.

Some other pioneering works were also carried out around 60's by Manabe [3][4][5]. However, the FOC concept was not widely incorporated into control engineering mainly due to the unfamiliar idea of taking fractional order, so few physical applications and limited computational power available at that time [6].

1.2 Present Situation

In last few decades, researchers pointed out that fractional order differential equations could model various materials more adequately than integer order ones and provide an excellent tool for describing complex dynamic features [1] [7]. Especially for the modeling and identification of flexible structures with increasing application of lighter materials, fractional order differential equations could provide a natural solution since these structures are essentially distributed-parameter systems [8]. Obviously, the fractional order models need fractional order controllers for more effective control of the "real" systems. This necessity motivated renewed interest in various applications of FOC [9] [10] [11]. And with the rapid development of computer performances, realization of FOC systems also became possible and much easier than before.

The researches on FOC are mainly centered in European universities at present. The CRONE team in France is leaded by Alain Oustaloup and Patrick Lanusse from Bordeaux University, France. CRONE is the French abbreviation for Contrôle Robuste d'Ordre Non-Entier (non-integer order robust control in English). Their practices include applying FOC into car suspension control [12], flexible transmission [13], hydraulic actuator [14], etc. Denis Matignon, a researcher from École Nationale Supérieure des Télécommunications (the Institute of Telecom Paris in English), France, contributed to the theoretical aspects of FOC concept, such as stability [15], controllability, and observability [16] of the fractional order systems; while Slovak researchers, Ivo Petras and Igor Podlubny from the Technical University of Kosice, are playing an important part for their efforts in modeling, realization and implementation of fractional order systems. J. A. Tenreiro Machado and Yangquan Chen, from Polytechnic Institute of Porto, Portugal, and Utah State University, Logan, are also well-known for their outstanding works in implementation methods of fractional order controllers, applying FOC in robotics control, etc. Their works will be cited in following chapters.

FOC research has been internationally accepted. The first symposium on Fractional Derivatives and Their Applications (FDTA) of the 19th Biennial Conference on Mechanical Vibration and Noise was held from September 2-6, 2003 in Chicago, IL, USA [17]. This conference was a part of ASME 2003 Design Technical Conferences. 29 papers concerning FDTA in automatic control, automatic control and system, robotics and dynamic systems, analysis tools and numerical methods, modeling, visco-elasticity and thermal systems were presented in the symposium. A sub-committee called "Fractional Dynamic Systems" under ASME "Multi-body Systems and Nonlinear Dynamics" committee was also formed during the symposium. The formation of the new sub-committee is expected to promote future researches and international cooperations in FDTA.

And the first IFAC Workshop on Fractional Differentiation and its Applications will be held in this year's summer, July 19-21, in Bordeaux, France [18]. The following areas will be covered by the workshop: representation tools, analysis tools, synthesis tools, simulation tools, modeling, identification, observation, control, vibration insulation, filtering, pattern recognition, edge detection. Besides the presentations of theoretical works and applications, this workshop will also give rise to benchmark, testing bench and software presentations.

The author thinks that generally there are three main advantages for introducing fractional order calculus to control engineering:

- Adequate modeling of control plant's dynamic features
- Effective and clear-cut robust control design
- Reasonable realization by approximation

1.3 Outline of Chapters

In motion control field, the FOC research is still in a primitive stage. This dissertation represents one of the first systematic efforts towards applying FOC to motion control. Especially, realization issues and control design of FOC system will be discussed in detail. The reader will find that FOC is just as tangible as conventional Integer Order Control (IOC) and a new dimension opens to control engineering when the orders of controllers and plant models become arbitrary numbers. The author believes that FOC is a natural and powerful choice in control design and its design process should be clear-cut. There is no reason that the knowledge of extremely well developed conventional IOC theories is not made full use of in FOC research.

Based on above considerations, the dissertation aims to study the most fundamental and important issues of FOC with regards to its applications to motion control. In order to achieve this objective, this dissertation is organized as follows:

Chapter 2 describes the necessary mathematic preliminary for understanding FOC research. Especially the definitions of fractional order calculus and their Laplace and Fourier transforms are mentioned in detail. Time-domain analysis tool, Mittag-Leffler function, will also be introduced.

Chapter 3 gives fundamental issues for FOC. For example, the mathematic representations, linearity of FOC systems. The modeling and identification of fractional order system are discussed in detail.

Chapter 4 reveals the impacts of introducing FOC concept to control engineering. The conventional control concepts, such as control system type and stability determination, are reviewed. Since FOC systems' frequency responses can be exactly known, the wealth of graphical methods and analysis tools in frequency domain are still available for FOC research. The effective gain-phase tradeoff and less model error imply introducing FOC could achieve an effective and clear-cut design of robust control system. A two-stage approach for design of FOC system is also proposed in this chapter.

Chapter 5 explores the sampling time scaling property for discrete fractional order controllers. This time-domain explanation provides more insight into FOC as control with self-scaled memory. A novel realization method is also proposed based on the sampling time scaling property.

Chapter 6 mentioned and compared different methods, frequency-band approximation and direct discretization methods, for realizing fractional order controllers. Especially the realization method proposed in Chapter 5 is used to establish baseline cases with full memory length.

Chapter 7, 8 and 9 concern the applications of FOC to various conventional control methods, PID control, low pass filter and disturbance observer. The proposed FOC approaches are verified by real experiments using torsional system. The control design and experimental results show an effective and clear-cut robust control design could be obtained through FOC approach.

Chapter 10 concludes the above chapters and discusses the future works for FOC research.

CHAPTER II

MATHEMATIC PRELIMINARY

2.1 Mathematic Definitions

The idea of fractional order calculus that allows calculus' order to be any arbitrary real number, in fact, is a natural generalization of the notions of classical integer order calculus, which are usually presented separately by integer order derivatives and integrals in classical analysis. The mathematical definitions of fractional derivatives and integrals have been the subject of several different approaches [1][7].

2.1.1 Grünwald-Letnikov definition

One of the most frequently encountered definitions is called Grünwald-Letnikov definition:

$$ {}_aD_t^{\alpha} = \lim_{\substack{h\to 0\\ nh=t-a}} h^{-\alpha}\sum_{j=0}^{n}(-1)^j \begin{pmatrix}\alpha\\ j\end{pmatrix} f(t-jh) \tag{6}$$

where the binomial coefficients are

$$ \begin{pmatrix}\alpha\\ 0\end{pmatrix} = 1, \quad \begin{pmatrix}\alpha\\ j\end{pmatrix} = \frac{\alpha(\alpha-1)\dots(\alpha-j+1)}{j!} \quad \text{for } j\geq 1 \tag{7}$$

The Grünwald-Letnikov definition can be also written as [7]:

$$\begin{aligned} {}_aD_t^{\alpha}f(t) &= \sum_{j=0}^{m}\frac{f^{(j)}(a)(t-a)^{-\alpha+j}}{\Gamma(-\alpha+j+1)} \\ &+ \frac{1}{\Gamma(-\alpha+m+1)}\int_a^t (t-\tau)^{m-\alpha}f^{(m+1)}(\tau)d\tau \end{aligned}\tag{8}$$

under the assumption that the derivatives $f^{(j)}(t)$ $(j = 1, 2, \dots, m+1)$ are continuous in $[a,\ t]$ with $m \leq \alpha < m+1$.

The Grünwald-Letnikov definition describes the unification of two notions, integer order derivatives and integrals. For a continuous function $y = f(t)$, the well-known definition of

m-order derivative of function $f(t)$ is

$$
{}_aD_t^m f(t) = \lim_{\substack{h\to 0\\ nh=t-a}} h^{-m} \sum_{j=0}^{n} (-1)^j \begin{pmatrix} m \\ j \end{pmatrix} f(t-jh) = \frac{d^m f(t)}{dt^m} \tag{9}
$$

as all the binomial coefficients after $\begin{pmatrix} m \\ m \end{pmatrix}$ are equal to 0. Similarly, considering negative values of order $-m$ leads to

$$
\begin{aligned}
{}_aD_t^{-m} f(t) &= \lim_{\substack{h\to 0\\ nh=t-a}} h^{m} \sum_{j=0}^{n} (-1)^j \begin{pmatrix} -m \\ j \end{pmatrix} f(t-jh) \\
&= \frac{1}{(m-1)!} \int_a^t (t-\tau)^{m-1} f(\tau) d\tau
\end{aligned} \tag{10}
$$

Integrating the relationships

$$
\begin{aligned}
{}_aD_t^{-1} f(t) &= \lim_{\substack{h\to 0\\ nh=t-a}} h \sum_{j=0}^{n} (-1)^j \begin{pmatrix} -1 \\ j \end{pmatrix} f(t-jh) \\
&= \lim_{\substack{h\to 0\\ nh=t-a}} h \sum_{j=0}^{n} f(t-jh) \\
&= \int_a^t f(\tau) d\tau
\end{aligned} \tag{11}
$$

and

$$
\frac{d}{dt}\left({}_aD_t^{-m} f(t)\right) = \frac{1}{(m-2)!} \int_a^t (t-\tau)^{m-2} f(\tau) d\tau =_a D_t^{-m+1} f(t) \tag{12}
$$

give

$$
\begin{aligned}
{}_aD_t^{-m} f(t) &= \int_a^t \int_a^t \left({}_aD_t^{-m+2} f(t)\right) dt \\
&= \int_a^t dt \int_a^t dt \int_a^t \left({}_aD_t^{-m+3} f(t)\right) dt \\
&\cdots \\
&= \int_a^t dt \int_a^t dt \ldots \int_a^t f(t) dt
\end{aligned} \tag{13}
$$

actually m-fold integral.

2.1.2 Riemann-Liouville definition

Another most widely known definition of fractional order calculus is called Riemann-Liouville definition with an integro-differential expression. The definition for fractional order integral is

$$ {}_aD_t^{-\alpha} f(t) = \frac{1}{\Gamma(\alpha)} \int_a^t (t-\xi)^{\alpha-1} f(\xi) d(\xi) \tag{14} $$

while the definition of fractional order derivatives is

$$ {}_aD_t^{\alpha} f(t) = \frac{d^\gamma}{dt^\gamma} \left[{}_aD_t^{-(\gamma-\alpha)} \right] \tag{15} $$

where

$$ \Gamma(x) = \int_0^\infty y^{x-1} e^{-y} dy \tag{16} $$

is the Gamma function, a and t are limits and α ($\alpha > 0$ and $\alpha \in R$) is the order of the operation. γ is an integer that satisfies $\gamma - 1 < \alpha \leq \gamma$. Obviously, the Riemann-Liouville definition is also a unification of integer order derivatives and integrals since integer order α actually equals γ.

Performing integration repeatedly by parts and differentiation on the Riemann-Liouville definition under the assumption that $f(t)$ must be $m+1$ times continuously differentiable [7], which is satisfied by most of dynamical processes, gives

$$ \begin{aligned} {}_aD_t^{-\alpha} f(t) &= \frac{1}{\Gamma(\alpha)} \int_a^t (t-\xi)^{\alpha-1} f(\xi) d(\xi) \\ &= \sum_{j=0}^{m} \frac{f^{(j)}(a)(t-a)^{-\alpha+j}}{\Gamma(-\alpha+j+1)} \\ &+ \frac{1}{\Gamma(-\alpha+m+1)} \int_a^t (t-\tau)^{m-\alpha} f^{(m+1)}(\tau) d\tau \end{aligned} \tag{17} $$

where $m \leq \alpha < m+1$. Therefore, if $f(t)$ has $m+1$ continuous derivatives, the Riemann-Liouville definition is equivalent to the Grünwald-Letnikov definition.

Similarly to integer order calculus, fractional order calculus is also a linear operation following directly from the above two definitions:

$$ D^\alpha(\lambda f(t) + \mu g(t)) = \lambda D^\alpha f(t) + \mu D^\alpha g(t) \tag{18} $$

2.2 Laplace and Fourier Transforms

Fractional order calculus is quite complicated in time domain, as shown in its two definitions. Fortunately one of the features most important to control engineers, its Laplace transform, is very straightforward. Based on the Riemann-Liouville definition, fractional order integral of order $\alpha > 0$ can be written as a convolution of the functions $g(t) = t^{\alpha-1}$ and $f(t)$:

$$ {}_0D_t^{-\alpha} f(t) = \frac{1}{\Gamma(\alpha)} \int_0^t (t-\tau)^{\alpha-1} f(\tau) d(\tau) = \frac{1}{\Gamma(\alpha)} t^{\alpha-1} * f(t) \tag{19} $$

The Laplace transforms of the function $t^{\alpha-1}$ is [7]

$$ L\{t^{\alpha-1}\} = \Gamma(\alpha) s^{-\alpha} \tag{20} $$

Therefore, using the convolution formula for the Laplace transform, the Laplace transform of fractional order integral can be obtained:

$$ L\{{}_0D_t^{-\alpha} f(t)\} = s^{-\alpha} F(s) \tag{21} $$

For fractional order derivative, it can be rewritten in the form:

$$ L\{{}_0D_t^{\alpha} f(t)\} = g^{(n)}(t) \tag{22} $$

$$ g(t) =_0 D_t^{-(n-\alpha)} f(t) = \frac{1}{\Gamma(n-\alpha)} \int_0^t (t-\tau)^{n-\alpha-1} f(\tau) d(\tau) \tag{23} $$

where $n - 1 < \alpha < n$.

Using formula for the Laplace transform of an integer order derivative leads to

$$ L\{g^{(n)}(t)\} = s^n G(s) - \sum_{k=0}^{n-1} s^k g^{(n-k-1)}(0) \tag{24} $$

The Laplace transform of the function $g(t)$ is evaluated by Equ. (21):

$$ G(s) = s^{-(n-\alpha)} F(s) \tag{25} $$

Additionally, from the definition of derivative it follows that

$$ g^{n-k-1}(t) = \frac{d^{n-k-1}}{dt^{n-k-1}} {}_0D_t^{-(n-\alpha)} f(t) =_0 D_t^{\alpha-k-1} f(t) \tag{26} $$

Substituting Equ. (25) and Equ. (26) into Equ. (24), the final expression of the Laplace transform of fractional order derivative is

$$L\{{}_0D_t^{\alpha}f(t)\} = s^{\alpha}F(s) - \sum_{k=0}^{n-1} s^k_0 D_t^{\alpha-k-1}f(0) \tag{27}$$

where $n-1 < \alpha < n$ again. If all the initial conditions are zero, the Laplace transform of fractional order derivative is simply

$$L\{{}_0D_t^{\alpha}f(t)\} = s^{\alpha}F(s) \tag{28}$$

Form Equ. (21) and Equ. (28), the Laplace transforms of fractional $\pm\alpha$ order calculus lead to the use of fractional order Laplace operator $s^{\pm\alpha}$. The transfer functions of models and controllers, which are described by fractional order differential equations, can be derived conveniently using fractional order Laplace operator $s^{\pm\alpha}$.

By Laplace transforming fractional order calculus into s domain, complicated manipulations of the Gamma function, $\Gamma(x)$, can be reduced to simple algebraic manipulations of the $s^{\pm\alpha}$ operator. This result is intuitively reassuring and greatly simplifies the analysis of FOC system.

As same as Laplace transform, using the convolution formula for Fourier transform gives

$$F_e\{{}_0D_t^{-\alpha}f(t)\} = F_e\left\{\frac{1}{\Gamma(\alpha)}t^{\alpha-1}\right\} * F_e\{f(t)\} \tag{29}$$

Therefore, from Equ. (21) the Fourier transform of fractional order integral is

$$F_e\{{}_0D_t^{-\alpha}f(t)\} = (j\omega)^{-\alpha}F(j\omega) \tag{30}$$

Similarly, the Fourier transform of fractional order derivative is

$$F_e\{{}_0D_t^{\alpha}f(t)\} = (j\omega)^{\alpha}F(j\omega) \tag{31}$$

Frequency response of FOC system can be exactly obtained by substituting $s^{\pm\alpha}$ with $(j\omega)^{\pm\alpha}$ in its transfer function. This advantage implies frequency-domain analysis of FOC system is as convenient as IOC system's. The graphical tools in frequency domain are still available for FOC analysis and design.

2.3 *Time-domain Analysis*

Some simple functions' fractional order calculus can be derived straightforwardly using the two mathematical definitions [1]. For example, based on the Riemann-Liouville definition, the unit-step response of open-loop $1/s^{\alpha}$ system is given based on the properties of the Gamma function [1] [2]:

$$\begin{aligned} L^{-1}\left\{\frac{1}{s^{\alpha}}\cdot\frac{1}{s}\right\} &= \frac{1}{\Gamma(\gamma+\alpha)}\frac{d^{\gamma}}{dt^{\gamma}}\int_0^t \frac{1}{(t-\xi)^{-\alpha-\gamma+1}}f(\xi)d\xi \\ &= \frac{1}{\Gamma(\gamma+\alpha)}\frac{d^{\gamma}}{dt^{\gamma}}\frac{t^{\gamma+\alpha}}{\gamma+\alpha} \\ &= \frac{1}{(\gamma+\alpha)\Gamma(\gamma+\alpha)}(\gamma+\alpha)\ldots(\alpha+1)t^{\alpha} \\ &= \frac{1}{\Gamma(\alpha+1)}t^{\alpha} \end{aligned} \tag{32}$$

When the fractional order α equals integer n, the response is well-known result for the unit-step input:

$$L^{-1}\left\{\frac{1}{s^{n}}\cdot\frac{1}{s}\right\} = \frac{1}{n!}t^{n} \tag{33}$$

As shown in Fig. 3, the unit-step responses of open-loop fractional order $1/s^{\alpha}$ systems $(\alpha = 0.2, \ldots, 0.8)$ display quite different behaves compared to their integer order counterparts $(\alpha = 0, 1)$ in time domain.

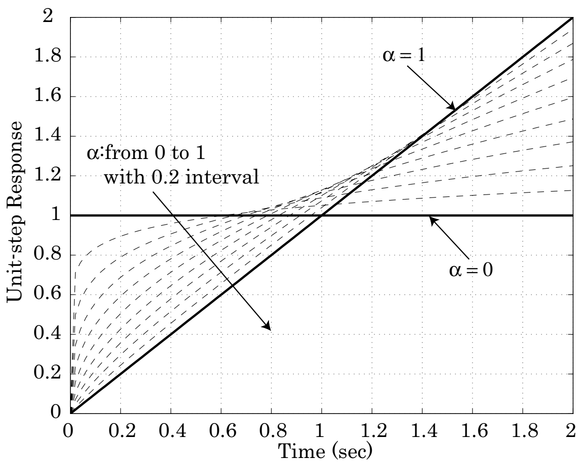

Figure 3: Unit-step responses of open-loop $1/s^{\alpha}$ systems

[1] $\Gamma(x-1) = \Gamma(x)/(x-1)$

[2] $\Gamma(1) = 1$

For more general time-domain analysis of fractional order systems, an effective tool called Mittag-Leffler function [7] [19] can be introduced. The Mittag-Leffler function in two parameters $E_{\alpha,\ \beta}(z)$ is defined as

$$E_{\alpha,\ \beta}(z) = \sum_{j=0}^{\infty} \frac{z^j}{\Gamma(\alpha j + \beta)} \quad (\alpha > 0,\ \beta > 0) \tag{34}$$

Its kth derivative is given by

$$E_{\alpha,\ \beta}^{(k)}(z) = \sum_{j=0}^{\infty} \frac{(j+k)! z^j}{j!\Gamma(\alpha j + \alpha k + \beta)} \quad (k = 0, 1, 2, \ldots) \tag{35}$$

It is convenient to introduce the function

$$\varepsilon_k(t, y; \alpha, \beta) = t^{\alpha k + \beta - 1} E_{\alpha,\beta}^{(k)}(y t^{\alpha}) \quad (k = 0, 1, 2, \ldots) \tag{36}$$

The Laplace transform of the function $\varepsilon_k(t, y; \alpha, \beta)$ is

$$\int_0^{\infty} e^{-st} \varepsilon_k(t, \pm y; \alpha, \beta) dt = \frac{k! s^{\alpha - \beta}}{(s^{\alpha} \mp y)^{k+1}} \quad (Re(s) > |y|^{1/\alpha}) \tag{37}$$

Another convenient property of $\varepsilon_k(t, y; \alpha, \beta)$ is its simple fractional differentiation:

$$_0D_t^{\lambda} \varepsilon_k(t, y; \alpha, \beta) = \varepsilon_k(t, y; \alpha, \beta - \lambda) \quad (\lambda < \beta) \tag{38}$$

For the unit-step response of the close-loop $1/s^{\alpha}$ system with unity feedback, its Laplace transform can be rewritten as:

$$\frac{1}{s} \cdot \frac{1}{1 + s^{\alpha}} = \frac{s^{-1}}{s^{\alpha} + 1} = \frac{0! s^{\alpha - (\alpha + 1)}}{(s^{\alpha} + 1)^{0+1}} \tag{39}$$

Therefore, by using Equ. (36) and Equ. (37) the inverse Laplace transform can be given:

$$L^{-1}\left\{\frac{1}{s} \cdot \frac{1}{1 + s^{\alpha}}\right\} = t^{\alpha} \sum_{j=0}^{\infty} \frac{(-t^{\alpha})^j}{\Gamma[(1+j)\alpha + 1]} \tag{40}$$

and the unit-step responses are plotted in Fig. 4. It can be seen the time responses of close-loop fractional order $1/s^{\alpha}$ systems show a nice interpolation between the responses of the integer order systems.

For general transfer functions, firstly consider a special fractional order transfer function given by the following form:

$$G_n(s) = \frac{1}{a_n s^{\beta_n} + a_{n-1} s^{\beta_{n-1}} + \ldots + a_1 s^{\beta_1} + a_0 s^{\beta 0}} \tag{41}$$

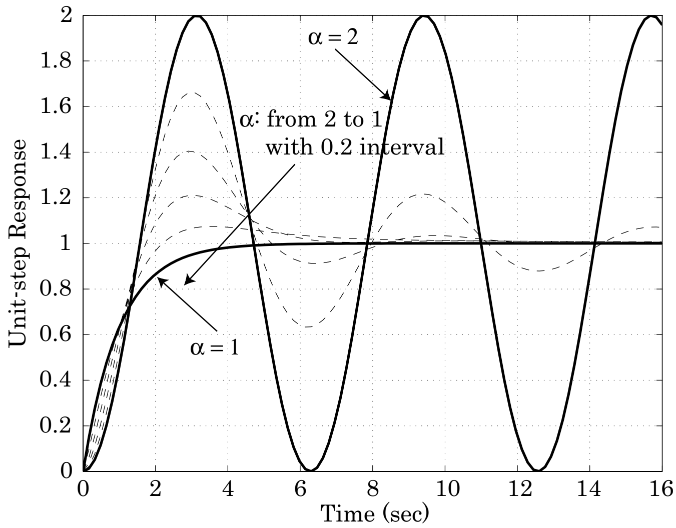

Figure 4: Unit-step responses of close-loop $1/s^{\alpha}$ systems

where β_k $(k = 0, 1, \ldots, n)$ is an arbitrary real number

$$\beta_n > \beta_{n-1} > \ldots > \beta_1 > \beta_0 \tag{42}$$

and a_k $(k = 0, 1, 2, \ldots, n)$ are arbitrary constants.

Based on Equ. (37), the infinite series expansion of $\frac{1}{1+x}$ [3] and the multinomial theorem [4], the inverse Laplace transform of Equ. (41) can be rewritten as follows:

$$\begin{aligned}
G_n(s) &= \frac{1}{a_n s^{\beta_n} + a_{n-1} s^{\beta_{n-1}}} \frac{1}{1 + \frac{\sum_{k=0}^{n-2} a_k s^{\beta_k}}{a_n s^{\beta_n} + a_{n-1} s^{\beta_{n-1}}}} \\
&= \frac{a_n^{-1} s^{-\beta_n - 1}}{s^{\beta_n - \beta_{n-1}} + \frac{a_{n-1}}{a_n}} \frac{1}{1 + \frac{a_n^{-1} s^{-\beta_{n-1}} \sum_{k=0}^{n-2} a_k s^{\beta_k}}{s^{\beta_n - \beta_{n-1}} + \frac{a_{n-1}}{a_n}}} \\
&= \sum_{m=0}^{\infty} \frac{(-1)^m a_n^{-1} s^{-\beta_n - 1}}{(s^{\beta_n - \beta_{n-1}} + \frac{a_{n-1}}{a_n})^{m+1}} \left[\sum_{k=0}^{n-2} \left(\frac{a_k}{a_n} \right) s^{\beta_k - \beta_{n-1}} \right]^m \\
&= \sum_{m=0}^{\infty} \frac{(-1)^m a_n^{-1} s^{-\beta_n - 1}}{(s^{\beta_n - \beta_{n-1}} + \frac{a_{n-1}}{a_n})^{m+1}} \\
&\times \sum_{\substack{k_0 + k_1 + \ldots + k_{n-2} = m \\ k_0 \geq 0; \ldots k_{n-2} \geq 0}} (m; k_0, k_1, \ldots, k_{n-2}) \\
&\times \prod_{i=0}^{n-2} \left[\left(\frac{a_i}{a_n} \right)^{k_i} s^{(\beta_i - \beta_{n-1}) k_i} \right]
\end{aligned}$$

[3] $\frac{1}{1+x} = \sum_{n=0}^{\infty} (-1)^n x^n$

[4] Multinomial theorem: $(x_1 + \ldots + x_k)^n = \sum (n; n_1, n_2, ..., n_k) x_1^{n_1} x_2^{n_2} \ldots x_k^{n_k}$. where the sum is over all $(n_1, \ldots, n_k)$ such that n_i is a non-negative integer for each i and $n_1 + \ldots + n_k = n$.

$$= \frac{1}{a_n}\sum_{m=0}^{\infty}(-1)^m \sum_{\substack{k_0+k_1+\ldots+k_{n-2}=m\\ k_0\geq 0;\ldots k_{n-2}\geq 0}} (m;k_0,k_1,\ldots,k_{n-2})$$
$$\times \prod_{i=0}^{n-2}\left(\frac{a_i}{a_n}\right)^{k_i} \frac{s^{-\beta_{n-1}+\sum_{i=0}^{n-2}(\beta_i-\beta_{n-1})^{k_i}}}{(s^{\beta_n-\beta_{n-1}}+\frac{a_{n-1}}{a_n})^{m+1}} \tag{43}$$

where $(m;k_0,k_1,\ldots,k_{n-2})$ are the multinomial coefficients. [5]

The term-by-term inversion by using Equ. (37) gives the final expression for the inverse Laplace transform of the function $G_n(s)$:

$$g_n(t) = \frac{1}{a_n}\sum_{m=0}^{\infty}\frac{(-1)^m}{m!} \sum_{\substack{k_0+k_1+\ldots+k_{n-2}=m\\ k_0\geq 0;\ldots k_{n-2}\geq 0}} (m;k_0,k_1,\ldots,k_{n-2})$$
$$\times \prod_{i=0}^{n-2}\left(\frac{a_i}{a_n}\right)^{k_i} \varepsilon_m\left(t,-\frac{a_{n-1}}{a_n};\beta_n-\beta_{n-1},\beta_n+\sum_{j=0}^{n-2}(\beta_{n-2}-\beta_j)k_j\right) \tag{44}$$

Therefore, the unit-impulse response of the fractional order system with the transfer function Equ. (41) is given by Equ. (44):

$$y_{impluse}(t) = g_n(t) \tag{45}$$

Integrating Equ. (44) with the help of Equ. (38) gives the unit-step response $y_{step}(t)$:

$$y_{step}(t) = \frac{1}{a_n}\sum_{m=0}^{\infty}\frac{(-1)^m}{m!} \sum_{\substack{k_0+k_1+\ldots+k_{n-2}=m\\ k_0\geq 0;\ldots k_{n-2}\geq 0}} (m;k_0,k_1,\ldots,k_{n-2})$$
$$\times \prod_{i=0}^{n-2}\left(\frac{a_i}{a_n}\right)^{k_i} \varepsilon_m\left(t,-\frac{a_{n-1}}{a_n};\beta_n-\beta_{n-1},\beta_n+\sum_{j=0}^{n-2}(\beta_{n-2}-\beta_j)k_j+1\right) \tag{46}$$

Further inverse Laplace transforms can be obtained by combining Equ. (37) and Equ. (38). For example, let $F(s)$ be general form of transfer functions

$$F(s) = \frac{b_n s^{\alpha_n}+b_{n-1}s^{\alpha_{n-1}}+\ldots+b_1 s^{\alpha_1}+b_0 s^{\alpha 0}}{a_n s^{\beta_n}+a_{n-1}s^{\beta_{n-1}}+\ldots+a_1 s^{\beta_1}+a_0 s^{\beta 0}}$$
$$= \sum_{i=0}^{n} b_i s^{\alpha_i} G_n(s) \tag{47}$$

where $\alpha_i \leq \beta_n,\ (i=0,1,\ldots,n)$. Then the inverse Laplace transform of $F(s)$ is

$$f(t) = \sum_{i=0}^{n} b_i D^{\alpha_i} g_n(t) \tag{48}$$

where the fractional derivatives of $g_n(t)$ can be evaluated using Equ. (38).

[5]The coefficients $(n;n_1,n_2,\ldots,n_k)$ in the multinomial theorem are called multinomial coefficients.

CHAPTER III

FUNDAMENTAL ISSUES

3.1 *Representations*

The fractional order system can be represented by a fractional SISO model using fractional differential equation:

$$\begin{aligned} & a_n D_t^{\alpha_n} y(t) + \ldots + a_1 D_t^{\alpha_1} y(t) + a_0 D_t^{\alpha_0} y(t) \\ = \; & b_m D_t^{\beta_m} u(t) + \ldots + b_1 D_t^{\beta_1} u(t) + b_0 D_t^{\beta_0} u(t) \end{aligned} \tag{49}$$

where ${}_0D_t^{(*)} := D_t^{(*)}$ and $\alpha_k,\ \beta_k$ $(k = 0, 1, 2, \ldots)$ are arbitrary real numbers, $\beta_n > \ldots > \beta_1 > \beta_0,\ \alpha_n > \ldots > \alpha_1 > \alpha_0$ and a_k, b_k $(k = 0, 1, 2, \ldots)$ are constants.

By Laplace transform, the transfer function of fractional order system can be obtained in following general expression:

$$G(s) = \frac{Y(s)}{U(s)} = \frac{b_m s^{\beta_m} + \ldots + b_1 s^{\beta_1} + b_0 s^{\beta_0}}{a_n s^{\alpha_n} + \ldots + a_1 s^{\alpha_1} + a_0 s^{\alpha_0}} \tag{50}$$

For special fractional order systems, $R(s^\alpha) = N(s^\alpha)/D(s^\alpha)$, a state-space model described in vector and matrix relations is given as:

$$\begin{aligned} \mathbf{x}^{(\alpha)}(t) &= \mathbf{A}\mathbf{x}(t) + \mathbf{B}u(t) \\ y(t) &= \mathbf{C}\mathbf{x}(t),\ t \geq 0 \end{aligned} \tag{51}$$

The controllability and observability of the fractional order $R(s^\alpha)$ systems can be discussed based on the state-space model description [15] [16]. Obviously, this description is convenient only for simple models with integer order s^α operator, $(s^\alpha)^n$ $(n = 0, 1, \ldots)$.

Another type state-space model of fractional order system can be written as [20]:

$$\begin{aligned} \dot{\mathbf{x}}(t) &= \mathbf{f}(\mathbf{x}^{(fr)}(t),\ u(t)) \\ y(t) &= \mathbf{g}(\mathbf{x}^{(fr)}(t),\ u(t)),\ t \geq 0 \end{aligned} \tag{52}$$

which expresses the 1st-order derivative in the state-space equations and has the classical state-space interpretation for the fractional order systems too. On the right side of these equations, more than one fractional order derivatives of the state-space variables can be transferred. This state-space model cannot be expressed in vector and matrix relations in time domain. But in s-plane, it is possible by using transfer function matrixes:

$$\begin{aligned} s\mathbf{X}(s) &= \mathbf{A}(s)\mathbf{X}(s) + \mathbf{B}(s)U(s) \\ Y(s) &= \mathbf{C}(s)\mathbf{X}(s) \end{aligned} \tag{53}$$

Similarly, the overall transfer function can be derived as:

$$\frac{Y(s)}{U(s)} = \frac{\mathbf{C}adj(s\mathbf{I} - \mathbf{A})\mathbf{B}}{det(s\mathbf{I} - \mathbf{A})} \tag{54}$$

Therefore, the characteristic equation of the closed-loop system can be determined by solving the determinant in the denominator of the transfer function, which is a fractional order polynomial in s:

$$a_n s^{\alpha_n} + \ldots + a_1 s^{\alpha_1} + a_0 s^{\alpha_0} = 0 \tag{55}$$

3.2 Linearity

As mentioned in Chapter 2, systems' linearity is obviously kept when their orders are expanded to fractional orders:

$$D^{\alpha}\left(\lambda f(t) + \mu g(t)\right) = \lambda D^{\alpha} f(t) + \mu D^{\alpha} g(t) \tag{56}$$

The linearity of fractional order systems follows directly from the two mathematical definitions. For the Riemann-Liouville definition of α order ($k-1 < \alpha < k$), it can be seen:

$$\begin{aligned} {}_aD_t^{\alpha}\left(\lambda f(t) + \mu g(t)\right) &= \frac{1}{\Gamma(k-\alpha)}\frac{d^k}{dt^k}\int_a^t (t-\tau)^{k-\alpha-1}\left(\lambda f(\tau) + \mu(\tau)\right)) d\tau \\ &= \frac{\lambda}{\Gamma(k-\alpha)}\frac{d^k}{dt^k}\int_a^t (t-\tau)^{k-\alpha-1} f(\tau) d\tau \\ &+ \frac{\mu}{\Gamma(k-\alpha)}\frac{d^k}{dt^k}\int_a^t (t-\tau)^{k-\alpha-1} g(\tau) d\tau \\ &= \lambda_a D_t^{\alpha} f(t) + \mu_a D_t^{\alpha} g(t) \end{aligned} \tag{57}$$

Similarly, based on the Grünwald-Letnikov definition, the same result can be arrived:

$$\begin{aligned}
{}_aD_t^{\alpha}\left(\lambda f(t)+\mu g(t)\right) &= \lim_{\substack{h\to 0\\ nh=t-a}} h^{-\alpha}\sum_{j=0}^{n}(-1)^j\begin{pmatrix}\alpha\\ j\end{pmatrix}\left(\lambda f(t-jh)+\mu g(t-jh)\right)\\
&= \lambda\lim_{\substack{h\to 0\\ nh=t-a}} h^{-\alpha}\sum_{j=0}^{n}(-1)^j\begin{pmatrix}\alpha\\ j\end{pmatrix}f(t-jh)\\
&+ \mu\lim_{\substack{h\to 0\\ nh=t-a}} h^{-\alpha}\sum_{j=0}^{n}(-1)^j\begin{pmatrix}\alpha\\ j\end{pmatrix}g(t-jh)\\
&= \lambda_a D_t^{\alpha}f(t)+\mu_a D_t^{\alpha}g(t) \qquad (58)
\end{aligned}$$

Although FOC is conceptually unfamiliar, it is in fact a natural generalization and expansion of IOC theory. The FOC systems are also linear systems whose Laplace and Fourier transforms are similar to integer order systems' but with fractional order operators.

3.3 Modeling and Identification

There is a growing significant demand for better mathematic models to describe real objects recently. The fractional order model can provide a new possibility to acquire more adequate modeling of dynamic processes. Fractional order models have been applied to describe reheating furnace [7], visco-elasticity [1][7][8], chemical processes [22] and Chaos system [21], etc.

Actually, using fractional order model for describing distributed-parameter systems is quite natural since the Laplace transform of partial differential equations will inevitably introduce fractional order s operator. For a simple example, see semi-infinite cable in Fig. 5 with voltage $v(t,0)$ applied in $x=0$ [3]. R and C are cable's electrical resistance and capacity at unit length. The physical model of the system can be described by following equations:

$$Ri(t,x) = -\frac{\partial v(t,x)}{\partial x} \qquad (59)$$

$$C\frac{\partial v(t,x)}{\partial t} = -\frac{\partial i(t,x)}{\partial x} \qquad (60)$$

The Laplace transform of the above equations gives:

$$RI(s,x) = -\frac{\partial V(s,x)}{\partial x} \qquad (61)$$

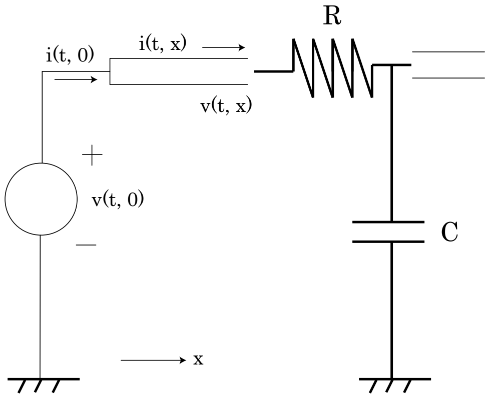

Figure 5: Semi-infinite cable

$$CsV(s,x) \quad = \quad -\frac{\partial I(s,x)}{\partial x} \tag{62}$$

Therefore,

$$\frac{\partial^2 V(s,x)}{\partial x^2} - RCsV(s,x) = 0 \tag{63}$$

The general solution for the 2nd-order differential equation is:

$$V(s,x) = C_1 e^{\sqrt{RCs}x} + C_2 e^{-\sqrt{RCs}x} \tag{64}$$

For the semi-infinite cable, it gives

$$V(s,0) \quad = \quad C_1 + C_2 \tag{65}$$

$$V(s,\infty) \quad = \quad C_1 e^{\sqrt{RCs}\infty} + C_2 e^{-\sqrt{RCs}\infty} = 0 \tag{66}$$

Finally,

$$V(s,x) \quad = \quad V(s,0)e^{-\sqrt{RCs}}x \tag{67}$$

$$I(s,x) \quad = \quad \sqrt{\frac{C}{R}}V(s,0)s^{0.5} \tag{68}$$

As another example, consider a torsional model as shown in Fig. 6, which consists of a flexible shaft attached to a rigid disk [23]. The rigid body equation of the disk is given as

$$I_1 s^2 \theta_1 = T_1 + T_{12} \tag{69}$$

Take a small element of length dx along the shaft axis and observe the cylindrical surface, as shown in Fig. 7(a). This element will deform through a small angle $d\theta$.

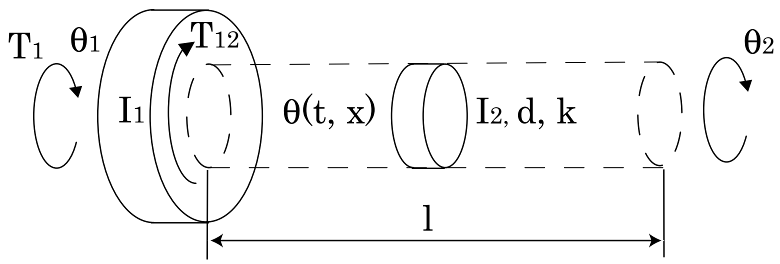

Figure 6: The flexible shaft attached to a rigid disk

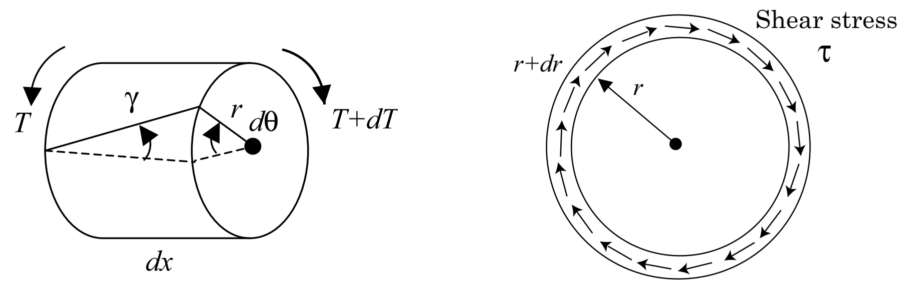

(a) Small element of the torsional shaft

(b) Shear stress in a small annular cross section

Figure 7: Deformation of the torsional shaft

Based on the theory of elasticity [24], γ is the shear strain:

$$\gamma = r\frac{\partial \theta(t,x)}{\partial x} \tag{70}$$

The corresponding shear stress at the deformed point at radius r is

$$\tau = G\gamma = Gr\frac{\partial \theta(t,x)}{\partial x} \tag{71}$$

where G is shear modulus [24].

As shown in Fig. 7(b), since this shear stress acts tangentially, the overall torque at the shaft cross section is

$$T = \int r \times (\tau \times 2\pi r dr) = G\frac{\partial \theta(t,x)}{\partial x}\int 2\pi r^3 dr = GJ\frac{\partial \theta(t,x)}{\partial x} \tag{72}$$

Now apply Newton's second law for rotatory motion of the small element dx shown in Fig. 7(a), the equation of motion is

$$\rho J dx\frac{\partial^2 \theta(t,x)}{\partial t^2} = T + dT - T = \frac{\partial T(t,x)}{\partial x}dx \tag{73}$$

Substitute Equ. (72) and cancel dx to get the equation of a circular shaft as

$$\rho J \frac{\partial^2 \theta(t,x)}{\partial t^2} = \frac{\partial}{\partial x} GJ \frac{\partial \theta(t,x)}{\partial x} \tag{74}$$

For a uniform shaft segment of length l with associated overall angular deformation θ, the torsional stiffness k is

$$k = \frac{T}{\theta} = GJ \frac{\partial \theta(t,x)}{\partial x} \cdot \frac{1}{\theta} = \frac{GJ}{l} \tag{75}$$

Therefore, Equ. (74) can be rewritten as

$$\frac{I_2}{l} \frac{\partial^2 \theta(t,x)}{\partial t^2} - kl \frac{\partial^2 \theta(t,x)}{\partial x^2} = 0 \tag{76}$$

For Equ. (74), the Laplace transform in t can be obtained:

$$\frac{I_2}{l} s^2 \theta(x) - kl \frac{d^2 \theta(x)}{dx^2} = 0 \tag{77}$$

where $\theta(s,x)$ is abbreviated as $\theta(x)$ for simplicity. Let $\mu^2 = \frac{I_2}{kl}$, the solution of Equ. (77), a 2nd-order differential equation, is

$$\theta(x) = C_1 e^{\mu s x} + C_2 e^{-\mu s x} \tag{78}$$

For the free end of the shaft, there is no deformation and the shear stress in zero. Therefore, the below two boundary conditions can be obtained:

$$\theta(x)|_{x=0} = \theta_1, \quad \left.\frac{d\theta(x)}{dx}\right|_{x=l} = 0 \tag{79}$$

Therefore, the two constants C_1 and C_2 can be calculated as:

$$C_1 = \frac{e^{-\mu l s}\theta_1}{2cosh(\mu l s)} \text{ and } C_2 = \frac{e^{\mu l s}\theta_1}{2cosh(\mu l s)} \tag{80}$$

Torque T_{12} in Fig. 6 can be obtained:

$$T_{12}(s) = (kl) \left.\frac{d\theta(x)}{dx}\right|_{x=0} = -tanh(\mu l s)\theta_1 \tag{81}$$

Finally, substitute T_{12} in Equ. (69), the transfer function between T_1 and θ_1 can be achieved:

$$\begin{aligned} \frac{T_1}{\theta_1} &= I_1 s^2 + kl \cdot \mu s \cdot tanh(\mu l s) \\ &= I_1 s^2 + \sqrt{klI_2} tanh\left(\sqrt{\frac{lI_2}{k}} s\right) s \end{aligned} \tag{82}$$

However, in conventional modeling method, the torsional system in Fig. 6 are usually modeled as a rigid body system with inertia $I = I_1 + I_2$:

$$\frac{T_1}{\theta_1} = (I_1 + I_2)s^2 \tag{83}$$

As shown in the Bode plots of Fig. 8, the fractional order transfer function model in Equ. (82) displays the mechanical resonance effect naturally. At low-frequency range, the two models give similar frequency responses. At high frequency range, the fractional model can describe the distributed nature of the torsional system; while in conventional integer order model, this nature is totally ignored. Fractional order modeling is a useful tool to give more adequately description of system's "real" dynamic features.

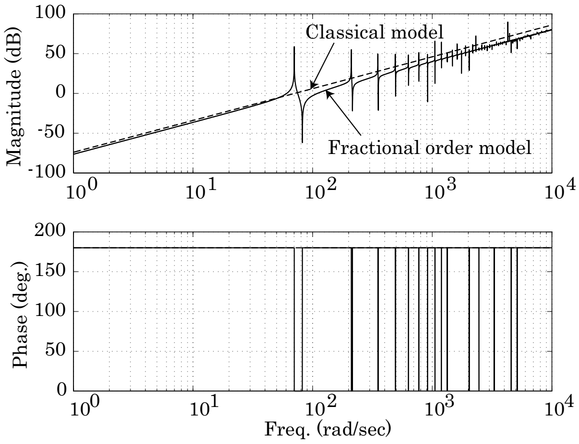

Figure 8: Bode plots of the torsional system's fractional order model and conventional integer order model

From the above two examples, it can be seen that distributed-parameter systems are naturally described by a set of partial differential equations. However, these equations will lead to transfer functions that are quotients of transcendental functions.

Using fractional order transfer function model, a quotient of polynomials in s^α, it is also possible to fit better a set of experimental data. For example, the frequency-domain identification of a flexible structure by fractional order model can take into account not only material damping, but also other variety of physical phenomena such as visco-elasticity and anomalous relaxation. This fact indicts fractional order models can be an appropriate and hopeful tool to model the dynamic features of flexible structure more accurately which is becoming more and more important due to lighter materials and faster motions [7][8].

For fractional order models like Equ. (50), frequency-domain identification methods to determine the coefficients $\alpha_k,\ \beta_k\ (k = 0, 1, 2, \ldots)$ and $a_k, b_k\ (k = 0, 1, 2, \ldots)$ are as routine as conventional integer order models. Various identification methods for determination of the coefficients were developed [7][8][25], based on minimization of the difference between the measured frequency response $F(\omega)$ and the frequency response of the model $G(j\omega)$. For example, the quadratic criterion for the optimization can be in following form:

$$Q = \sum_{m=0}^{M} W^2(\omega_m) \left| F(\omega_m) - G(j\omega_m) \right|^2 \tag{84}$$

where $W(\omega_m)$ is a weighting function and M is the number of measured values of frequencies $\omega = (\omega_0,\ \omega_2,\ \ldots,\ \omega_M)$.

Compared to the general fractional order model as in Equ. (50), a special model can be introduced, in which only integer orders of fractional order operator s^α are used:

$$G(s) = \frac{\sum_{i=0}^{m} a_i (s^\alpha)^i}{(s^\alpha)^n + \sum_{j=0}^{n-1} b_j (s^\alpha)^j},\ n \geq m \tag{85}$$

It is interesting to notice that the selection of α can actually be seen as selecting the phenomena that can be modeled. For example, when modeling a flexible structure, using $\alpha = 2$ can not model damping. In $\alpha = 1$ case, we can model the damping. If we can further take $\alpha = 0.5$, other phenomena such as visco-elasticity and anomalous relaxation will be described. The other advantage of this model is that existing optimization methods can still be use since only integer order s^α is introduced.

CHAPTER IV

CONTROL IMPACTS

4.1 Control System Type

Control system type is defined as the number of poles that $G(s)$ has at $s = 0$. Here $G(s)$ is the forward-path transfer function for unity feedback systems. In order to investigate the impacts of s^α upon conventional integer order control, consider a unity feedback with open-loop transfer function:

$$G(s) = \frac{K(s - z_1)(s - z_2)\dots(s - z_m)}{s^\alpha(s - p_1)(s - p_2)\dots(s - p_n)} \tag{86}$$

It is well-known that for system with a step-function input of magnitude R, R/s, the steady-state error is:

$$e_{ss} = \frac{R}{1 + \lim_{s\to 0} G(s)} = \frac{R}{1 + \lim_{s\to 0} \frac{K\prod_{i=1}^{m}(s - z_i)}{s^\alpha \prod_{j=1}^{n}(s - p_j)}} \tag{87}$$

For system with a ramp-function input R/s^2:

$$e_{ss} = \frac{R}{\lim_{s\to 0} sG(s)} = \frac{R}{\lim_{s\to 0} \frac{K\prod_{i=1}^{m}(s - z_i)}{s^{\alpha-1} \prod_{j=1}^{n}(s - p_j)}} \tag{88}$$

For system with a parabolic function input R/s^3:

$$e_{ss} = \frac{R}{\lim_{s\to 0} s^2G(s)} = \frac{R}{\lim_{s\to 0} \frac{K\prod_{i=1}^{m}(s - z_i)}{s^{\alpha-2} \prod_{j=1}^{n}(s - p_j)}} \tag{89}$$

Obviously, since the fractional order s^α does not exactly cancel the integer orders of s for the various inputs, there will always be a fractional order s term in the numerator or the denominator, which accounts for the fact that the steady-state error e_{ss} is always either 0 or infinite. The following table Table. 1 shows the effects of fractional s^α on steady-state error.

Based on root locus condition on magnitude, the values of K along the root locus can be determined by

$$|K| = |s^\alpha| \frac{|s - p_1||s - p_2|\dots|s - p_n|}{|s - z_1||s - z_2|\dots|s - z_m|} \tag{90}$$

System type of α	Input	Error Constant	Steady-state Error
$0 < \alpha < 1$	Unit step	∞	0
	Ramp	0	∞
	Parabolic	0	∞
$1 < \alpha < 2$	Unit step	∞	0
	Ramp	∞	0
	Parabolic	0	∞
$2 < \alpha < 3$	Unit step	∞	0
	Ramp	∞	0
	Parabolic	∞	0

Table 1: State-state error of fractional type system

and condition on angels:

$$\angle G(s) = -\alpha \angle s + \sum_{k=1}^{m} \angle(s - z_k) - \sum_{j=1}^{n} \angle(s - p_j) \tag{91}$$

Obviously by choosing α small enough, the fractional pole at 0 can be reduced to $1\angle 0$ and is thereby made transparent to the rest of the system. A weak pole ($0 < \alpha \ll 1$) behaves like a linear multiplier of value 1. On the other hand, a strong pole, for example $\alpha = 1$, tends to shift the root locus to the right which may lead to instability. As α is reduced from 1 to zero, the fractional pole at the origin can be adjusted to exhibit different pole-like behavior. This suggests that the tendency of a pole to shift the entire root locus plot can now be scaled to accommodate a particular application by introducing the fractional order operator s^{α}.

For a type α system, $0 < \alpha < 1$, with a unit step input, the steady-state error of the system is 0, a characteristic usually found in a system of at least TYPE 1. However, when $0 < \alpha \ll 1$, the root locus plot would resemble that of a TYPE 0 system since the weak pole at s^{α} has little effect to root locus. A fractional type system seems to combine some of the characteristics of TYPE N and TYPE N+1 systems.

For a simple example, consider the unit-step responses of $G(s) = 1/s^{\alpha}$ for a very small $\alpha = 0.00001$ and $\alpha = 0$ (see Fig. 9). The steady-state error of $1/s^{0.00001}$ is zero, which is the characteristic of TYPE 1 system; while for $1/s^0$, a TYPE 0 system, the error is 0.5.

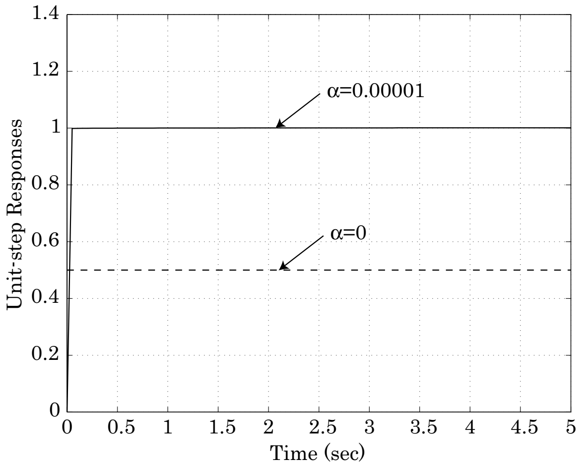

Figure 9: Unit-step responses of $1/s^{0.00001}$ and $1/s^0$

In above example, even with very small fractional order 0.00001, the system's characteristics are greatly changed and show a combinatorial effects of the neighbor integer order 0 and 1 systems. More extensive analysis which examines this combinatorial effects of fractional poles and zeros, and their relationship to system damping coefficients and other performance criteria are beyond the scope of this dissertation and still largely open research problems.

4.2 Stability Determination

The question of stability is of main interest in control theory. A fractional order system is stable if all its roots in the main sheet of the Riemann surface are negative or have negative real parts [26]. However, It is quite difficult to find a general stability criterion like Routh criterion for integer order systems.

For the special fractional order systems with only integer order s^α operators, this question can be easily resolved. For example, the characteristic equation of $R(s^\alpha) = N(s^\alpha)/D(s^\alpha)$ systems can be expressed as:

$$(s^\alpha)^n + a_{n-1}(s^\alpha)^{n-1} + \ldots + a_1 s^\alpha + a_0 = 0 \tag{92}$$

where $0 < \alpha < 1$. Let $\sigma := s^\alpha$, Equ. (92) can be rewritten as

$$\sigma^n + a_{n-1}\sigma^{n-1} + \ldots + a_1\sigma + a_0 = 0 \tag{93}$$

The requirement of stability for Equ. (92) is the roots p_i of the characteristic equation in the main sheet of the Riemann surface ($-\pi < arg(s) < \pi$) must be all located in the left-half s-plane. As shown in Fig. 10, using the mapping $\sigma := s^\alpha$, the corresponding stability condition for Equ. (93) is that all its roots $p_i^{'}$ must be located outside the sector of $-\frac{\pi}{2}\alpha < arg(p_i^{'}) < \frac{\pi}{2}\alpha$ in the σ-plane.

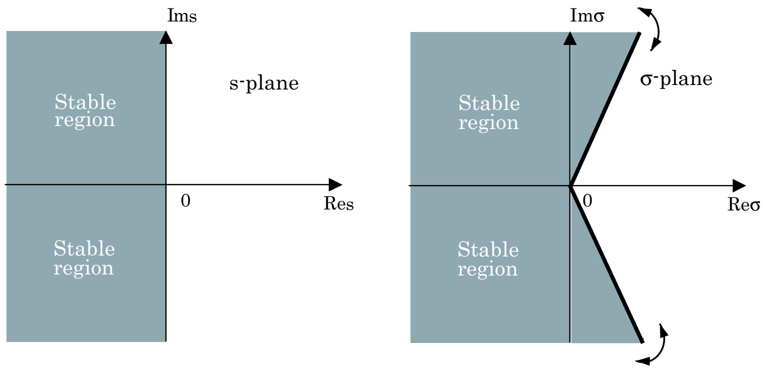

Figure 10: Larger stable root region for fractional order $R(s^\alpha)$ system

Namely, the stabilities for $R(s^\alpha)$ systems are guaranteed iff the roots of the polynomial Equ. (93) lie outside the closed angular sector:

$$|arg(\delta)| \leq \alpha\frac{\pi}{2} \tag{94}$$

For state-space representation of the $R(s^\alpha)$ fractional order systems, all the eigenvalues of the state-transition matrix $\mathbf{A}$ should be outside the above sector. This result generalizes the well-known results for the integer case $\alpha = 1$ in a stupendous way.

As a qualitative explanation in time domain, compared with the characteristic equations of integer order control systems with same coefficients $\{a_{n-1}, \ldots, a_1, a_0\}$, the stability requirement of the FOC systems is looser (see Fig. 10). When uncertainties occur, the coefficients of characteristic equation change and consequently roots move about the complex plane. Looser stability requirement of FOC systems means better robustness performance against uncertainties.

Like IOC systems, frequency-domain approaches are more convenient to determinate the stabilities of FOC systems . In chapter 2, it has been shown that the Fourier transform of fractional order systems can be easily obtained by substituting the s operator with $j\omega$, just as same as conventional integer order systems.

Here, the close-loop $1/s^{\alpha}$ system is used again as an example to illustrate the effectiveness of stability analysis by classical frequency-domain approaches, such as the Nyquist criterion. In the Bode plots of Fig. 11(a), the phase margin is negative for 2.2 order α and zero for 2 order α. For the other orders smaller than 2, the phase margin is positive and the system should be stable. The time responses of close-loop $1/s^{\alpha}$ systems verify this stability analysis. Obviously when taking α as 2 and 2.2, the system will be unstable (see Fig. 11(b)).

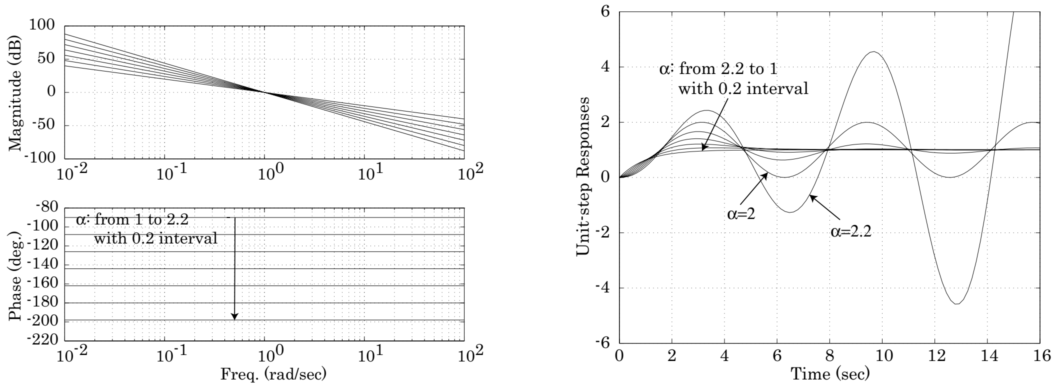

(a) Bode plots with fractional α orders

(b) Time responses with fractional α orders

Figure 11: Example of stability determination using Nyquist criterion

4.3 Frequency-domain Analysis

As a starting point for frequency-domain analysis of FOC system, consider the classical way of introducing a sinusoidal input with amplitude R and frequency ω:

$$r(t) = Rsin(\omega t) \tag{95}$$

In order to obtain steady-state output, $y(t)$, fractional order calculus of $sin(\omega t)$ need be known. Since $sin(\omega t)$ is a periodic function, it's fractional α order calculus $(-1 < \alpha < 1)$ can be expressed in following form

$${}_0D_t^{\alpha} sin(\omega t) = \frac{{}_0D_t^{\alpha} e^{j\omega t} - {}_0 D_t^{\alpha} e^{-j\omega t}}{2j} \tag{96}$$

When t tends to infinity, the fractional α order derivative of $e^{j\omega t}$ can be expanded using an asymptotic expansion of the incomplete gamma function [1]:

$$\begin{aligned} {}_0D_t^{\alpha} e^{j\omega t}\Big|_{t\to\infty} &= (j\omega)^{\alpha} e^{j\omega t} - \sum_{k=0}^{\infty} \frac{(j\omega t)^{-1-k} t^{-\alpha}}{\Gamma(-\alpha-k)} \\ &= \omega^{\alpha} e^{j(\omega t + \frac{\pi}{2}\alpha)} - \sum_{k=0}^{\infty} \frac{(j\omega t)^{-1-k} t^{-\alpha}}{\Gamma(-\alpha-k)} \end{aligned} \tag{97}$$

Based on this expansion, Equ. (96) can be rewritten as

$$\begin{aligned} \frac{{}_0D_t^{\alpha} e^{j\omega t} + {}_0D_t^{\alpha} e^{-j\omega t}}{2j}\Bigg|_{t\to\infty} &= \omega^{\alpha} sin(\omega t + \frac{\pi}{2}\alpha) - \sum_{k=0}^{\infty} \frac{1-(-1)^{-1-k}}{2j\Gamma(-\alpha-k)} (j\omega t)^{-1-k} t^{-\alpha} \\ &= \omega^{\alpha} sin(\omega t + \frac{\pi}{2}\alpha) + \sum_{n=0}^{\infty} \frac{(-1)^n}{\omega^{1+2n}\Gamma(-\alpha-2n)} \cdot \frac{1}{t^{1+2n+\alpha}} \\ &= \omega^{\alpha} sin(\omega t + \frac{\pi}{2}\alpha) \end{aligned} \tag{98}$$

Namely,

$${}_0D_t^{\alpha} sin(\omega t)|_{t\to\infty} = \omega^{\alpha} sin(\omega t + \frac{\pi}{2}\alpha) \tag{99}$$

Therefore, the steady-state output, $y(t)$, of fractional order s^{α} system will also be a sinusoid with same frequency ω, but different amplitude, $R\omega^{\alpha}$, and phase, $\omega t + \frac{\pi}{2}\alpha$:

$$y(t) = Y sin(\omega t + \phi) \tag{100}$$

where Y is the amplitude of the output sine wave scaled by ω^{α} and ϕ is the phase shift of $\frac{\pi}{2}\alpha$. The utility of being able to vary α fractionally is apparent when considering that control system's frequency responses can be further adjusted accurately between existing IOC systems through FOC approach.

As discussed in chapter 2, for a general FOC system with transfer function $G(s)$, the amplitude and phase of the output sinusoid are

$$Y = R\left|G(j\omega)\right|, \quad \phi = \angle G(j\omega) \tag{101}$$

Unlike the complicated time-domain analysis, frequency responses of FOC systems can be easily and exactly known. The wealth of graphical methods and analysis tools in frequency domain are still available for fractional order systems and can be used as conveniently as in conventional IOC system analysis and design. Most importantly, the Nyquist stability criterion can be a general solution for determining FOC system's stability. Due to these reasons, FOC researches are mainly carried out in frequency domain.

To investigate the impacts of introducing FOC upon system's frequency responses, the Bode plots of unity-feedback control system $G(s)$ with fractional order operator s^α are shown from Fig. 12 to Fig. 15.

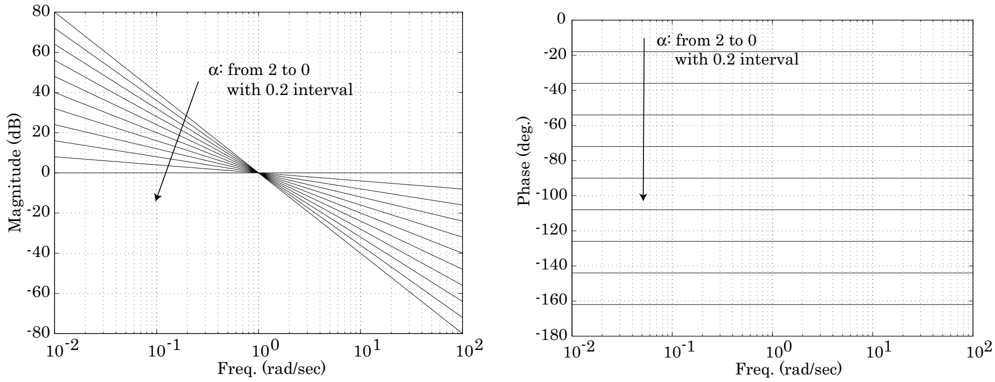

(a) Gain (b) Phase

Figure 12: Bode plots of $G(s) = \frac{1}{s^\alpha}$

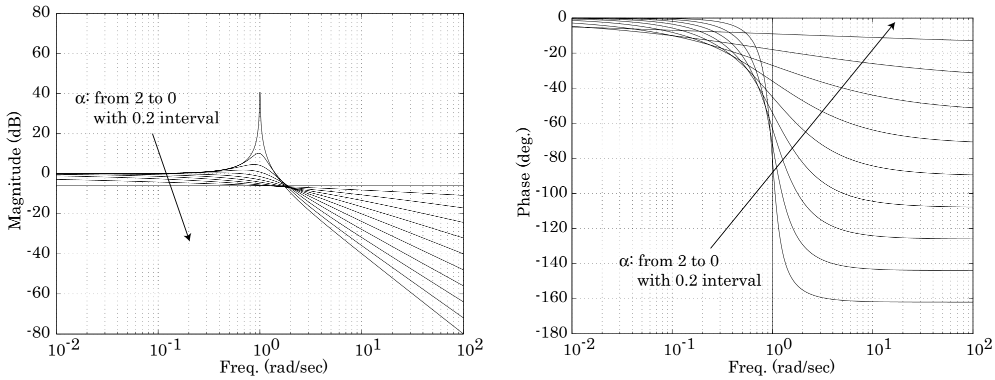

(a) Gain (b) Phase

Figure 13: Bode plots of $G(s) = \frac{1}{s^\alpha+1}$

By adjusting fractional order α, the control system's frequency responses are significantly changed. Even fractional order is a natural interpolation between integer orders, the FOC system's properties exhibit distinct differences between conventional IOC systems. It implies some complicated frequency characteristics, which were obtained by high-order transfer

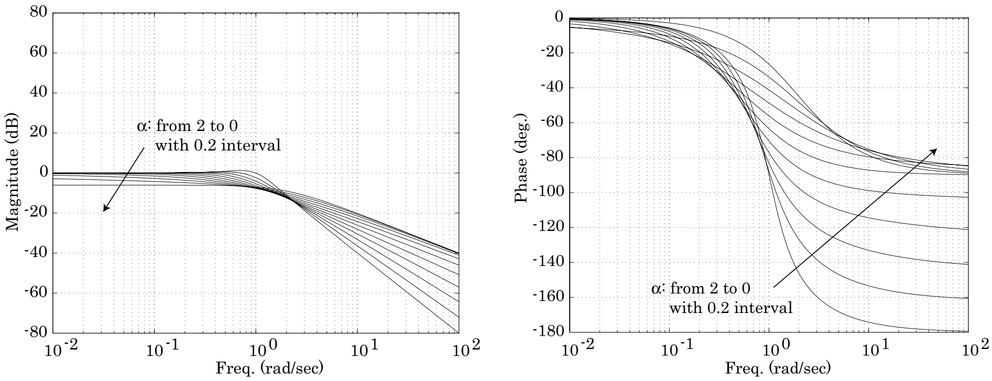

(a) Gain (b) Phase

Figure 14: Bode plots of $G(s) = \frac{1}{s+s^{\alpha}+1}$

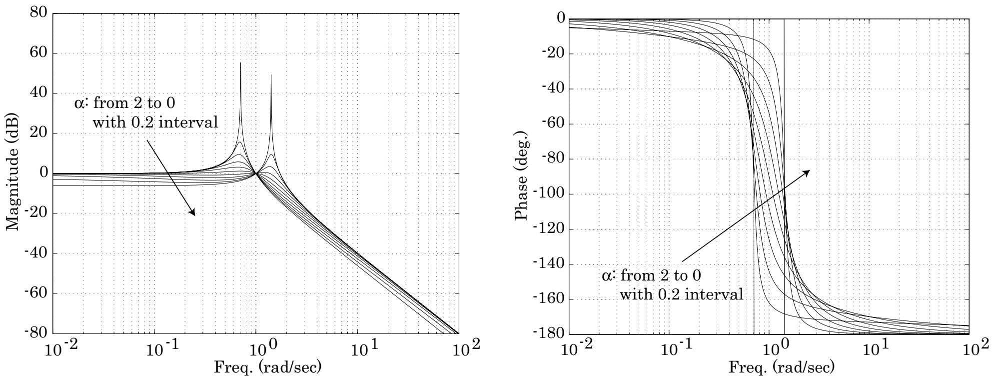

(a) Gain (b) Phase

Figure 15: Bode plots of $G(s) = \frac{1}{s^2+s^{\alpha}+1}$

functions in IOC before, could be realized easily by FOC with simpler structures and less control parameters.

It is of interest to consider the effects on frequency-domain responses when fractional order poles and zeros are added to the prototype forward-path transfer function of a unity-feedback control system. As an example, consider a more general unity-feedback control system $G(s)$:

$$G(s) = \frac{K(s+2)}{s^{\alpha}(s+1)} \tag{102}$$

then

$$\begin{aligned} |G(j\omega)|_{dB} &= -20\alpha log_{10}|j\omega| + 20log_{10}|K| + 20log_{10}|j\omega+2| - 20log_{10}|j\omega+1| \\ \angle G(j\omega) &= -\alpha\frac{\pi}{2} + \angle(j\omega+2) - \angle(j\omega+1) \end{aligned} \tag{103}$$

Here the advantage of introducing s^α is more obvious. Recall that when $\alpha = 1$, $j\omega$ is considered to have a constant phase characteristic of -90 degree. By introducing s^α, Equ. (103) shows that an arbitrary phase shift can be obtained with different value of α. Moreover, this phase is independent of frequency ω. By choosing α between 0 and 2, the phase response of the system can be precisely offset (increased or decreased) by any amount from 0 to -180 degree.

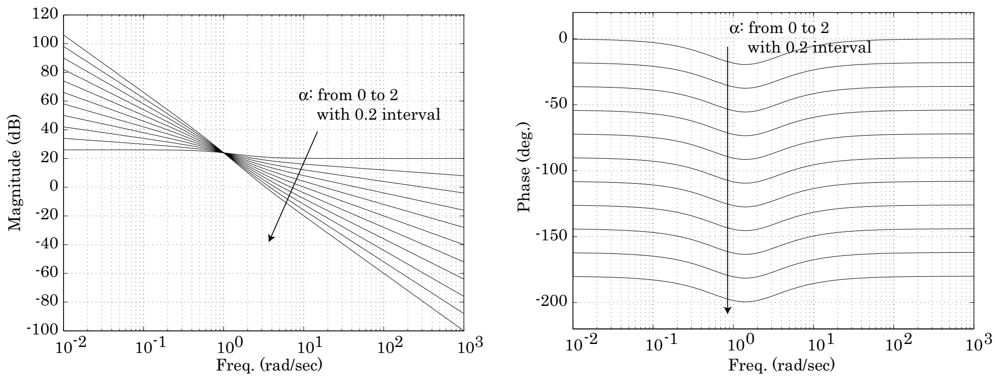

(a) Gain (b) Phase

Figure 16: Bode plots of $G(s)$ with selected α (K=10)

As shown in Equ. (103) and Fig. 16, when the type of system, α, is reduced from 2 to 0, the effect is to reduce the system gain at constant rate $-20\alpha \ dB/decade$; while adding phase in a linear fashion. In phase plot's bottom trace, -180 degree in low frequency range is the standard response of two strong poles located at the origin. As α is reduced, phase is added and the whole response is shifted upward. This is an interesting result when contrasted with conventional lead, lag networks or PID-type controllers which have undesirable phase-margin and phase-gain trade-offs at certain frequencies. This advantage implies a clear-cut control design could be achieved by introducing FOC approach.

4.4 Design of Robust Control System

Robustness of control systems to disturbances and uncertainties has always been a central issue in feedback control. Feedback would not be needed for most control systems if there were no disturbances and uncertainties. Developing robust control methods has be the focal point in the last two decades in the control community. The state-of-the-art $H\infty$ robust control theory is the result of this effort [27]. Despite its past successes in various applications, $H\infty$ control is notorious for its high-order, conservative controllers and complicated mathematics.

A new dimension opens to control engineering when the order of Laplace operator s becomes an arbitrary real number. A controller, which is neither too conservative nor too aggressive, can be easily designed by choosing proper fractional order. More adequate fractional order model also leads to less model error used in control design.

4.4.1 Less model error

A good model should be simple enough to facilitate design, yet complex enough to give the control engineer confidence that designs based on the model will work on the true plant. Fractional order modeling and identification rightly fit this category. As mentioned in section 3.3, fractional order model can give a natural description of complex dynamic features, especially for distributed-parameter systems. On the contrary, the conventional integer order model can only describe lumped-parameter systems. For flexible structures expressed by integer order model, additional modal analysis is needed [23].

Adequate fractional order modeling could give us a reliable understanding of control plants before control design. At the same time, obtaining lower order fractional model for control plant, low order controllers could be designed. This implies the controlled system is more robust against noises and disturbances [8]. Finally, fractional order plant models naturally need fractional order controllers for more effective control [19].

4.4.2 Effective gain-phase tradeoff

In robust control, it is well-known that a good performance requires large loop gain in some frequency range, typically some low-frequency range $(0, \omega_l)$; while good robustness and good sensor noise rejection require small loop gain in some frequency range, typically some high-frequency range (ω_h, ∞).

The transition frequency range $(\omega_l,\ \omega_h)$ is crucial for robust control design. A "strong" transition will cause stability problem due to the possibility of negative relative stability margin, phase margin; while a "weak" transition will lead to poor robust performance against noises and disturbances since the loop gain in high-frequency range is relatively large. As shown in Fig. 17, adoption of fractional order controllers can easily obtain a smooth transition and give proper phase margin by using only one control parameter, the fractional order α.

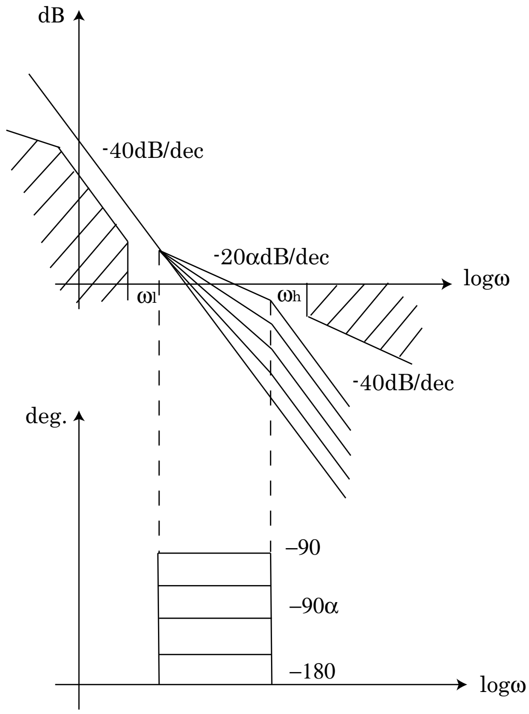

Figure 17: Smooth transition by adoption of fractional order controllers

It has been mentioned that the conventional IOC methods have undesirable phase-gain tradeoff at certain frequency. Mainly due to this reason, high-order controllers were designed. By introducing fractional order controllers, gain and phase can be shifted precisely and easily by any amount with less control parameters, mostly the fractional orders. Consider a unity-feedback system $G(s)$ with gain $K = 4$

$$G(s) = \frac{K}{s(s+1)(s+2)} \tag{104}$$

Obviously, the control system has poor relative stability due to the small phase margin (see Fig. 18(b)). This may cause robustness problem when uncertainties such as parameter variation occurs. For example, larger $K = 6$ will shift gain response upward and lead to zero phase margin.

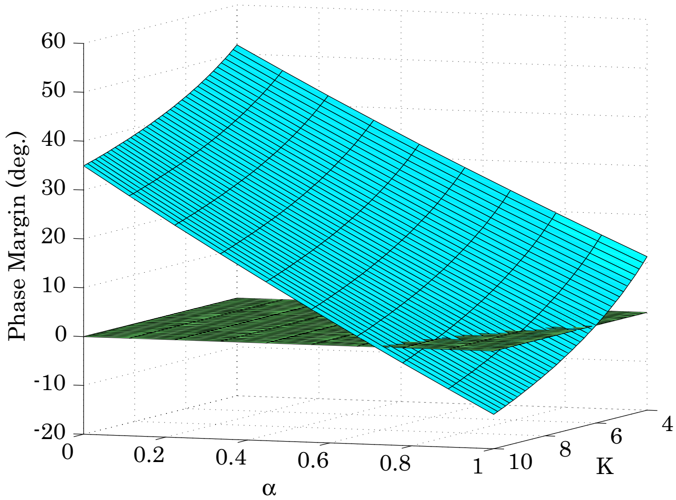

(a) The change of phase margin with α and K

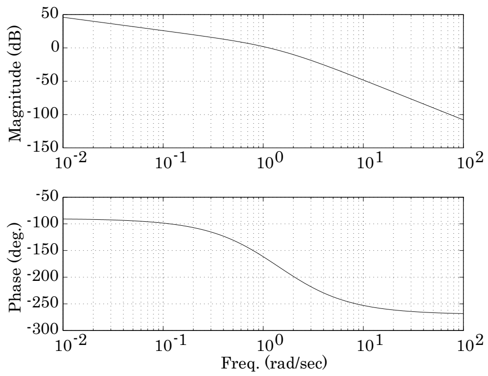

(b) Bode plots of $G(s)$ with integer α order (α=1 and K=4)

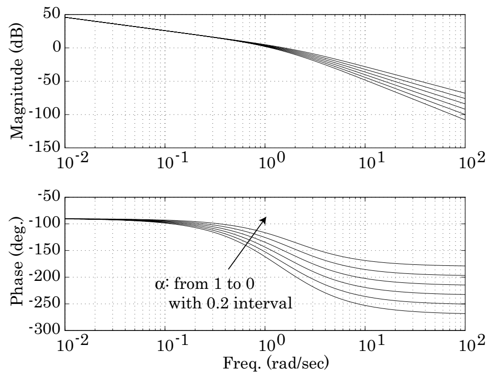

(c) Bode plots of $G(s)$ with fractional α order (K=4)

Figure 18: Gain-phase tradeoff with fractional α order

In order to improve the system's robustness with less gain loss, introducing fractional order low-pass filter $1/(s+1)^\alpha$ is an effective approach. The system's open-loop transfer function is now

$$G(s) = \frac{K}{s(s+1)^\alpha(s+2)} \tag{105}$$

where order α can be any real number from 1 to 0. As shown in Fig. 18(c), with proper fractional order α, the phase margin can be offset to any desired amount.

Fig. 18(a) plots the relationship among phase margin, α and K. Even taking K as 10, selecting α smaller than 0.6 can still give positive phase margin. With novel tuning knob α, the possibility of gain-phase tradeoff is greatly increased. It can been seen in Fig. 18(a) adjusting fractional order α is much more effective to obtain proper phase margin with less gain loss than changing gain K.

The advantage of FOC is not restricted to phase margin analysis. Consider the $M-\Delta$ loop shown in Fig. 19. From Small Gain Theorem [27], robust stability of the loop is assured with

(a) $\parallel \Delta \parallel_\infty \leq 1/\gamma$ *if and only if* $\parallel M(s) \parallel_\infty < \gamma$

(b) $\parallel \Delta \parallel_\infty < 1/\gamma$ *if and only if* $\parallel M(s) \parallel_\infty \leq \gamma$

where $\gamma > 0$.

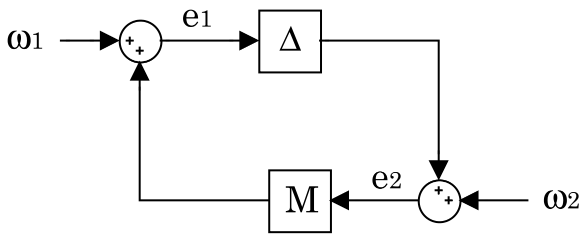

Figure 19: $M-\Delta$ loop for robust stability analysis

To illustrate FOC's advantage, let M be a low-pass filter but with fractional order:

$$M(s) = \frac{1}{(\tau s + 1)^\alpha} \tag{106}$$

and Δ be a time delay uncertainty, e^{-sT_d}, which is the only source of unmodeled dynamics:

$$\Delta(s) = e^{-sT_d} - 1 \tag{107}$$

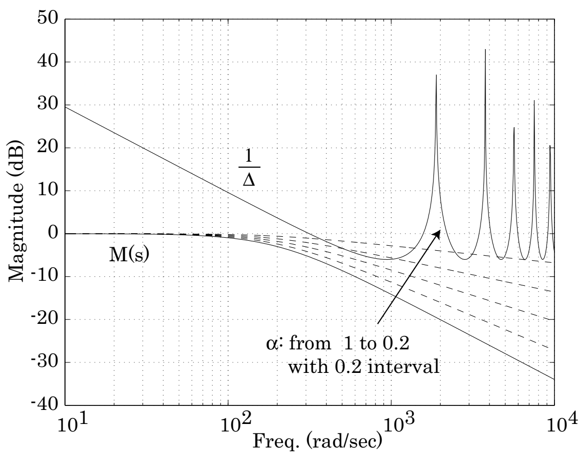

Figure 20: $M(s)$ with time delay uncertainty Δ ($T_d = 1/300$ and $\tau = 1/200$)

The magnitude plot of $1/\Delta$ and different α order $M(s)$ are shown in Fig. 20. For conventional integer order filter, 1 is the smallest order that can be taken. Clearly there is still room to recover some control performance. To do this, raising the filter's cut-off frequency or expanding nominal plant model to account for uncertainties can be choices. Large cut-off frequency will lead to worse noise rejection. And reflecting uncertainties in nominal plant model maybe too complicated in calculation to make this approach unattractive. Taking proper fractional order α, for example 0.8 and 0.6 in Fig. 20, can further and easily recover some control performance with less noise rejection loss. For low orders, 0.4 and 0.2, obviously the robust stability criteria is violated.

By introducing FOC concept, control system's performance can be further and easily adjusted between conventional IOC systems. The more effective gain-phase tradeoff of fractional order controllers implies FOC could be an effective and clear-cut design tool for real control applications.

4.4.3 Design method for FOC

Systematic design method for FOC still largely keeps being an open problem. Various methods have been reported for FOC design. A method based on pole distribution of the characteristic equation in complex plane was proposed [28]. Since it is more convenient to analyze FOC system in frequency domain, H_2, H_∞ and other optimal control methods were expanded to design FOC system [12][29][13]. However, the optimal algorithm might become very complicated due to the necessity of optimizing fractional orders. The cost-effectiveness of above optimal methods are questionable. To decrease the difficulty of optimization, Genetic Algorithm (GA) can be applied [30].

The author believes that the design and application of FOC should be clear-cut. Because FOC provides us a novel and powerful tool in control design, we should make full use of its power to solve complex control problems in a simpler and more straightforward way. It has been mentioned that FOC can further and easily improve the performance of IOC system designed by IOC methods. And for most control problems in motion control, integer order models may be not as adequate as fractional order model. But they can still provide a good description of control plant's dynamic features considering its simplicity.

Based on these considerations, the author designed FOC in a two-stage or hybrid approach: use IOC design method firstly and then improve the performance of designed control system by adding proper fractional order controller (see Fig. 21). Namely, design IOC system to give a good sense of direction and fine tune it's performance using novel FOC design method. This two-stage design could make the most of well developed IOC knowledge and novel FOC advantages. Therefore, a clear-cut and cost-effective design approach would be obtained. In below chapters, the control design issues will be mentioned in detail with theoretical analysis and experimental verifications.

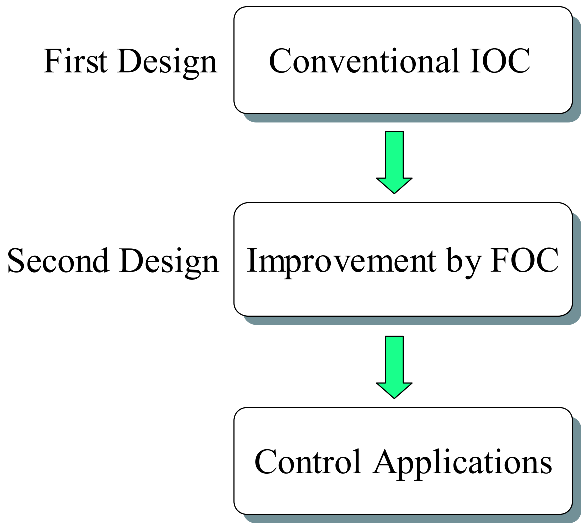

Figure 21: Illustration for the two-stage design approach

CHAPTER V

SAMPLING TIME SCALING PROPERTY

While FOC system's analysis and design in frequency domain are as convenient as conventional IOC systems due to the availability of existing graphical tools, in practice the performance of a control system is more realistically measured by its time-domain characteristics. At the same time, most modern control systems are controlled by digital controllers. It is well-known that continuous-data controllers such as PID controllers can be approximated digitally with clear time-domain interpretations. For example, the backward-difference rule for derivative controller means the change of sampled inputs between one sampling time period. The trapezoidal-integration rule approximates the area under the sampled inputs by a series of trapezoids. These clear time-domain interpretations significantly simplified their use in various control applications. Classical control theory was extremely well developed based on integer order differential equations.

On the contrary, for fractional order controllers, it was not so. Podlubny proposed a simple geometric interpretation of fractional integrals as "changing shadows on the wall (g_t, f)" and some pictures describing this changing were given [31]. However, since most modern controllers are realized by digital computers, clear interpretation of fractional order controllers in discrete domain should be much more concerned with practical importance. Especially insights in discrete fractional order controllers would be enlightening for the future development of FOC research.

5.1 Scaled Sampling Time

From the Riemann-Liouville definition, fractional order integral with order between 0 and 1 can be rewritten in following form

$$ {}_0D_t^{-\alpha} f(t) = \int_0^t f(\tau) dg_t(\tau), \ 0 < \alpha < 1 \tag{108}$$

where

$$g_t(\tau) = \frac{1}{\Gamma(1+\alpha)}[t^\alpha - (t-\tau)^\alpha] \tag{109}$$

Let $t := nT$, where T is sampling time and n is the step currently under execution, then

$$g_{nT}(kT) = \frac{n^\alpha - (n-k)^\alpha}{\Gamma(1+\alpha)} T^\alpha, \;\; k = 1, ..., n \tag{110}$$

Based on the same consideration of trapezoidal integration method, the constant sampling time T is adjusted to $T_n(k)$ for the kth step in discrete fractional order integral controller:

$$\begin{aligned} T_n(k) &= \Delta g_{nT}(kT) \\ &= g_{nT}(kT) - g_{nT}[(k-1)T] \\ &= \frac{(n-k+1)^\alpha - (n-k)^\alpha}{\Gamma(1+\alpha)} T^\alpha \end{aligned} \tag{111}$$

Thus

$$\begin{aligned} T_n(n) &= \frac{1^\alpha - 0^\alpha}{\Gamma(1+\alpha)} T^\alpha \\ T_n(n-1) &= \frac{2^\alpha - 1^\alpha}{\Gamma(1+\alpha)} T^\alpha \\ &\cdots \\ T_n(1) &= \frac{n^\alpha - (n-1)^\alpha}{\Gamma(1+\alpha)} T^\alpha \end{aligned} \tag{112}$$

Finally, the integral $\int_0^t f(\tau) dg_t(\tau)$ in Equ. (108) can approximated as a series of trapezoids with the scaled sampling time $T_n(k)$

$${}_0D_{nT}^{-\alpha} \approx \sum_{k=1}^{n} \frac{f(kT) + f[(k-1)T]}{2} T_n(k) \tag{113}$$

and if $T \to 0$, then

$${}_0D_{nT}^{-\alpha} = \sum_{k=1}^{n} \frac{f(kT) + f[(k-1)T]}{2} T_n(k) \tag{114}$$

From Equ. (112), the interpretation of discrete fractional order integrals is the "deformation" of their integer order counterparts by internal sampling time scaling. As shown in Fig. 22, with same sampled inputs $f(kT)$ as integer order integral, the scaled sampling time $T_n(k)$ leads to different characteristics of fractional order integral. Based on this sampling time scaled version of trapezoidal integration rule, it is easily to understand that the past inputs are “forgotten” gradually in discrete fractional order integral due to their scaled tiny sampling time while in integer order ones all the values are “remembered” with same weights. Therefore, a link to known classical trapezoidal-integration rule has been found, but with scaled sampling time in fractional order case.

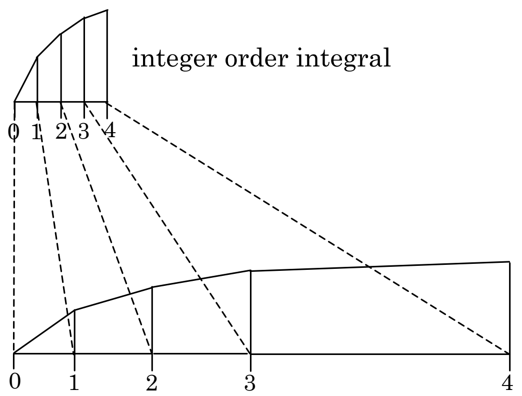

Figure 22: Trapezoidal-integration rules with the scaled sampling time

Similarly, discrete fractional order derivatives with order between 0 and 1 can also be written as

$$
\begin{aligned}
{}_0D_t^{\alpha} f(t) &= \frac{1}{\Gamma(1-\alpha)} \frac{d}{dt} \int_0^t \frac{f(\tau)}{(t-\tau)^{\alpha}} d\tau \\
&= \frac{d[\int_0^t f(\tau) dg_t^{'}(\tau)]}{dt}, \quad 0 < \alpha < 1 \qquad (115)
\end{aligned}
$$

where

$$
g_t^{'}(\tau) = \frac{1}{\Gamma(2-\alpha)} [t^{1-\alpha} - (t-\tau)^{1-\alpha}] \qquad (116)
$$

Therefore,

$$
\begin{aligned}
T_n^{'}(n) &= \frac{1^{1-\alpha} - 0^{1-\alpha}}{\Gamma(2-\alpha)} T^{1-\alpha} \\
T_n^{'}(n-1) &= \frac{2^{1-\alpha} - 1^{1-\alpha}}{\Gamma(2-\alpha)} T^{1-\alpha} \\
&\cdots \\
T_n^{'}(1) &= \frac{n^{1-\alpha} - (n-1)^{1-\alpha}}{\Gamma(2-\alpha)} T^{1-\alpha} \qquad (117)
\end{aligned}
$$

Again based on the trapezoidal integration rule, the integral $\int_0^t f(\tau)dg_t^{'}(\tau)$ in Equ. (115) can be also approximated as

$$\int_0^{nT} f(\tau)dg_t^{'}(\tau) \approx \sum_{k=1}^{n} \frac{f(kT) + f[(k-1)T]}{2} T_n^{'}(k) \tag{118}$$

and if $T \to 0$, then

$$\int_0^{nT} f(\tau)dg_t^{'}(\tau) = \sum_{k=1}^{n} \frac{f(kT) + f[(k-1)T]}{2} T_n^{'}(k) \tag{119}$$

The interpretation of discrete fractional order derivatives is the derivatives of fractional $(1-\alpha)$ order integrals $\int_0^{nT} f(\tau)dg_t^{'}(\tau)$. Namely, it can be understood geometrically as the changing ratio of the "scaled integral area" due to the scaled sampling time, as shown in the shadow area of Fig. 23.

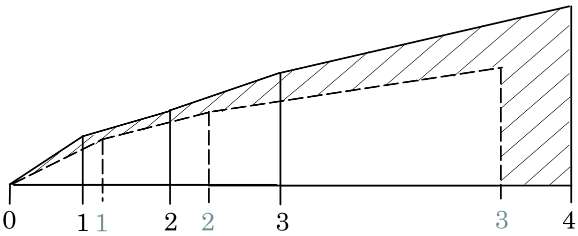

Figure 23: Changing of the "scaled integral area"

Clearly, when order α equals 1, the sampling time will not be scaled any more. From the viewpoint of sampling time scaling, in discrete domain FOC is also a natural generalization and interpolation of conventional integer order control.

5.2 *Control with Self-scaled Memory*

Viewing in terms of sampling time scaling can gain more insight into discrete FOC systems. The fractional order controllers are controllers with self-adjustable parameters and a mechanism for adjusting the parameters. As shown in Fig. 24, a fractional order controller can be considered conceptually as the series of a sampling time scaler and conventional integer order controller. Namely, the sampling time of input sequence is pre-adjusted by the sampling time scaler before entering integer order controller.

Therefore, fractional order control can be regarded as a special control strategy, which apply strong control action to latest sampled inputs by using "forgetting factors" $\lambda_n(k)$.

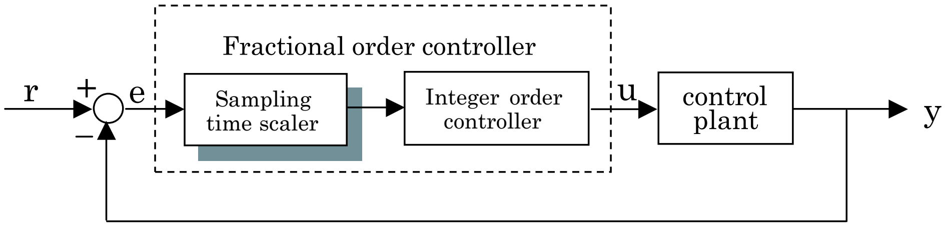

Figure 24: Sampling time scaler of FOC systems

Large scaled sampling time of latest values means small "forgetting factors" and vice versa. For example, the control law of a pure fractional order integral controller can be rewritten in "forgetting factor" form, where $\lambda_n(k)$ equals $2/T_n(k)$ in Equ. (112):

$$u(n) = \sum_{k=1}^{n} \frac{1}{\lambda_n(k)}[e(k) + e(k-1)] \tag{120}$$

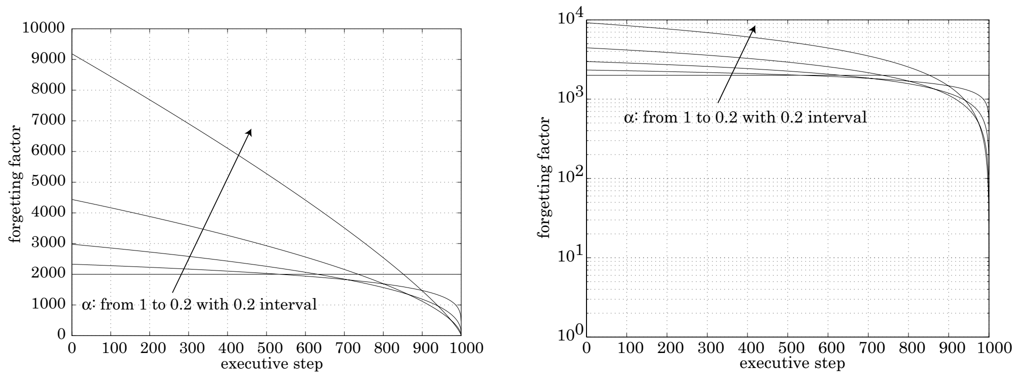

(a) Normal chart

(b) Semi-log chart

Figure 25: Plots of the forgetting factor $\lambda_n(s)$ (T=0.001sec)

It can be seen in Fig. 25 that in fractional order integral controllers the sampled inputs are memorized with time-scaled weights, while the integer order controllers give all the inputs same weights. More fractional order differs from the integer order 1, more obvious the sampling time scaling is. Fig. 25 shows discrete fractional order controllers memorize the latest inputs more strongly and also "forget" the old inputs more completely than conventional integer order controllers.

An adaptive controller can be defined as a controller with adjustable parameters and a mechanism for adjusting parameters [32]. The adaptive controller modifies its parameters in response to changes in the dynamics of the control plant. Due to the parameter adjustment mechanism, the adaptive control system becomes nonlinear, which is difficult to analyze. For fractional order controller, the internal sampling time is adjusted by the sampling time scaling mechanism. However, this adjustment is not in response to outer changes and the control system keeps being linear, which means the wealth of analysis tools can still be used. The rapidly fading influences of the old inputs and dominance of the latest ones make fractional order controllers "passively adaptive" to the changes of the control plant. This distinct characteristic could also be a time-domain explanation for FOC system's robustness against various uncertainties.

5.3 Realization by Sampling Time Scaling

It is common knowledge that fractional order systems have an infinite dimension while integer order systems are finite dimensional. Discretization of fractional order controller by the time-scaled trapezoidal integration rule is not an exception. Proper approximation by finite difference equation is needed to realize fractional order controller.

Based on the observation that the scaled sampling time near "starting point" t_0 is small enough to be "forgotten" for large t (see Fig. 26), a novel realization method is proposed to take into account only the behavior of $f(t)$ in "recent past", i.e. in the interval $[t-L, t]$, where L is the length of "memory":

$$ {}_{t_0}D_t^k f(t) \approx {}_{t-L} D_t^k f(t), \;\; t > t_0 + L \tag{121} $$

Therefore this realization method can be considered as a kind of "short memory principle" approach but based on the Riemann-Liouville definition [7].

From Equation (113) and Equation (118), it is easy to give the discrete equivalent of fractional α order integral or derivative controllers as follows:

$$ Z\{D^\alpha[x(t)]\} \approx \frac{1}{T^\alpha} \sum_{j=0}^{[L/T]} c_j z^{-j} \tag{122} $$

For integral controllers ($\alpha < 0$), coefficients c_j are

$$ c_0 \;\; = \;\; \frac{1}{2\Gamma(1+|\alpha|)} $$

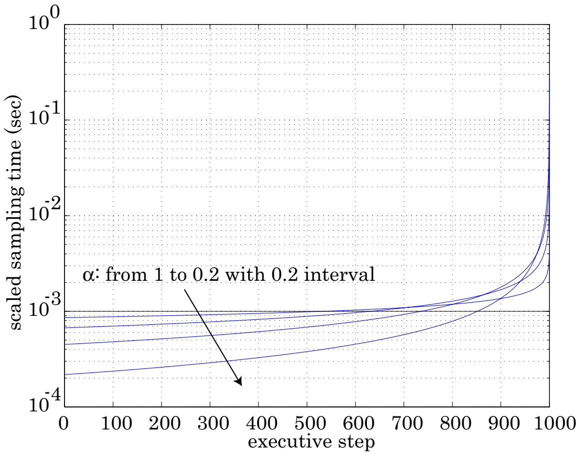

Figure 26: Discrete I^α controller's scaled sampling time ($T = 0.001sec$)

$$c_j = \frac{(j+1)^{|\alpha|} - (j-1)^{|\alpha|}}{2\Gamma(1+|\alpha|)}, \; j \geq 1 \tag{123}$$

And the coefficients of derivative controllers ($\alpha > 0$) are a little more complicated:

$$\begin{aligned} c_0 &= \frac{1}{2\Gamma(2-\alpha)} \\ c_1 &= \frac{2^{1-\alpha}-1}{2\Gamma(2-\alpha)} \\ c_j &= \frac{1}{2\Gamma(2-\alpha)}\Big[(j+1)^{1-\alpha} - j^{1-\alpha} \\ &- (j-1)^{1-\alpha} + (j-2)^{1-\alpha}\Big], \; j \geq 2 \end{aligned} \tag{124}$$

Figure 27 shows the Bode plot of discrete $Z\{1/s^{0.5}\}$ controller for sampling time $T = 0.001sec$ realized by different [L/T] (solid line) compared with the ideal case of continuous controller $1/s^{0.5}$ (dash line). Clearly, in order to have a better approximation in discrete domain, shorter sampling time and larger $[L/T]$ (memory length) are preferable.

5.4 Example: One-mass Position Control

In order to verify the sampling time scaling property of discrete fractional order controllers, one-mass position control is used as a simple prototype, where $J_m = 0.001kgm^2$, $K_d = 0.1$ and a torque limitation of $\pm 5NM$ is introduced (see Fig. 28). Sampling time T is taken as $0.001sec$. Time responses with fractional order derivative controllers D^α are simulated using the above realization method with full memory length. Namely, all the past sampled inputs

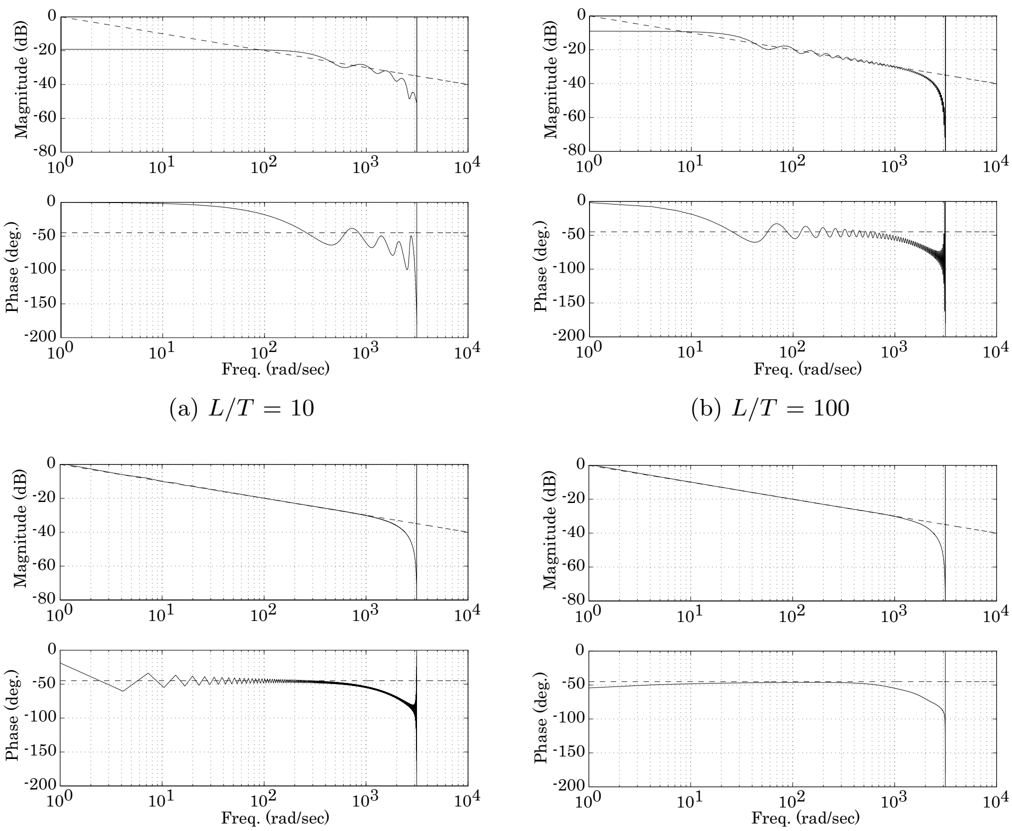

(a) $L/T = 10$ (b) $L/T = 100$

(c) $L/T = 1000$ (d) $L/T = 10000$

Figure 27: Bode plots of $Z(1/s^{0.5})$ with different memory length L/T (solid line: approximation cases; dashed line: ideal case)

e during the simulation will be memorized. The integer order D^1 controller is discreted by the backward-difference rule:

$$Z\left\{ \left.\frac{df(t)}{dt}\right|_{t=kT} \right\} = Z\left\{ \frac{1}{T}\left(f(kT) - f[(k-1)T]\right) \right\} = \frac{z-1}{Tz}F(z) \tag{125}$$

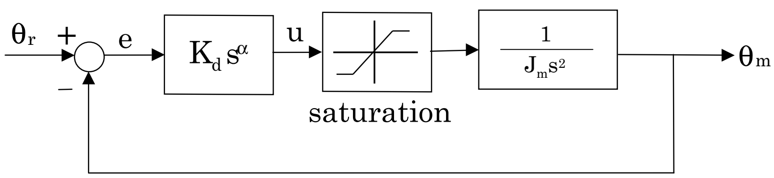

Figure 28: The one-mass position control loop

The time responses with different α order derivative controllers are shown in Fig. 29. Obviously, the FOC systems are much more robust than conventional IOC systems. The system with D^1 controller has the best time response when torque saturation does not exist (see Fig. 29(a)). However, as shown in Fig. 29(b), its robustness against torque saturation is very poor and the time response is totally no good. On the contrary, the control systems with fractional order D^α controllers display much better robustness. Among them, $D^{0.4}$ controller has the best robust performance.

The comparisons of the integer order and fractional order derivative controllers are shown in Fig. 30 and Table. 2. Obviously, the self-scaled sampling time gives fractional order D^α controllers an intermediate and different characteristic among conventional integer order D controllers. The mechanism of sampling time scaling property could give a qualitative analysis for FOC's robustness.

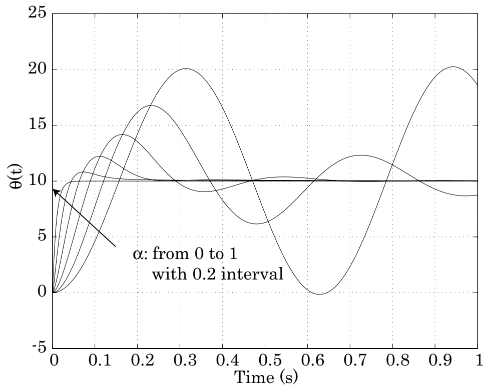

(a) without saturation

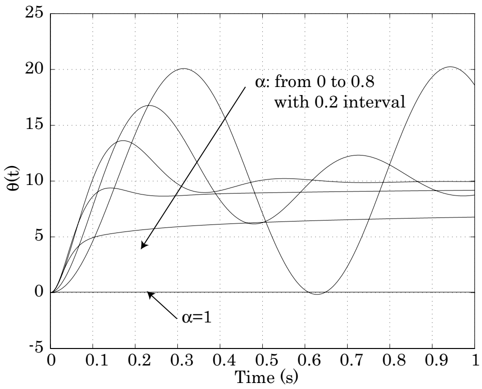

(b) with saturation

Figure 29: Time responses $\theta_m(t)$ with D^α controllers

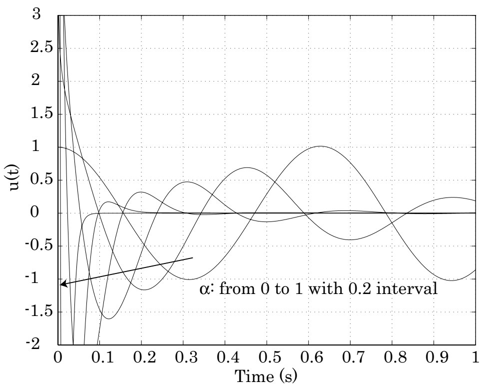

(a) without saturation

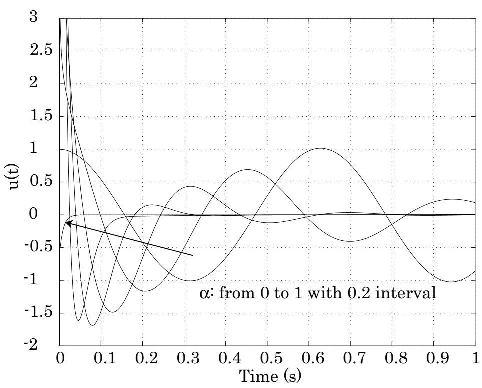

(b) with saturation

Figure 30: Plots of D^α controllers' output $u(t)$

	$\mathbf{D^0}$	$\mathbf{D^\alpha}$	$\mathbf{D^1}$
Inputs Memorized	Newest one	Whole	Newest two
Forgetting Factor	1	Scaled	$\pm T$
Control Action	Weak	Middle and Scaled	Strong
Robustness	-	Good	Poor

Table 2: The comparison of integer order D controllers and fractional order D$^\alpha$ controllers $(0 < \alpha < 1)$ based on the one-mass position control example

Just like conventional integer order control, to give a quantitative analysis in time domain is quite difficult. It is often convenient and with more valuable information to analyze fractional order control system in frequency domain. For stability analysis, Fig. 11 in chapter 4 can be referred. The D$^\alpha$ controllers' robustness could be understood as keeping proper phase margin between 0 and 90 degree. Therefore, a better tradeoff between stability and robustness can be easily obtained. The "in-between" characteristic of D$^\alpha$ control's time responses could be analyzed by their close-loop frequency-domain specifications, as shown in Fig. 31 and Table. 3.

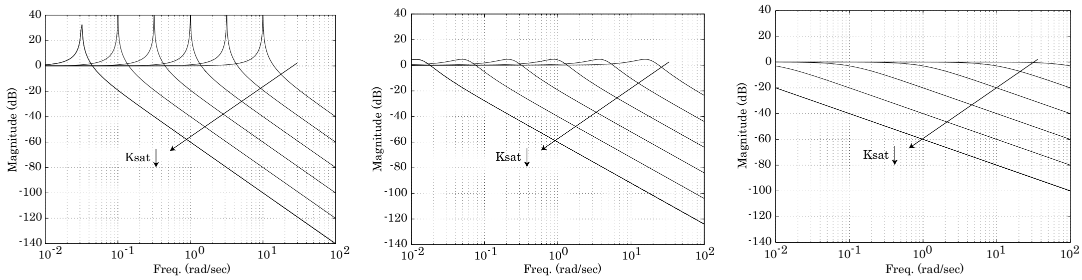

(a) D^0 (b) $D^{0.4}$ (c) D^1

Figure 31: Close-loop gain plots with D$^\alpha$ controllers (saturation is consider as a gain variation K_{sat} reduced from 1 to 0.00001)

	$\mathbf{D^0}$	$\mathbf{D^\alpha}$	$\mathbf{D^1}$
Resonant Peak M_r	Large	Intermediate	Small
Bandwidth BW	Small	Intermediate	Large
Change of BW	Small	Intermediate	Large
Cut-off Rate	Large	Intermediate	Small

Table 3: The comparison of frequency-domain specifications based on Fig. 31

CHAPTER VI

REALIZATION METHODS

Though it is not difficult to understand the theoretical advantages of FOC, especially in frequency domain, realization issue kept being somewhat problematic and perhaps was one of the most doubtful points for the application of FOC. As shown in the Riemann-Liouville definition, fractional order systems have an infinite dimension; while the conventional integer order systems are finite dimension. To realize fractional order controllers perfectly, all the past inputs should be memorized. It is impossible in real applications. Proper approximation by finite differential or difference equation must be introduced.

Frequency-band fractional order controller can be realized by broken line approximation in frequency domain. But further discretization is required for this method [33]. As to direct discretization, various methods have been proposed such as Sampling Time Scaling, Short Memory Principle [7], Tustin Taylor Expansion [34], Lagrange Function Interpolation method [9], while all the approximation methods need truncation of the expansion series.

6.1 Frequency-band Approximation

6.1.1 Frequency-band fractional order controller

Since fractional order system's frequency responses can be exactly known, approximating fractional order controllers by frequency-domain approaches is natural. At the same time, it is neither practicable nor desirable to try to make the order be fractional in whole frequency range. The frequency-band fractional order controllers are required and practical in most control applications. The broken-line approximation method can introduced to realize frequency-band fractional order I$^\alpha$ controller. Let

$$\left(\frac{\frac{s}{\omega_h}+1}{\frac{s}{\omega_b}+1}\right)^\alpha \approx \prod_{i=0}^{N-1} \frac{\frac{s}{\omega_i'}+1}{\frac{s}{\omega_i}+1} \tag{126}$$

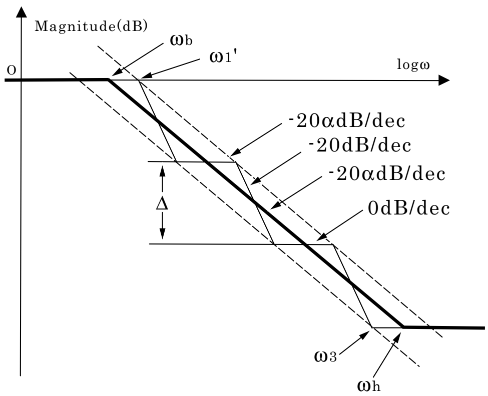

Figure 32: An example of broken-line approximation ($N = 3$)

Based on Fig. 32, two recursive factors ζ and η are introduced to calculate ω_i and $\omega_i^{'}$:

$$\zeta = \frac{\omega_i^{'}}{\omega_i},\ \eta = \frac{\omega_{i+1}}{\omega_i^{'}} \tag{127}$$

Since

$$\omega_0 = \eta^{\frac{1}{2}}\omega_b,\ \omega_{N-1}^{'} = \eta^{-\frac{1}{2}}\omega_h \tag{128}$$

Therefore

$$\zeta\eta = \left(\frac{\omega_h}{\omega_b}\right)^{\frac{1}{N}} \tag{129}$$

with

$$\omega_i = (\zeta\eta)^i\omega_0,\ \omega_i^{'} = \zeta(\zeta\eta)^i\omega_0 \tag{130}$$

The frequency-band fractional order controller has $-20\alpha dB/dec$ gain slope, while the integer order factors $1\Big/(\frac{s}{\omega_i^{'}}+1)$ have $-20dB/dec$ slope. For the same magnitude change Δ:

$$-20\alpha = \frac{\Delta}{log\zeta + log\eta},\ -20 = \frac{\Delta}{log\zeta} \tag{131}$$

Thus

$$(\zeta\eta)^\alpha = \zeta \tag{132}$$

Therefore ζ and η can be expressed respectively by

$$\zeta = \left(\frac{\omega_h}{\omega_b}\right)^{\frac{\alpha}{N}},\ \eta = \left(\frac{\omega_h}{\omega_b}\right)^{\frac{1-\alpha}{N}} \tag{133}$$

Finally

$$\omega_i = \left(\frac{\omega_h}{\omega_b}\right)^{\frac{i+\frac{1}{2}-\frac{\alpha}{2}}{N}}\omega_b,\ \omega_i^{'} = \left(\frac{\omega_h}{\omega_b}\right)^{\frac{i+\frac{1}{2}+\frac{\alpha}{2}}{N}}\omega_b \tag{134}$$

Figure. 33 shows the Bode plots of ideal frequency-band case ($\alpha = 0.4,\ \omega_b = 200Hz,\ \omega_h = 10000Hz$) and its 1st-order, 2nd-order and 3rd-order approximations by broken-line approximation method. Even taking $N = 2$ can give a satisfactory accuracy in frequency domain.

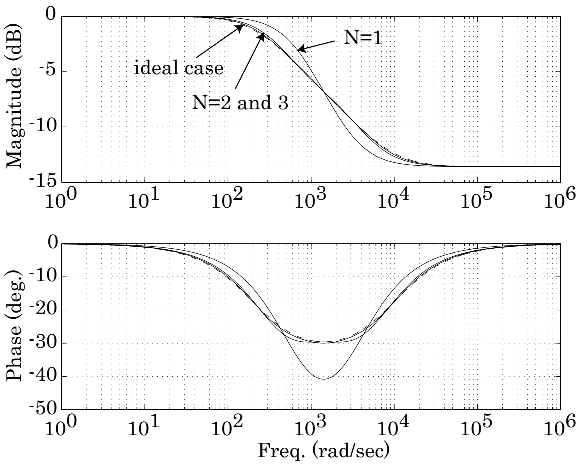

Figure 33: Bode plots of ideal case, 1st, 2nd and 3rd-order approximations

6.1.2 Digital implementation

The approximate controllers can be discreted using bilinear transformation method. For example, the 2nd-order approximation of fractional -0.4 order controller in frequency range $[200,\ 10000]$ is

$$\frac{0.2091(s+786.4471)(s+5561.0205)}{(s+359.6462)(s+2543.0828)} \tag{135}$$

Its digital implementation by bilinear transformation is

$$\frac{0.4110z^2+0.0146z-0.0843}{z^2-0.5756z-0.0831} \tag{136}$$

The Bode plots of the 2nd broken-line approximation and its digital implementation with sampling time $T = 0.001sec$ are shown in Fig. 34. The vertical line in the discrete-time Bode plots is located at the Nyquist frequency, which equals π/T (rad/sec).

6.2 Direct Discretization

Standard discrete control system is shown in Fig. 35. For simplification, the controller K_d is discrete fractional α order derivative $(0 < \alpha < 1)$ or integral $(-1 < \alpha < 0)$.

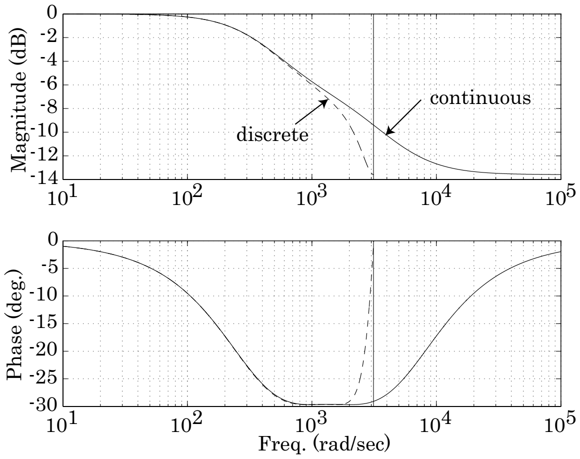

Figure 34: The Bode plots of the 2nd broken-line approximation and its digital implementation (sampling time T is 0.001sec)

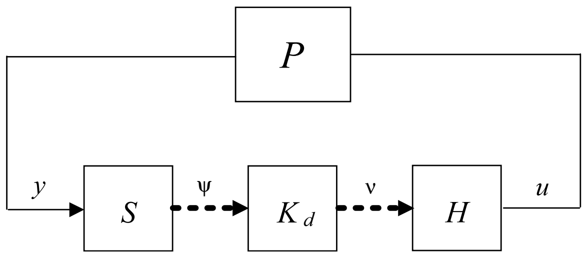

Figure 35: Block diagram of digital control system

6.2.1 Short memory principle

The discretization method is based on the observation that for the Grünwald-Letnikov definition, the values of the binomial coefficients near "starting point" $t = 0$ are small enough to be neglected or "forgotten" for large t. Therefore the principle takes into account the behavior of $x(t)$ only in "recent past", i.e., in the interval $[t - L,\ t]$, where L is the length of "memory":

$$ {}_0D_t^{\alpha} x(t) \approx {}_{t-L} D_t^{\alpha} x(t), \quad (t > L) \tag{137}$$

Based on approximation of the time increment h through the sampling time T, the discrete equivalent of the fractional order α derivative is given by

$$ Z\{D^{\alpha}[x(t)]\} \approx \left(\frac{1}{T^{\alpha}} \sum_{j=0}^{m} c_j z^{-j} \right) X(z) \tag{138}$$

where $m = [L/T]$ and the coefficients c_j are

$$\begin{aligned} c_0 &= 1, \\ c_j &= (-1)^j \begin{pmatrix} \alpha \\ j \end{pmatrix} = \frac{j-\alpha-1}{j} \cdot c^{\alpha}_{j-1}, \quad j \leq 1 \end{aligned} \tag{139}$$

6.2.2 Tustin taylor expansion

The direct discretization can also be obtained by using the well-known Tustin operator or trapezoidal rule as a generation function:

$$Z\{D^{\alpha}[x(t)]\} \approx \left(\frac{2}{T}\frac{1-z^{-1}}{1+z^{-1}}\right)^{\alpha} X(z) \tag{140}$$

Taylor expansion of the fractional α order Tustin operator gives

$$\left(\frac{2}{T}\frac{1-z^{-1}}{1+z^{-1}}\right)^{\alpha} = \frac{1}{T^{\alpha}}\sum_{j=0}^{\infty} c_j z^{-j} \tag{141}$$

Here the coefficients c_j are

$$c_j = \frac{2^{\alpha}}{j!}\left[\left(\frac{1-x}{1+x}\right)^{\alpha}\right]^{(j)}\Bigg|_{x=0} \tag{142}$$

Real implementation of Equ. (140) corresponds to m-term truncated series given by

$$\begin{aligned} Z\{D^{\alpha}[x(t)]\} &\approx Trunc_m\left[\left(\frac{2}{T}\frac{1-z^{-1}}{1+z^{-1}}\right)^{\alpha}\right] X(z) \\ &= \left(\frac{1}{T^{\alpha}}\sum_{j=0}^{m} c_j z^{-j}\right) X(z) \end{aligned} \tag{143}$$

6.2.3 Lagrange function interpolation

For example, quadratic Lagrange interpolation among $x(k-2)$, $x(k-1)$ and $x(k)$ in the interval $0 \leq t \leq 2T$ results

$$\begin{aligned} x(t) &= \frac{x(k)-2x(k-1)+x(k-2)}{2}\left(\frac{t}{T}\right)^2 \\ &- \frac{x(k)-4x(k-1)+3x(k-2)}{2}\frac{t}{T} \\ &+ x(k-2) \end{aligned} \tag{144}$$

The α order derivative of t^n is [1]

$${}_0D^{\alpha}_t(t^n) = \frac{n!t^{n-\alpha}}{\Gamma(n-\alpha+1)} \tag{145}$$

Therefore, for $t = 2T$ the α order derivative of $x(t)$ is

$$\begin{aligned} D^{\alpha}x(t)|_{t=2T} &= \frac{1}{T^{\alpha}} \cdot \frac{1}{2^{\alpha}\Gamma(3-\alpha)} \big[(2+\alpha)\cdot x(k) \\ &- 4\alpha \cdot x(k-1) + \alpha^2 \cdot x(k-2)\big] \end{aligned} \tag{146}$$

The z-transformation is

$$\begin{aligned} Z\{D^{\alpha}x(t)\} &= \frac{1}{T^{\alpha}} \cdot \frac{1}{2^{\alpha}\Gamma(3-\alpha)} [(2+\alpha) - 4\alpha z^{-1} \\ &+ \alpha^2 z^{-2}]X(z) \end{aligned} \tag{147}$$

Therefore, the m-order Lagrange Function Interpolation method can also be rewritten in the form:

$$Z\{D^{\alpha}[x(t)]\} \approx \left(\frac{1}{T^{\alpha}} \sum_{j=0}^{m} c_j z^{-j} \right) X(z) \tag{148}$$

6.3 Evaluation of Direct Discretization Methods

For comparison purpose, the one-mass position control is introduced again as a simple prototype for the case of $J_m = 0.001$ and $K_d = 0.01$ (see Fig. 36). Time responses with fractional order derivative controllers D^{α} are simulated and evaluated. The D^{α} controllers are discretized by using the above direct discretization methods.

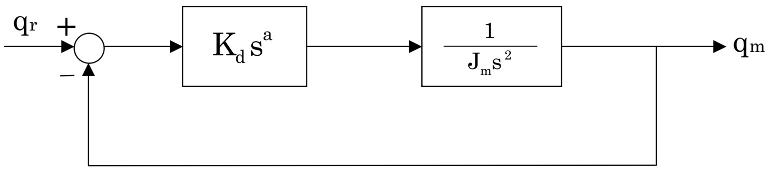

Figure 36: The position control loop with fractional α order derivative controller

Those methods' convergences must be analyzed before applying them to control implementation. The semi-log chart of Fig. 37 shows the amplitude absolute values of the coefficients $|c_j|$ versus term order j when approximating $\alpha = 0.4$ derivative. Short Memory Principle (SMP) and Sampling Time Scaling (STS) methods should have similar approximation performances, while the SMP's coefficients converge a little more rapidly than the STS's. The poor convergences of Tustin Taylor Expansion (TTE) and Lagrange Function Interpolation (LFI) methods seem problematic (see Fig. 37a and Fig. 37b).

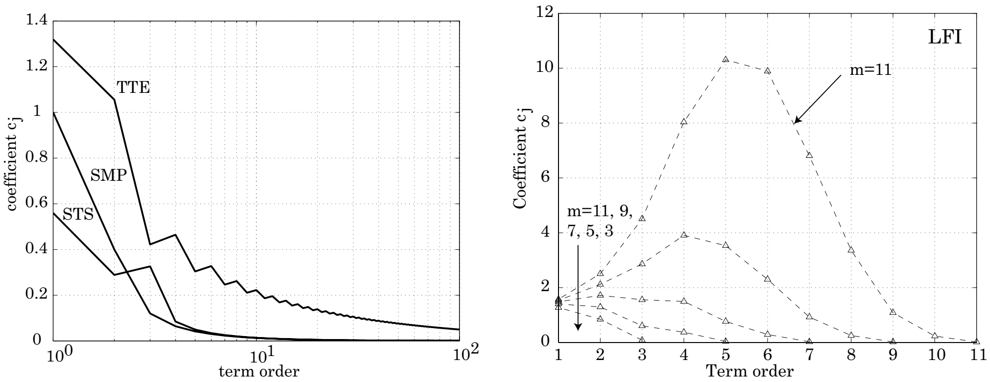

(a) SMP, STS and TTE methods (b) LFI method

Figure 37: $|c_j|$ versus j when approximating $\mathrm{D}^{0.4}$

6.3.1 Baseline establishment

In order to evaluate the discretization methods in time domain, a reliable baseline case must be established in advance. For simulation of FOC systems, using the truncated Grünwald-Letnikov expansion (Short Memory principle)[19], Mittag-Leffler function [19], Bromwich's integral with a numerical integration and B-spline series expansion [35] can be options. However those methods are either too abstract or too complicated for engineering applications. To simulate FOC systems with non-linear factors is also difficult.

As mentioned in chapter 5, the sampling time-scaled trapezoidal integration rule for discrete fractional order controllers can give a clear geometric interpretation and thus be a reliable simulation method. For a reasonable baseline, the whole past values will be memorized when simulating by STS method:

$$Z\{D^{\alpha}[x(t)]\} \approx \left(\frac{1}{T^{\alpha}} \sum_{j=0}^{\infty} c_j z^{-j} \right) X(z) \tag{149}$$

For integral controllers ($\alpha < 0$), coefficients c_j are

$$\begin{aligned} c_0 &= \frac{1}{2\Gamma(1+|\alpha|)} \\ c_j &= \frac{(j+1)^{|\alpha|} - (j-1)^{|\alpha|}}{2\Gamma(1+|\alpha|)}, \quad j \geq 1 \end{aligned} \tag{150}$$

And the coefficients of derivative controllers ($\alpha > 0$) are

$$c_0 = \frac{1}{2\Gamma(2-\alpha)}$$

$$
\begin{aligned}
c_1 &= \frac{2^{1-\alpha}-1}{2\Gamma(2-\alpha)} \\
c_j &= \frac{1}{2\Gamma(2-\alpha)}\Big[(j+1)^{1-\alpha} - j^{1-\alpha} \\
&- (j-1)^{1-\alpha} - (j-2)^{1-\alpha}\Big], \quad j \geq 2
\end{aligned} \tag{151}
$$

From above equations, it can be seen that the full memory length STS method would be a clear and easy way to establish baseline case. And the algorithm can be conveniently combined with other components such as non-linear factors during the simulation.

6.3.2 TTE and LFI methods

The simulations of TTE and LFI methods verify the convergence analysis. As shown in Fig. 38(a) with approximation order $m = 5$, the TTE method results poor performance. Actually the fractional order controllers realized by high order TTE methods can make control systems unstable; while higher the order better the approximation should be achieved. The time responses of LFI method for $D^{0.4}$ controller are also unsatisfied (see Fig. 38(b)). In addition, the programming complexity of calculating high order Lagrange interpolation and Tustin operator's high order derivative makes the two methods inferior to control applications.

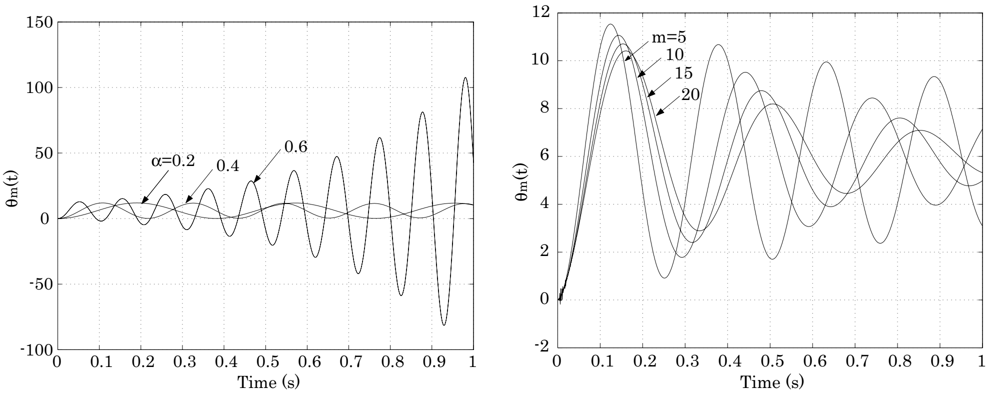

(a) TTE method

(b) LFI method

Figure 38: Time responses of TTE and LFI methods

6.3.3 SMP and STS methods

In order to investigate the influence of the memory length in SMP and TST methods, a quadratic performance index J is defined in an error function form:

$$J = \int_0^t [f_a(t) - f_b(t)]^2 \, dt \tag{152}$$

with $t(= 1sec)$ simulation time, $f_a(t)$ time responses of the two approximation cases, $f_b(t)$ the baseline time response. The baseline case is calculated by full memory length STS method. Fig. 39 shows performance index J versus memory length $n(\geq 5)$, in which the fractional order α is from 0.8 to 0.2 with 0.2 interval.

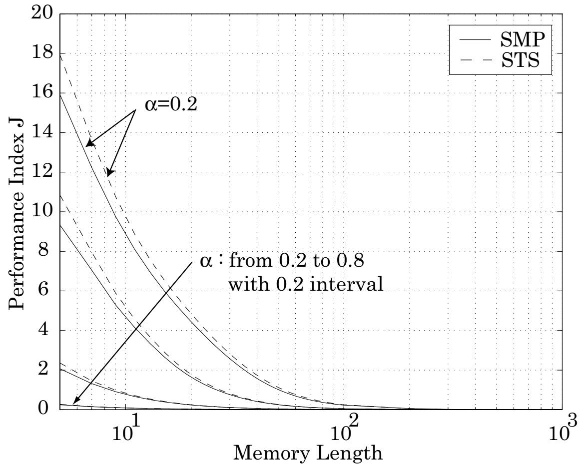

Figure 39: Performance index versus memory length

The four quantities of the step responses, maximum overshoot, delay time, rise time and settling time, are calculated for both methods. For clearness, only $\alpha = 0.4$ case is plotted in Fig. 40.

As shown in Fig. 39 and Fig. 40, clearly the approximation performance is remarkably improved when increasing the memory length from 10 to 100. Between 100 and 1000 memory length, the performance improvement is just slight; while hardware burden increases due to the necessity of storing and processing more data in short time. The step response's quantities plotted in Fig. 40 also show the same observation result.

The SMP method has a slightly better approximation than the STS method. The programming of SMP method is also much easier in which c_j can be calculated by simply

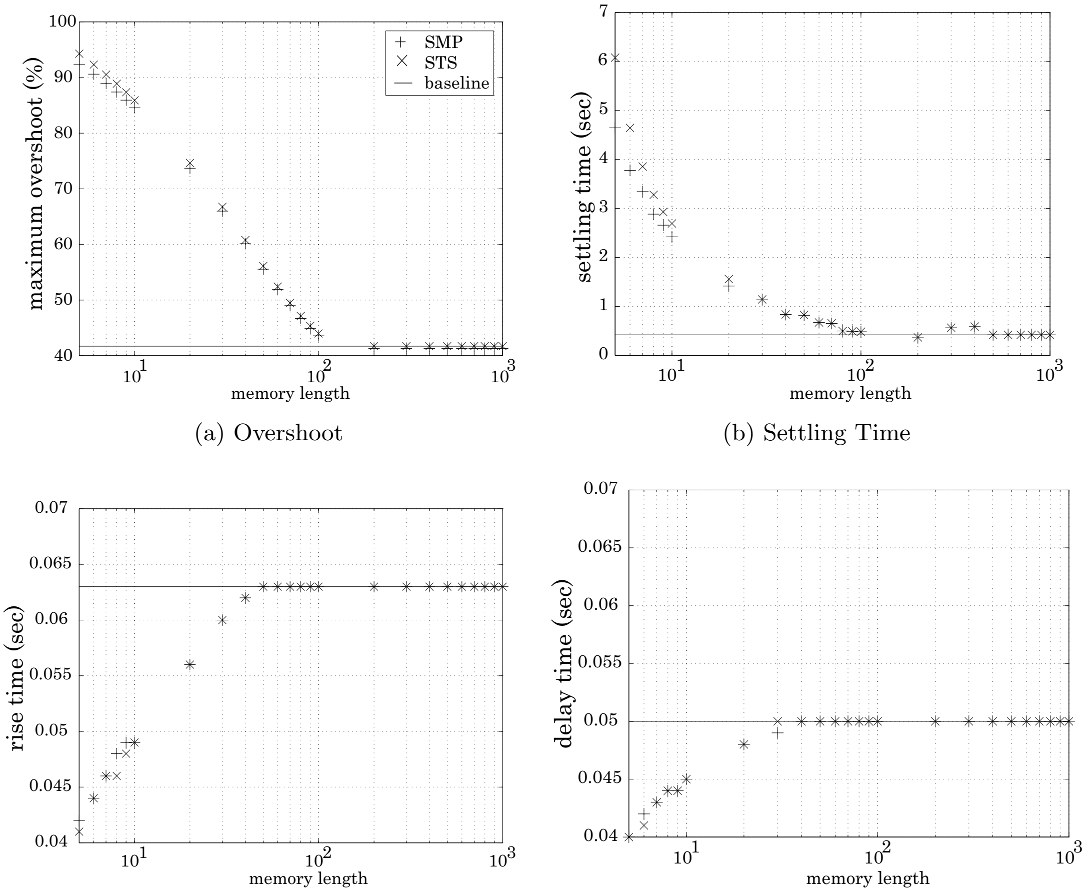

(a) Overshoot

(b) Settling Time

(c) Rise Time

(d) Delay Time

Figure 40: Time responses' four quantities

multiplying c_{j-1} and $(j-\alpha-1)/j$ together, as shown in Equ. (139). The SMP method is practically superior. Taking 100 memory length can have a good approximation in most cases (see Fig. 41). With highly-developed computational power, processing 100 sampling data with simple algorithm should not be problematic in mili-second level for modern digital control systems.

Fig. 42 verifies that the well-approximated fractional order $\mathrm{D}^{0.4}$ controllers are remarkably robust against saturation non-linearity. It was found that the fractional order controllers, like PID^{α} controller, are robust against other non-linearities such as gear backlash. This aspects will be mentioned in below chapters.

The digital implementation of $\mathrm{D}^{0.4}$ for SMP and STS methods are:

$$Z_{(SMP)}\{s^{0.4}\} \;=\; 15.8489 - 6.3396z^{-1} - 1.9019z^{-2} - 1.0143z^{-3} - 0.6593z^{-4} - 0.4747z^{-5}$$

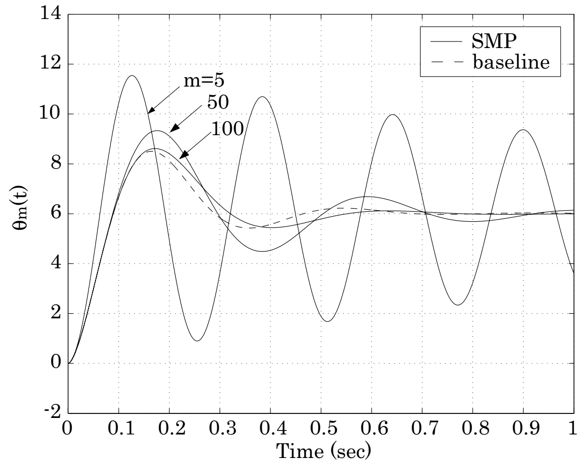

Figure 41: Time responses with different memory lengths ($\alpha = 0.4$)

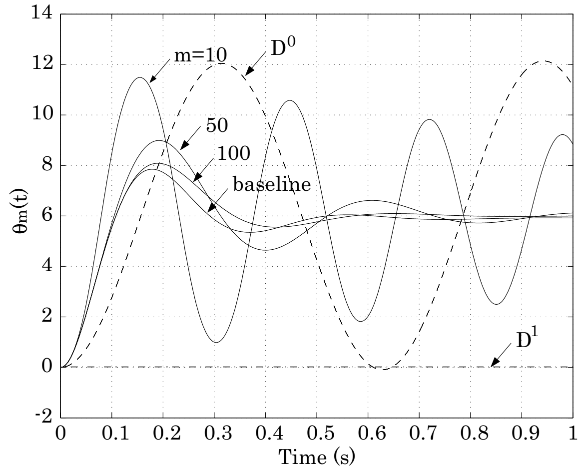

Figure 42: Robustness of approximated $\mathrm{D}^{0.4}$ controller against saturation non-linearity (dash lines are the time responses with integer 1 and 0 order D^{α} controllers)

$$- \quad 0.3639z^{-6} - 0.2912z^{-7} - 0.2402z^{-8} - 0.2028z^{-9} \tag{153}$$

$$\begin{aligned} Z_{(STS)}\{s^{0.4}\} &= 8.8689 + 4.5738z^{-1} - 5.1664z^{-2} - 1.3436z^{-3} - 0.7834z^{-4} - 0.5373z^{-5} \\ &- 0.4008z^{-6} - 0.3150z^{-7} - 0.2567z^{-8} - 0.2149z^{-9} \end{aligned} \tag{154}$$

where $m = 10$ and $T = 0.001sec$.

It must be pointed out that the necessary memory length, namely how good the approximation is needed, should be decided by the demand of specific control problem. Larger memory gives better performance, but also leads to longer computation time. This tradeoff is not restricted in FOC field, but actually a common problem in digital control.

6.3.4 Frequency responses of SMP and STS methods

The above direct discrete methods are based on different approaches, mathematical definition for SMP, simple Taylor expansion for TTE and geometric interpretation for STS and LFI. In order to verify the conclusion drawn in time domain, the Bode plots of $D^{0.4}$ controller discreted by STS and SMP methods are plotted and examined in Fig. 43.

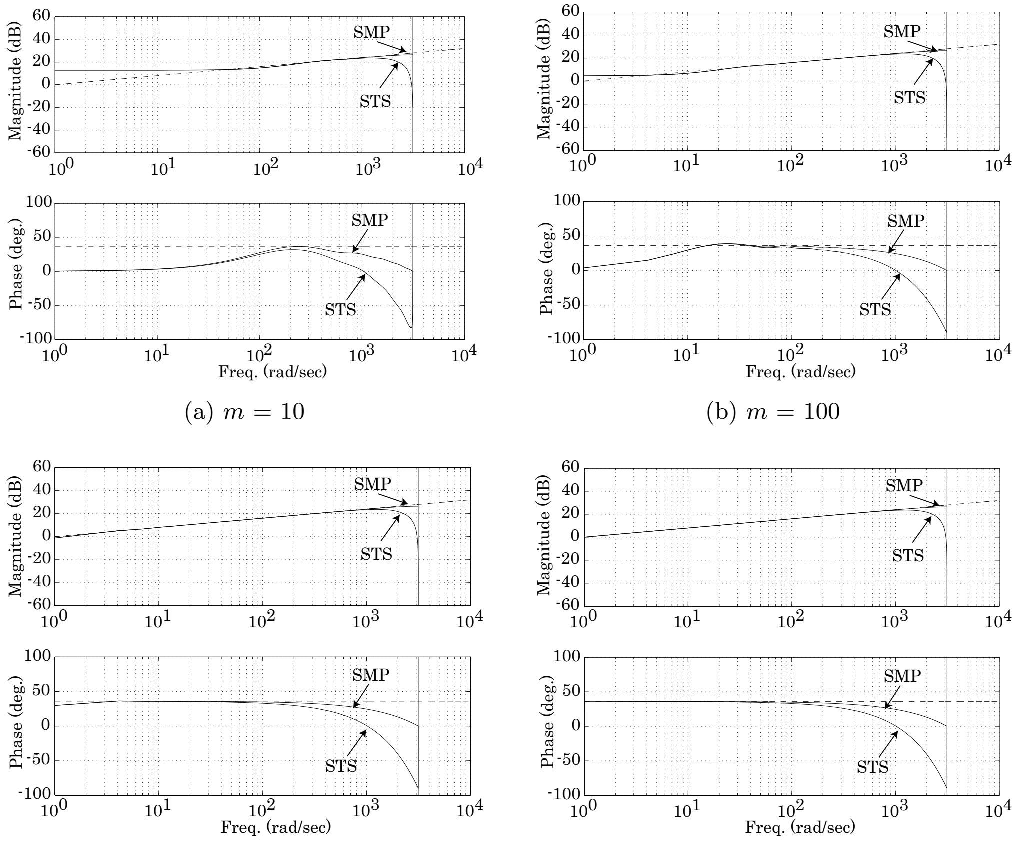

(a) $m = 10$ (b) $m = 100$

(c) $m = 1000$ (d) $m = 10000$

Figure 43: Bode plots of $Z\{s^{0.4}\}$ discreted by SMP and STS methods (dash line is the ideal responses for continuous $s^{0.4}$ and sampling time $T = 0.001sec$)

The above Bode plots show the effectiveness of the SMP and STS approximations for fitting the ideal responses in a wide range of frequency, especially in magnitude characteristic. SMP gives a better approximation than STS both in magnitude and phase, which is consistent with the conclusion obtained in time-domain evaluation. The accuracy of the approximations is greatly improved when increase memory length m from 10 to 100. And obviously, longer the memory length is taken, better the approximation will be.

CHAPTER VII

FRACTIONAL ORDER PI$^\alpha$D$^\beta$ CONTROL

7.1 Review of PID Control

The PID controller is by far the most dominating form of feedback control in use today. More than 90% of all control loops are PID. Integral, proportional and derivative feedback is based on the past(I), present(P) and future(D) control error. The PID controller is applied for a wide range of problems: process control, motor drives, magnetic and optic memories, automotive, flight control, instrumentation, etc. PID is the first solution that should be tried when feedback is used.

The transfer function of the PID controller is written as

$$G_c(s) = K_p + \frac{K_i}{s} + K_d s = (1 + K_{d1} s)\left(K_{p2} + \frac{K_{i2}}{s}\right) \tag{155}$$

Namely, the PID controller actually consists of a PD portion connected in cascade with a PI portion. The PD controller can improve the damping and rising time of a control system, but the steady-state response is not affected. The PI controller can improve the steady-state error, but the rise time is increased. This leads to the motivation of using a PID controller so that the best features of each of the PI and PD controllers are utilized.

The significance of the PID controller is that it can deal with lots of control problems

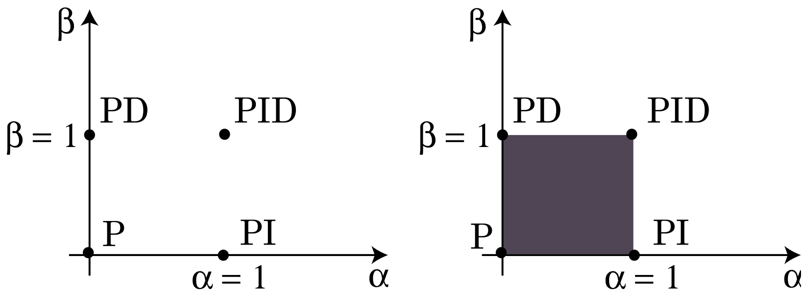

(a) Conventional PID

(b) Fractional PI$^\alpha$D$^\beta$

Figure 44: PID controllers from point to plane with fractional orders

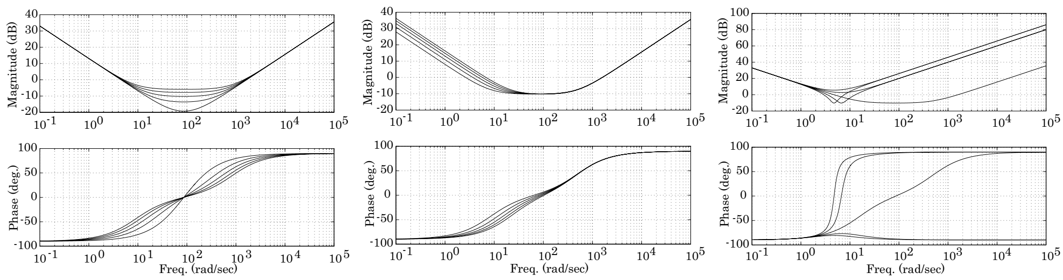

(a) Chaging K_p with 0.1 interval

(b) Chaging K_i with 1.0 interval

(c) Chaging K_d with 0.1 interval

Figure 45: Bode plots of PID controller with different K_p, K_i and K_d

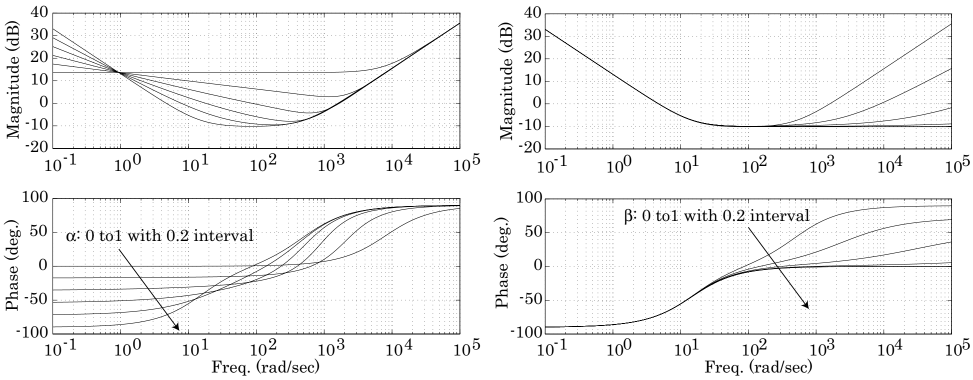

(a) Change α fractionally

(b) Change β fractionally

Figure 46: Bode plots of novel PI$^{\alpha}$D$^{\beta}$ controller with different α and β

with simple structure and few control parameters. Only three parameters K_p, K_i and K_d need to be designed. In order to further improve PID controller's performance, the fractional order version PI$^{\alpha}$D$^{\beta}$ is proposed:

$$G_c(s) = K_p + \frac{K_i}{s^{\alpha}} + K_d s^{\beta} \tag{156}$$

Namely, the orders α and β of I and D controllers are not necessarily integer order 1, but any real numbers. As shown in Fig. 44, the fractional order PI$^{\alpha}$D$^{\beta}$ controller generalizes the integer order PID controller and expands it from point to plane. This expansion could provide much more flexibility in PID control design.

For an example, $K_p = 0.309$, $K_i = 4.5$, and $K_d = 0.0006$ are selected as baseline case. By the comparison of Fig. 45 and Fig. 46, it can be seen that letting I and D portions' order be fractional can adjust the PID controller's frequency responses much more significantly than changing coefficients K_p, K_i, and K_d. And the change of the frequency responses is also more predictable. The real control applications of PI$^\alpha$D$^\beta$ controller will be mentioned in below sections.

7.2 I$^\alpha$ Controller for One-mass Speed Control

For one-mass speed control with gain variation, fractional order I$^\alpha$ controller could give good control and robust performances. The control loop for fractional one-mass speed control system is shown in Fig. 47, where the nominal inertia of the electric motor J_{m0}=6.53×10$^{-4}kgm^2$, friction coefficient D_m=1.25×10$^{-3}Nm \cdot sec/rad$, controller's coefficient K_i=0.11, sampling time T=0.001sec and an encoder (8000$pulse/rev$) is used as feedback speed sensor. Input torque saturation T_{max} and motor inertia variation $\Delta J_m (= J_m - J_{m0})$ will be introduced to verify the robustness against nonlinearity and parameter variation for the I$^\alpha$ control system.

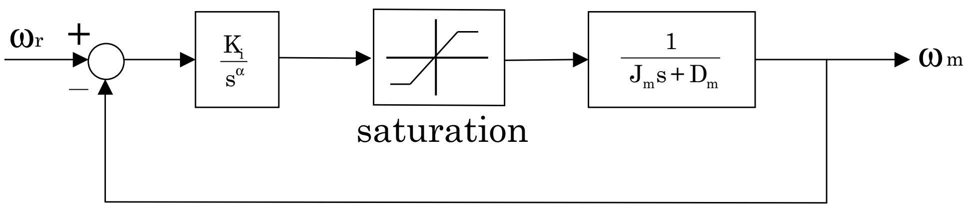

Figure 47: Fractional α order I control loop with non-linear factor

The Sampling Time Scaling method with full memory length is applied to implement I$^\alpha$ controller on digital computer. As shown in Fig. 48, the time responses of fractional order systems are clearly the "interpolation" between integer order ones. The time domain performances, such as overshoot and settling time, are changed greatly with different α orders. In Fig. 49, a constant overshoot can be ensured in face of inertia variation, showing a good robustness of the fractional I$^\alpha$ control system. In the same line, Fig. 50 also shows that fractional order controllers are much more robust against saturation non-linearity than their integer order counterparts.

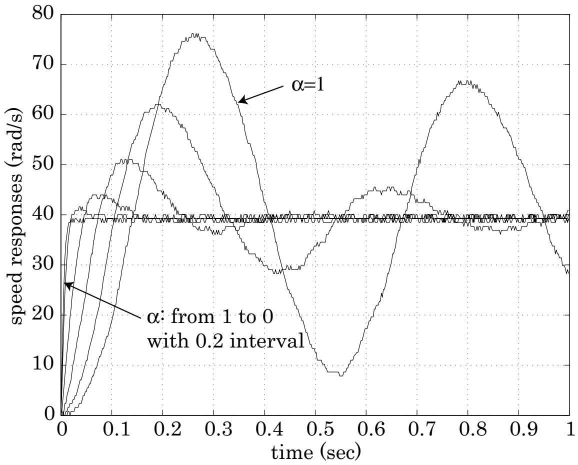

Figure 48: The time responses of I^{α} control system

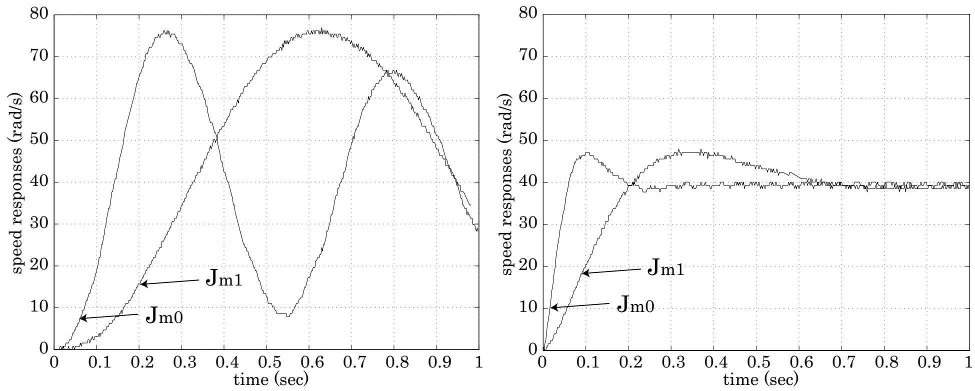

(a) $\alpha = 1$

(b) $\alpha = 0.5$

Figure 49: Robustness of the fractional I^{α} control system against inertia variation: $J_{m0} = 6.53 \times 10^{-4} kgm^2, J_{m1} = 3.36 \times 10^{-3} kgm^2$

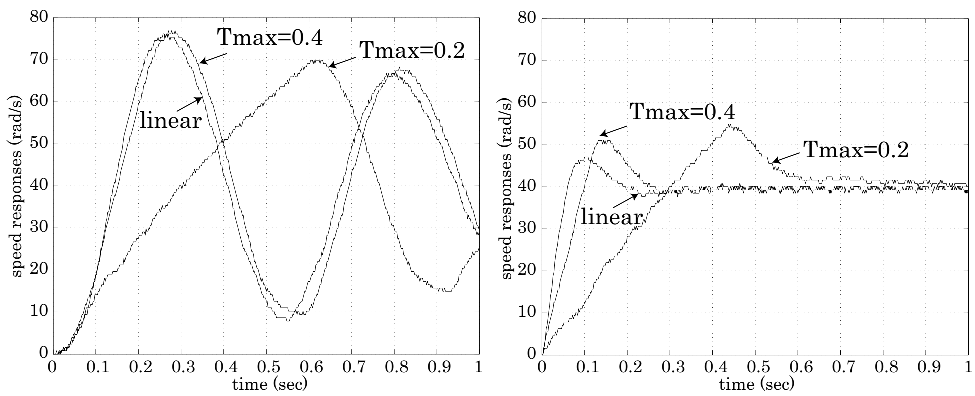

(a) $\alpha = 1$

(b) $\alpha = 0.5$

Figure 50: Robustness of the fractional I^{α} control system against torque limitation T_{max}

7.3 *Frequency-band $PI^{\alpha}D$ Control*

7.3.1 Experimental torsional system

Torsional system was chosen as testing bench, which is a typical oscillatory system. As shown in Fig. 51, two flywheels are connected with a long torsional shaft; while driving force is transmitted from driving servomotor to the shaft by gears with gear ratio 1:2. Some system parameters are adjustable, such as gear inertia, load inertia, shaft elastic coefficient and gear backlash angle. The encoders and tacho-generators are used as position and rotation speed sensors.

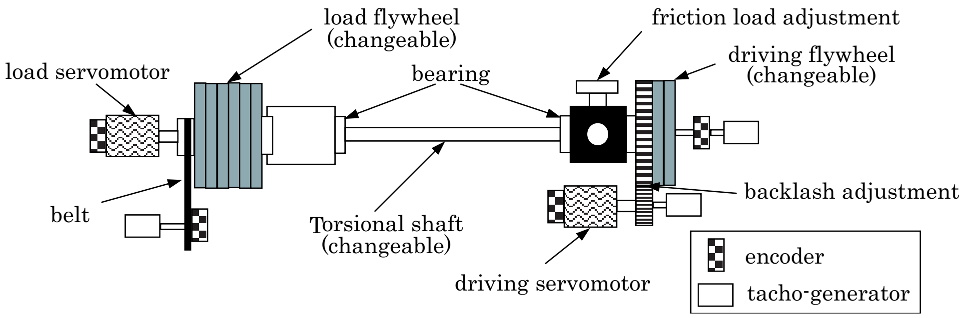

Figure 51: Experimental setup of the torsional system

The simplest model of the torsional system with gear backlash is three-inertia model, as shown in Fig. 52 and Fig. 53, where J_m, J_g and J_l are driving motor, gear (driving flywheels) and load inertias, K_s shaft elastic coefficient, ω_m and ω_l motor and load rotation speeds, T_m input torque and T_l disturbance torque. The gear backlash non-linearity is described by the classical dead zone models in which the shaft is modeled as a pure spring with zero damping [36]. Frictions between components are neglected due to their small values.

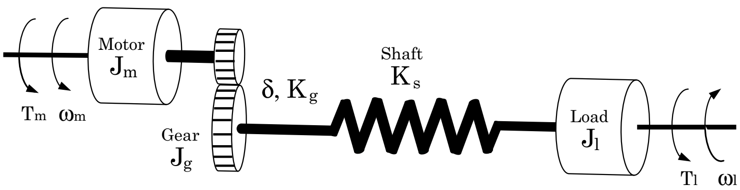

Figure 52: Torsional system's three-inertia model

Parameter setting of the experimental torsional system are shown in Table. 4 with

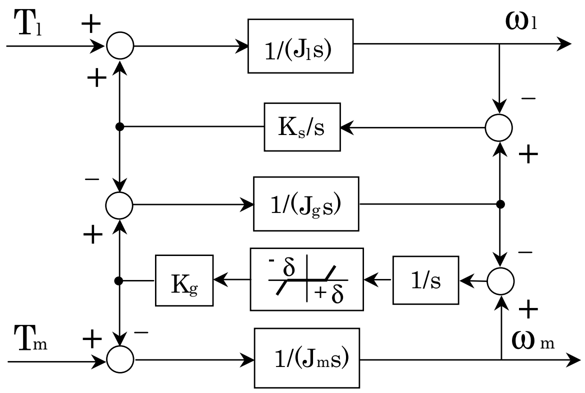

Figure 53: Block diagram of three-inertia model

backlash angle δ of $\pm 0.6deg$. Open-loop transfer function from T_m to ω_m is in following form:

$$P_{3m}(s) = \frac{(s^2+\omega_{h1}^2)(s^2+\omega_{h2}^2)}{J_m s(s^2+\omega_{o1}^2)(s^2+\omega_{o2}^2)} \tag{157}$$

where ω_{o1} and ω_{o2} are resonance frequencies while ω_{h1} and ω_{h2} are anti-resonance frequencies. ω_{o1} and ω_{h1} correspond to torsion vibration mode; while ω_{o2} and ω_{h2} correspond to gear backlash vibration mode (see Fig. 54).

Table 4: Parameters of the three-inertia system

J_m (Kgm^2)	J_g (Kgm^2)	J_l (Kgm^2)	K_g (Nm/rad)	K_s (Nm/rad)
0.0007	0.0034	0.0029	3000	198.4900

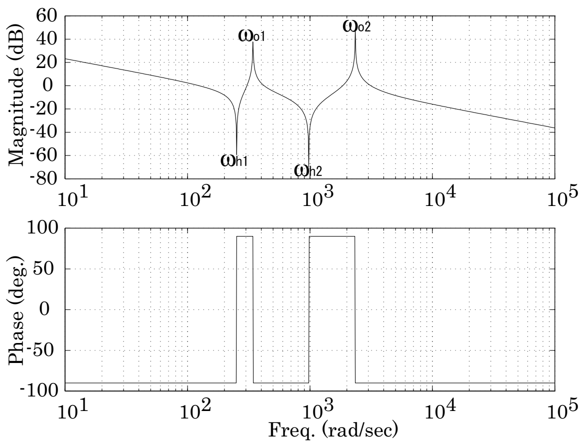

Figure 54: Bode plots of three-inertia model

Since gear elastic coefficient K_g is much larger than shaft elastic coefficient K_s ($K_g \gg K_s$), for speed control design the two-inertia model is commonly used in which driving motor inertia J_m and gear inertia J_g are simplified to a single inertia $J_{mg}(= J_m + J_g)$ (see Fig. 55).

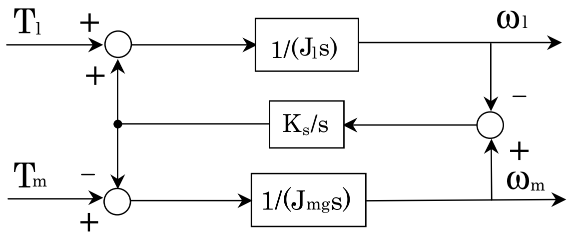

Figure 55: Block diagram of two-inertia model

The open-loop transfer function for two-inertia model is

$$P_{2m}(s) = \frac{s^2 + \omega_h^2}{J_{mg} s (s^2 + \omega_o^2)} \tag{158}$$

where ω_o is resonance frequency and ω_h is anti-resonance frequency corresponding to torsion vibration mode. Obviously the existence of backlash vibration mode is totally ignored in this simplified model.

7.3.2 PID controller design by CDM

Firstly, the conventional integer order PID control is designed by Coefficient Diagram Method (CDM), which is a direct characteristic polynomial design approach proposed by Manabe [37]. When backlash angle δ is set to zero, the experimental torsional system can looked as two-inertia system. As shown in Fig. 56, a set-point-I PID controller is introduced to the speed control of two-inertia system, which will be designed using the standard form of CDM [37] [38].

The characteristic equation of the close loop is

$$\begin{aligned} P(s) &= (J_l K_d + J_l J_{mg}) s^4 + J_l K_p s^3 + (J_l K_s + J_{mg} K_s + K_s K_d + J_l K_i) s^2 \\ &+ K_s K_p s + K_s K_i \\ &= a_4 s^4 + a_3 s^3 + a_2 s^2 + a_1 s + a_0 \end{aligned} \tag{159}$$

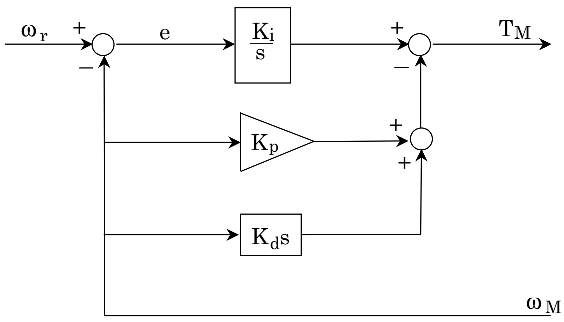

Figure 56: Set-point-I PID controller

Then the stability indexes are

$$\gamma_1 = \frac{a_1^2}{a_2 a_0} = \frac{K_s K_p^2}{K_i(J_l K_s + J_{mg} K_s + K_s K_d + J_l K_i)} \tag{160}$$

$$\gamma_2 = \frac{a_2^2}{a_3 a_1} = \frac{(J_l K_s + J_{mg} K_s + K_s K_d + J_l K_i)^2}{K_s J_l K_p^2} \tag{161}$$

$$\gamma_3 = \frac{a_3^2}{a_4 a_2} = \frac{J_l K_p^2}{(J_{mg} + K_d)(J_l K_s + J_{mg} K_s + K_s K_d + J_l K_i)} \tag{162}$$

Consider the same factor $a_2 = J_l K_s + J_{mg} K_s + K_s K_d + J_l K_i$, the relationship between γ_1, γ_2 and γ_3 can be written as

$$\begin{aligned} A &= \gamma_2 - \frac{1}{\gamma_1} - \frac{1}{\gamma_3} \\ &= \frac{J_l K_s + J_{mg} K_s + K_s K_d + J_l K_i}{K_p^2} \end{aligned} \tag{163}$$

Therefore, from Equ. (160), K_i can be derived as

$$K_i = \frac{K_s}{\gamma_1 A} \tag{164}$$

Similarly, K_d and K_p can be calculated as

$$K_d = \frac{J_l}{\gamma_3 A} - J_{mg} \tag{165}$$

$$K_p = \frac{\sqrt{\gamma_2 J_l K_s}}{A} \tag{166}$$

Finally, based on the CDM standard form ($\gamma_1 = 2.5,\ \gamma_2 = 2,\ \gamma_3 = 2$), the PID controller's parameters can be expressed as following

$$K_p = \frac{10\sqrt{2}}{11}\sqrt{J_s K_s},\ K_i = \frac{4}{11} K_s,\ K_d = \frac{5}{11} J_l - J_{mg} \tag{167}$$

Table 5: Two-inertia System's Parameters

$\mathbf{J_{mg}}$ (Kgm^2)	$\mathbf{J_l}$ (Kgm^2)	$\mathbf{K_s}$ (Nm/rad)
0.0040	0.0029	198.4900

Table. 5 and Equ. (167) give

$$K_p = 0.9789,\ K_i = 72.1782,\ K_d = -0.0027 \tag{168}$$

Time responses by simulation show the designed PID control system has satisfactory performances (see Fig. 57(a)) in nominal case (gear ratio is 1:1); while as shown in Fig. 57(b), in its frequency response, enough phase margin is not kept in the neighborhood of critical point. This would cause poor robustness of the integer order PID control system against non-linearities such as saturation and parameter variations.

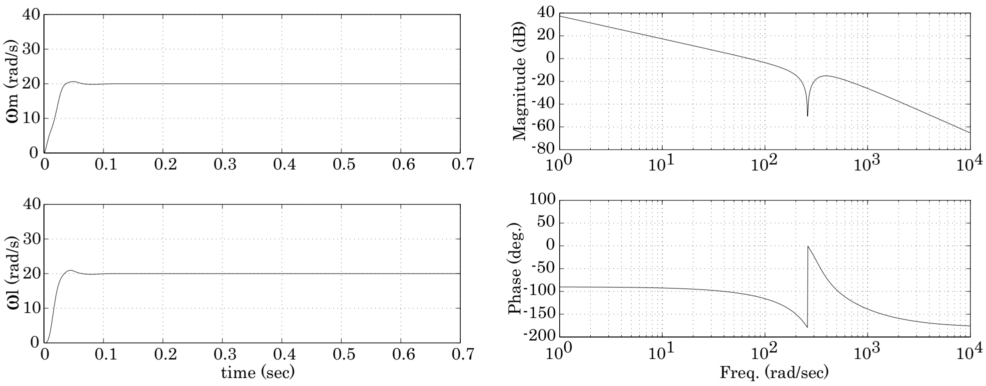

(a) Time responses by simulation

(b) Bode plots

Figure 57: Designed integer order PID control system

7.3.3 Frequency-band $\mathbf{I}^{\alpha}$ controller

The most straightforward way to improve the robustness of designed PID control system should be adjusting I controller's order to give control system more phase margin around the critical point. As mentioned in chapter 6, it is neither practicable nor desirable to try to make the order be fractional in whole frequency range. Frequency-band fractional order controller is a proper solution.

As shown in Equ. (169), a frequency-band I$^\alpha$ controller is proposed to substitute conventional integer order I controller. The low band frequency ω_b is taken as $10 rad/sec$ and high band frequency ω_h are $1000 rad/sec$:

$$\frac{1}{s}\left(\frac{\frac{s}{\omega_b}+1}{\frac{s}{\omega_h}+1}\right)^{1-\alpha} \tag{169}$$

By changing order α, the phase margin of proposed fractional order PI$^\alpha$D control system can be adjusted easily to any desired amount (see Fig. 58(a)). As shown in Fig. 58(b) and Fig. 58(c), when uncertainties such as saturation (gain variation) and load inertia variation exist, enough phase margin can be easily kept by choosing proper fractional order α.

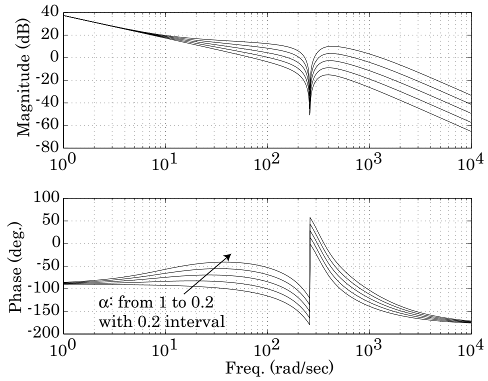

(a) Nominal case

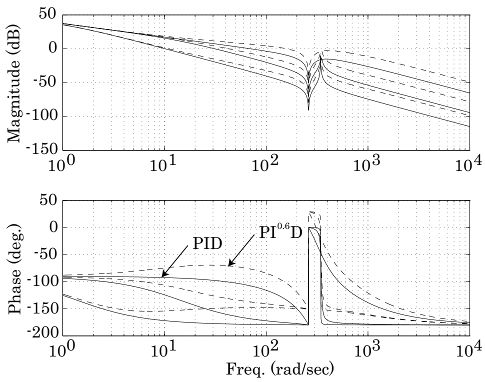

(b) With gain varation

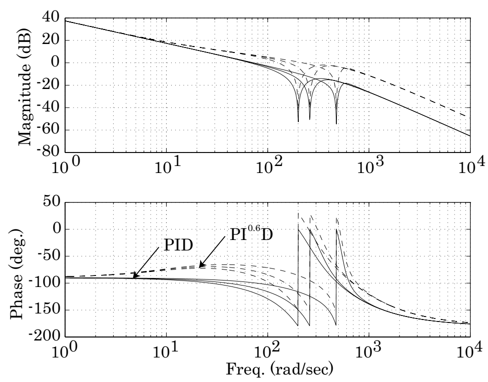

(c) With load inertia varation

Figure 58: Bode plots of fractional order PI$^\alpha$D control systems

7.3.4 Experimental results

The frequency-band I$^\alpha$ controllers are realized using broken-line approximation method. Experiments are carried out with sampling time T=0.001sec and 3nd-order broken-line approximation ($N = 3$).

As shown in Fig. 59, letting I controller's order be fractional can affect control system's time response greatly. It can be seen the frequency-band PI$^{\alpha}$D systems show better robustness to saturation non-linearity with smaller overshoots.

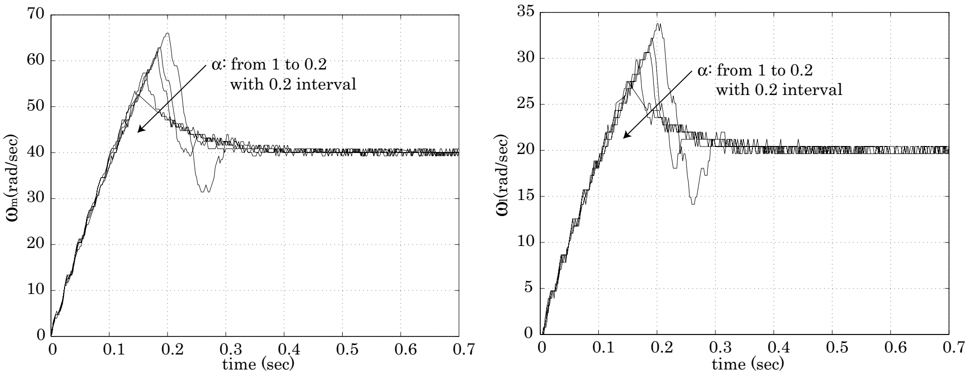

(a) Speed of driving motor (b) Speed of load side

Figure 59: Step responses with input torque saturation (T_m saturation is $\pm 3.84NM$)

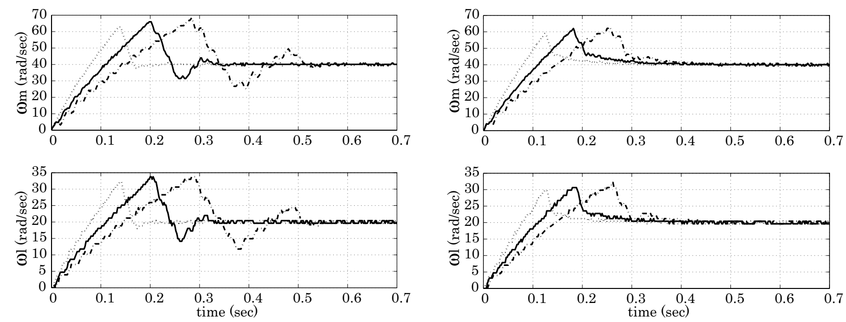

(a) $\alpha = 1$ (b) $\alpha = 0.6$

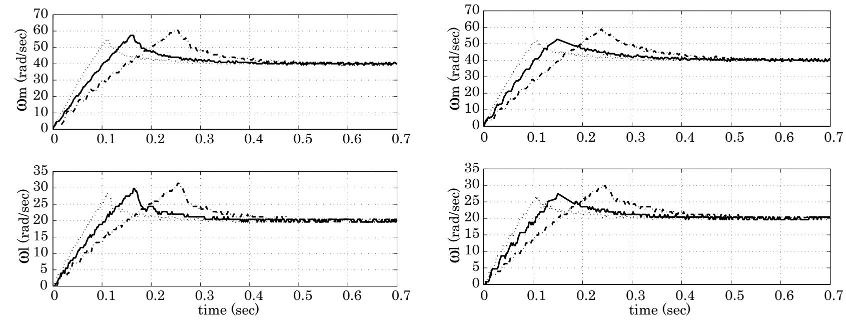

(c) $\alpha = 0.4$ (d) $\alpha = 0.2$

Figure 60: Step responses of PI$^{\alpha}$D system with load inertia variation. (solid line: nominal case; dotted line: $0.3J_l$; broken line: $1.7J_l$)

Figure 60 gives the step responses of PI$^{\alpha}$D control systems with different inertia on load side. Compared to severe change of integer order PID control system's time responses with large overshoot and overswing, the frequency-band PI$^{\alpha}$D control systems show better robustness against load inertia variation.

7.4 Fractional Order PID$^{\beta}$ Control

7.4.1 Unstable integer order PID control system

For two-inertia speed control, the history of control theory can be seen. Various design methods such as classical PID control, time derivative feedback, model following control, disturbance observer-based control, state feedback control and modern H∞ control have been proposed [38] [39] [40] [41]. Among them, the PID control is the most widely used in real industrial applications.

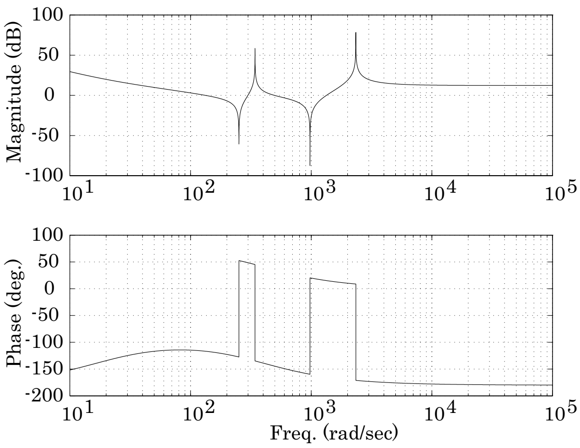

Figure 61: Bode plot of $G_l(s)$ for PID control system

Common weak point of the above methods is that the existence of backlash non-linearity is totally neglected. This weakness may make designed speed control systems unstable and give rise to backlash vibration. For example, when the torsional system's gear backlash angle δ is not zero, the three-inertia model must be used in control design. For three-inertia plant $P_{3m}(s)$, the close-loop transfer function of integer order PID control system from ω_r to ω_m is

$$G_{close}(s) = \frac{C_I(s)P_{3m}(s)}{1 + C_I(s)P_{3m}(s) + C_{PD}(s)P_{3m}(s)} \tag{170}$$

where $C_I(s)$ is I controller and $C_{PD}(s)$ is the parallel of P and D controllers in minor loop; therefore $G_{close}(s)$ is stable if and only if $G_l = C_I(s)P_{3m}(s) + C_{PD}(s)P_{3m}(s)$ has positive gain margin and phase margin. But as shown in Fig. 61, with same PID parameter setting designed by using two-inertia model, the gain margin of $G_l(s)$ will be negative. Therefore, with the existence of gear backlash, the designed integer order PID control system in above section will be unstable and lead to severe vibration.

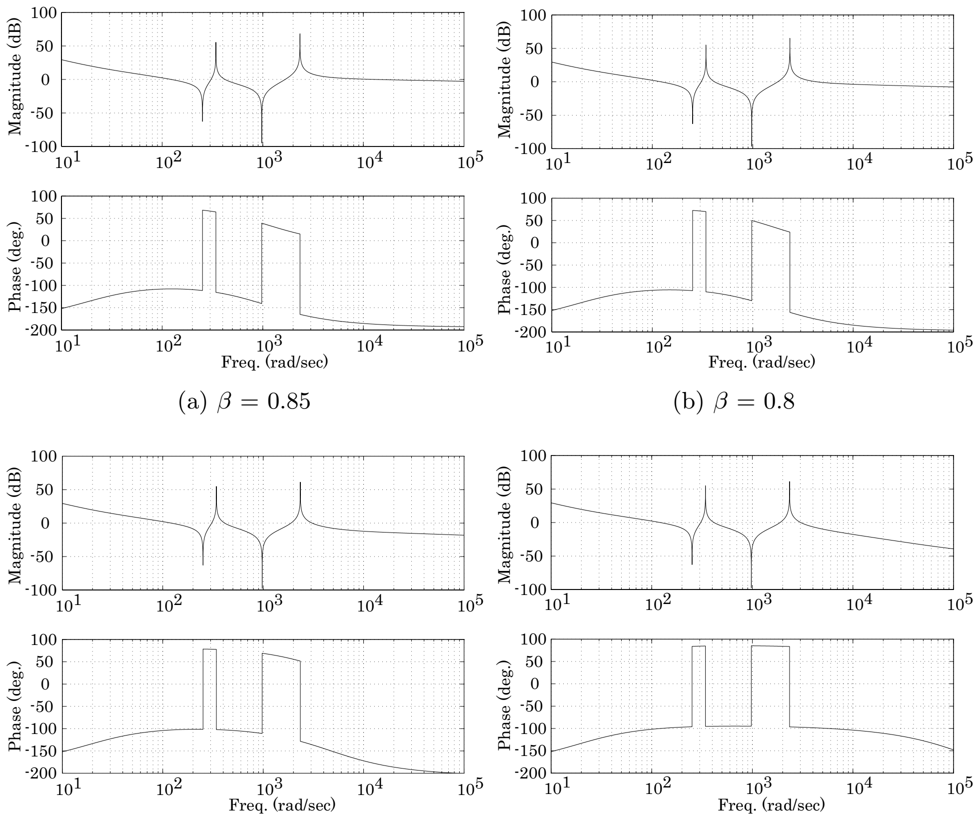

(a) $\beta = 0.85$ (b) $\beta = 0.8$

(c) $\beta = 0.7$ (d) $\beta = 0.5$

Figure 62: Bode plots of $G_l(s)$ for PID$^\beta$ control system

7.4.2 Design of fractional order β

In order to design a stable control system for three-inertia system, several methods have been proposed, but their design processes are very complicated. As an example, for PID control, introducing a low-pass filter $K_d s/(T_d s + 1)$ to substitute D controller and redesigning the whole control system with three-inertia model can be a solution [42]. Due to the necessity of solving high order equations, the design is not easy to be carried out. Clear-cut design approach is required in practical applications.

In this chapter, a novel fractional order PID$^\beta$ controller is proposed to achieve a clear-cut design of stable control system when gear backlash exists. Instead of solving high order equations, by changing D$^\beta$ controller's fractional order β, the frequency response of $G_l(s)$ can be effectively adjusted (see Fig. 62). As shown in Fig. 63, selecting proper fractional order β can improve PID$^\beta$ control system's gain margin quite easily. In nominal case, when $\beta < 0.84$ the PID$^\beta$ control system will become stable.

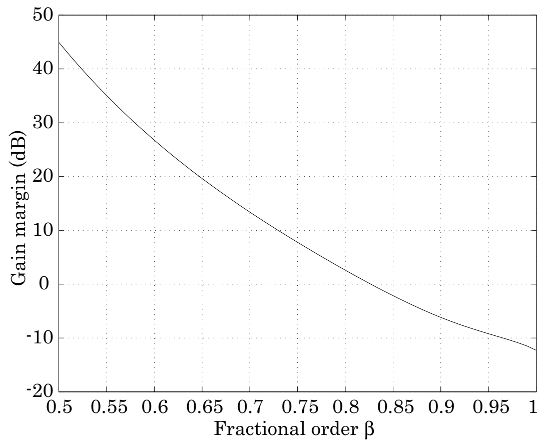

Figure 63: Gain margin versus fractional order β

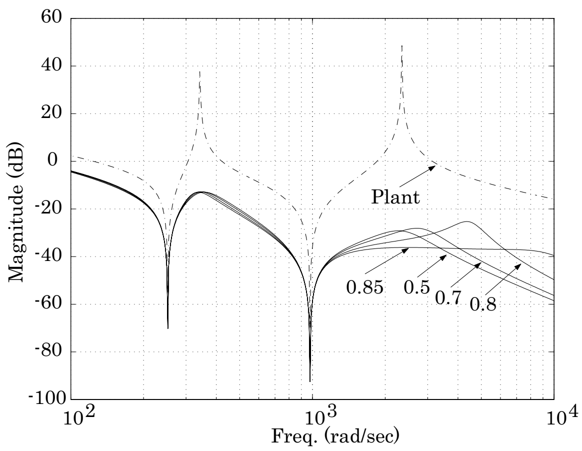

Figure 64: Gain plots of the PID$^\beta$ control systems and three-inertia plant

At the same time, for better backlash vibration suppression higher D$^\beta$ controller's order is more preferable. As shown in open-loop gain plots of 0.85, 0.8, 0.7 and 0.5 order PID$^\beta$ control systems (see Fig. 64), higher the D controller's order is taken lower the gain near gear backlash vibration mode is. Based on the tradeoff between robustness and vibration suppression strength, fractional order 0.7 is chosen as D^{β} controller's best order.

7.4.3 Realization of D^{β} controller

Short Memory Principle is adopted to realize discrete fractional order D^{β} controller. The discrete equivalent of D^{β} controller is in following form:

$$Z\{D^{\beta}[f(t)]\} \approx \left[T^{-\beta}\sum_{j=1}^{m} c_j^{\beta} z^{-(j-1)}\right] Z\{f(t)\} \tag{171}$$

For a comparison purpose, the Sampling Time Scaling method is also applied to realize discrete D^{β} controller, which has same form as Equ. (171). The semi-log charts of Fig. 65 show the two realization method's binomial coefficients c_j versus term order j when approximating $D^{0.5}$. Based on the observation of Fig. 65, memorizing 10 latest values (m=10) is assumed to have a good approximation.

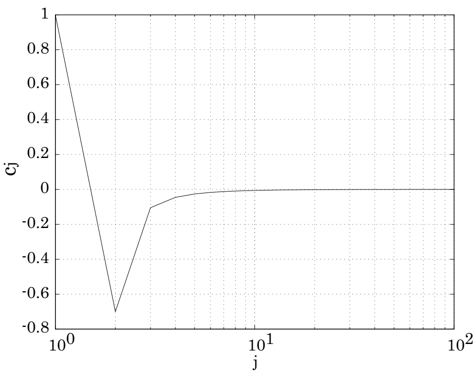

(a) Short Memory Principle method

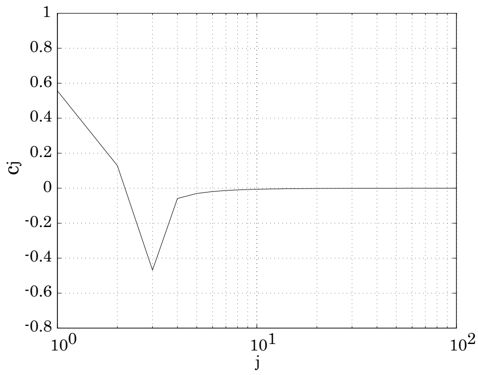

(b) Sampling Time Scaling method

Figure 65: Binomial coefficients c_j versus term order j when approximating $D^{0.5}$ (Sampling time $T = 0.001sec$)

7.4.4 Experimental results

Experiments are carried out with sampling time T=0.001sec. Since driving servomotor's input torque command T_m has a limitation of maximum ± 3.84 Nm, K_i is reduced to 20.2099 by trial-and-error to avoid large over-shoot caused by the input torque saturation.

Firstly, integer order PID speed control experiment is carried out. As shown in Fig. 66

the PID control system can achieve satisfactory response when the backlash angle is adjusted to zero degree ($\delta = 0$); while due to the existence of backlash non-linearity, severe vibration occurs and the PID control system is obviously unstable (see $\delta = 0.6$ case). This experimental result is consistent with above theoretical analysis.

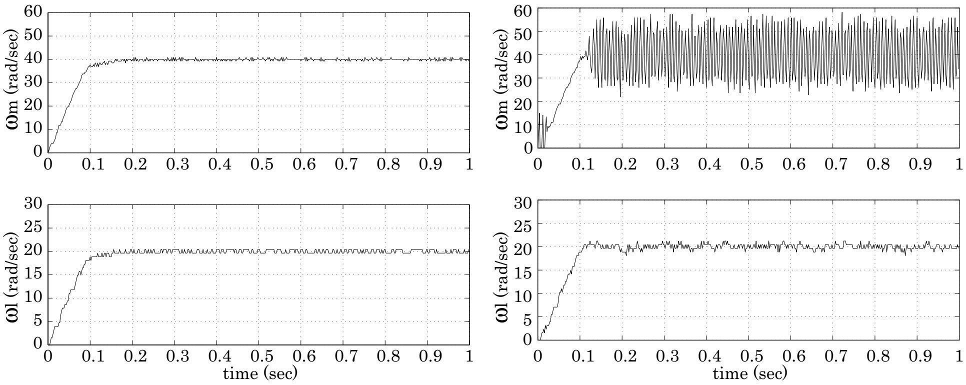

(a) $\delta = 0deg.$ (b) $\delta = 0.6deg.$

Figure 66: Time responses of the integer order PID control

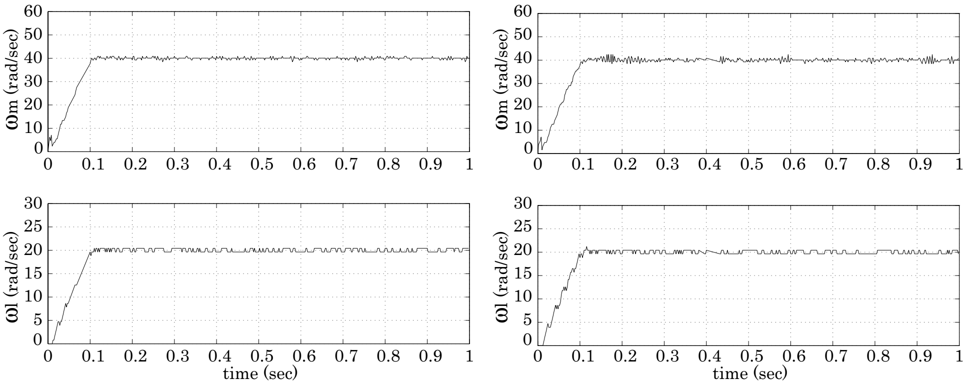

(a) $\beta = 0.7$ (b) $\beta = 0.5$

Figure 67: Time responses of PID$^\beta$ control with gear backlash (realized by Short Memory Principle method)

Realization by Short Memory Principle method: Figure 67 gives the experimental results of fractional order PID$^\beta$ control with 0.7 and 0.5 order D$^\beta$ controllers. Severe vibration in integer order PID control case is effectively suppressed. The control system's stability and robustness against gear backlash non-linearity can be greatly improved by introducing fractional order version D$^\beta$ controller. PID$^{0.7}$ control system has a good tradeoff between stability and backlash vibration suppression. The intermittent tiny vibrations in lower order 0.5 case are due to its relatively high gain near gear backlash vibration mode in open-loop frequency response.

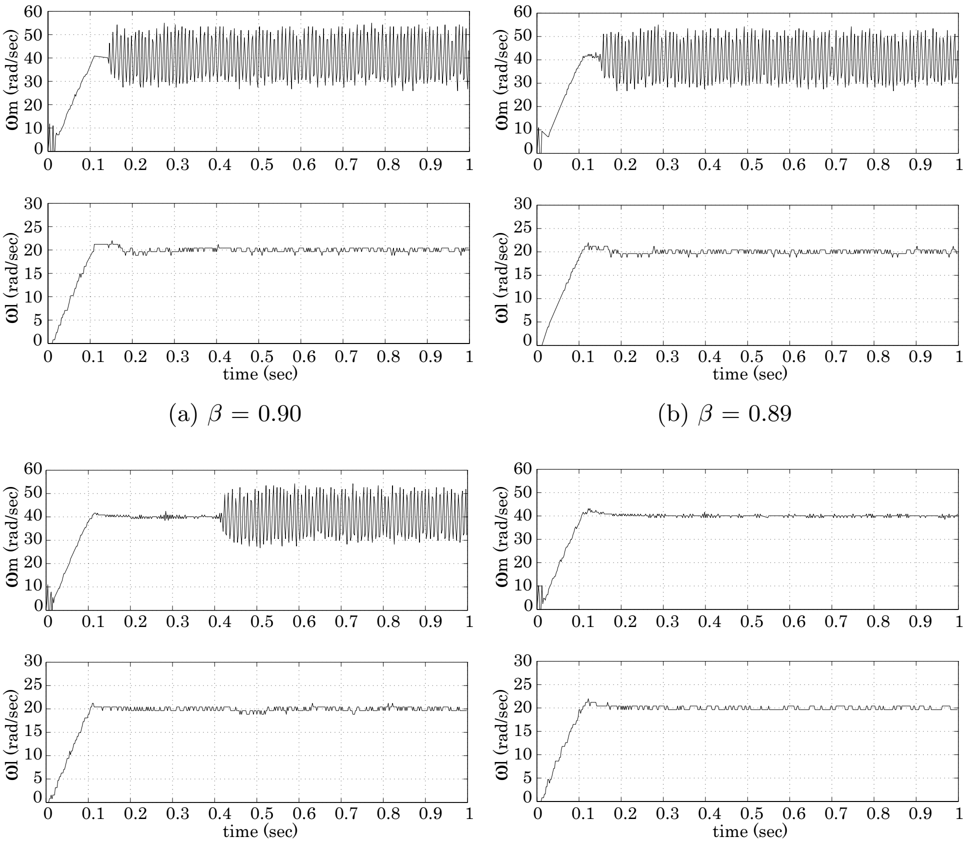

(a) $\beta = 0.90$ (b) $\beta = 0.89$

(c) $\beta = 0.88$ (d) $\beta = 0.87$

Figure 68: Continuity of PID$^\beta$ control's time responses with gear backlash (realized by Short Memory Principle method)

It is interesting to find the time responses of fractional order PID$^\beta$ control system show somewhat "interpolation" characteristic. As shown in Fig. 68, PID$^{0.9}$ control has the most severe vibration due to the instability, while PID$^{0.87}$ is on a critical state between instability and stability. PID$^{0.89}$ and PID$^{0.88}$ have intermediate time responses. This experimental result should be natural since these orders are continuously changed. The "interpolation" characteristic is one of main points to understand the superiority of FOC as providing a clear-cut and effective tool for adjust control system's characteristics further between conventional IOC approaches. At the same time, this experimental consistency with logicality also verifies the good approximation of the realization method based on Short Memory Principle.

Experiments of PID$^{0.7}$ control with different memory length m are also carried out. As shown in Fig. 69, even 2nd-order approximation can give a relatively good performance; while taking m=100 actually has almost same performance as m=10 case. These results show that in this control problem memorizing 10 latest values is a reasonable choice for applying the Short Memory Principle method.

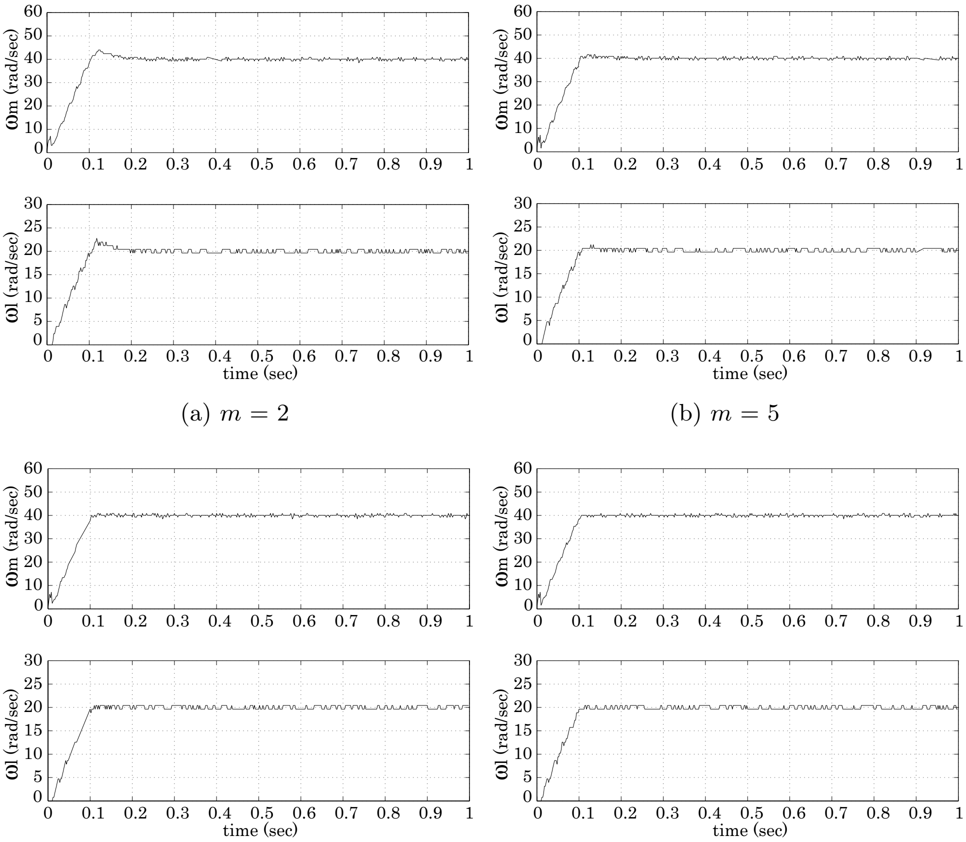

(a) m = 2

(b) m = 5

(c) m = 10

(d) m = 100

Figure 69: Time responses of PID$^{0.7}$ control with different memory length m (realized by Short Memory Principle method)

Realization by Sampling Time Scaling method: In chapter 6, it was concluded that Short Memory Principle Method and Sampling Time Scaling Method have similar approximation performance, but the Short Memory Principle method is practically superior due to its simple algorithm. The time responses of PID$^{0.7}$ control realized by Sampling Time Scaling method (memory length $m = 10$) are shown in Fig. 70. It can seen that the conclusion drawn in chapter 6 is verified by real experimental results.

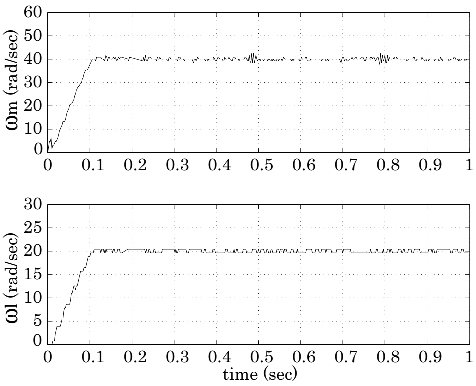

(a) $\beta = 0.1$

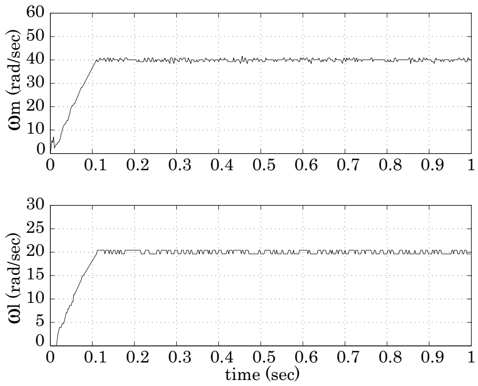

(b) $\beta = 0.3$

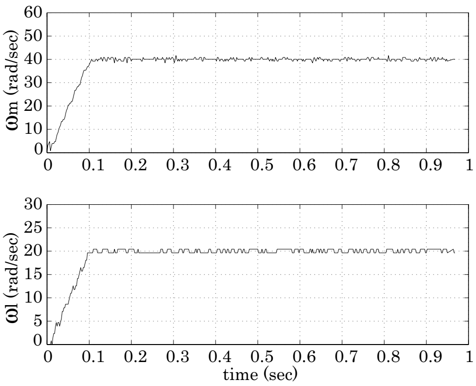

(c) $\beta = 0.5$

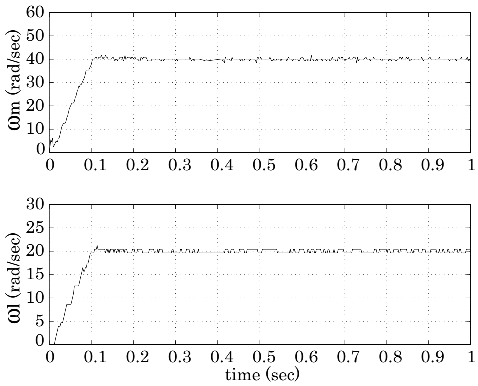

(d) $\beta = 0.7$

Figure 70: Time responses of PID$^{\beta}$ control with gear backlash (realized by Sampling Time Scaling method with $m = 10$)

7.5 Summary

In this chapter, PI$^{\alpha}$D$^{\beta}$ control, a fractional order version of conventional PID control, is proposed and verified by various control problems using the experimental torsional system. By letting controller's order be fractional, control system's frequency responses can be designed effectively and much more predictably with less control parameters, only fractional order α and β in this chapter.

Even having a little higher hardware demand, clear-cut design and better control performance of PI$^{\alpha}$D$^{\beta}$ control demonstrated in this chapter still highlight FOC's promising aspect. Rapid development of computational power also makes fractional order controller's implementation not really problematic.

However, care must be taken about the purpose of section 7.4. It is not to claim PID$^{\beta}$ controller as a good controller for three-inertia system, but to contribute to being a valuable experience and verification for novel but still primitive FOC research. Especially the section shows the possibility of straightforward and better tradeoff between stability margin loss and backlash vibration suppression strength through FOC approach. This tradeoff is a common and natural problem in oscillatory systems' control [45]. For such kind of systems, a fractional order controller in the following form

$$G_c(s) = \frac{K_p s + K_i}{(T_d s + 1)^{\alpha} s} \tag{172}$$

is expected to be a general solution, where better tradeoff between stability margin and vibration suppression can be achieved by choosing proper fractional order α. Namely, a PI controller with fractional low-pass filter $\frac{1}{(T_d s+1)^{\alpha}}$ is a proper choice for oscillatory systems' control design. This aspect will be discussed in next chapter, chapter 8.

CHAPTER VIII

FRACTIONAL ORDER FILTER

8.1 Redesign the PID Controller

In chapter 7, the PID controller was designed using the fixed gammas of CDM. Standard form was emphasized at CDM's early stage. When gammas are in standard form, pole pattern is fixed. Only variation of magnitude due to τ is allowed. The early version of CDM is actually nothing but an analytical pole assignment method, where robustness is not guaranteed at all. As discussed in Ref. [37], what is really needed for controller design of two-inertia resonant system is phase lag, not phase lead. For this reason, the value of D control becomes negative, which means phase lag. However positive feedback of D control will lead to poor robustness and should be avoided as much as possible in control design. Namely, the big value of negative K_d causes robustness problem for the integer order PID control design in chapter 7.

In recent development, the selection of the gammas is recommended. Designers should choose proper gammas that can guarantee not only stability but also robustness. The CDM formula for designing PID controller is repeated:

$$\begin{aligned} A &= \gamma_2 - \frac{1}{\gamma_1} - \frac{1}{\gamma_3} && (173) \\ K_d &= \frac{J_l}{\gamma_3 A} - J_{mg} && (174) \\ K_p &= \frac{\sqrt{\gamma_2 J_l K_s}}{A} && (175) \\ K_i &= \frac{K_s}{\gamma_1 A} && (176) \end{aligned}$$

In order to avoid D control, $K_d = 0$ is assigned. Therefore the following results are derived:

$$[A\ \gamma_3\ K_p\ K_i] = [0.6629\ 1.0671\ 1.6187\ 117.8528] \quad (177)$$

γ_3 can not be assigned previously any more and must be the value calculated under above assignment. Namely, a PI controller, where the assignment is $\gamma_1 = 2.5, \gamma_2 = 2$ and $\gamma_3 =$

1.0671, should give a better performance in both stability and robustness than the PID controller designed in chapter 7.

Redesigned set-point-I PI control is shown in Fig. 71. The PI controller is designed by revised CDM method with $K_i = 119.78$ and $K_p = 1.6187$. Simulation results with nominal three-inertia model (backlash angle is 0 deg.) show the redesigned PI control system has satisfactory time responses in nominal case. However, as demonstrated in chapter 7, control system's vibration suppression performance must be considered due to the existence of gear backlash.

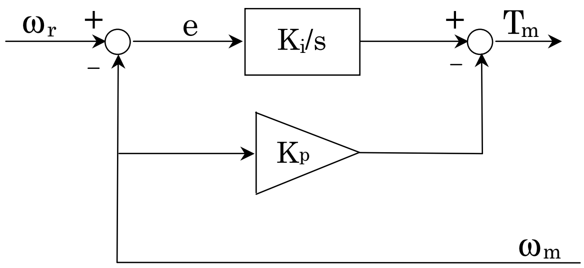

Figure 71: Set-point-I PI controller

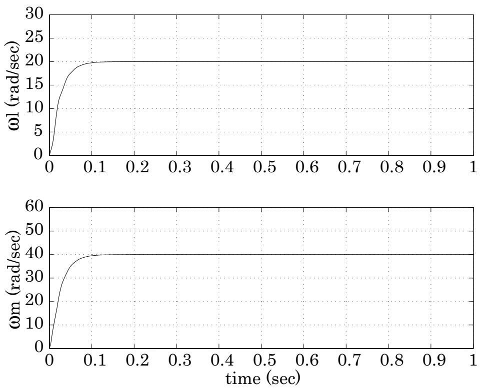

Figure 72: Simulation results with nominal three-inertia model

8.2 Necessity of Tradeoff Adjustment

For clearness, the stability analysis is repeated. With nominal three-inertia model $P_{3m}(s)$, the close-loop transfer function of integer order PI control system from ω_r to ω_m is

$$G_{close}(s) = \frac{C_I(s)P_{3m}(s)}{1 + C_I(s)P_{3m}(s) + C_P(s)P_{3m}(s)} \tag{178}$$

where $C_I(s)$ is I controller and $C_P(s)$ is P controller in minor loop; therefore $G_{close}(s)$ is stable if and only if $G_l = C_I(s)P_{3m}(s) + C_P(s)P_{3m}(s)$ has positive gain margin and phase margin.

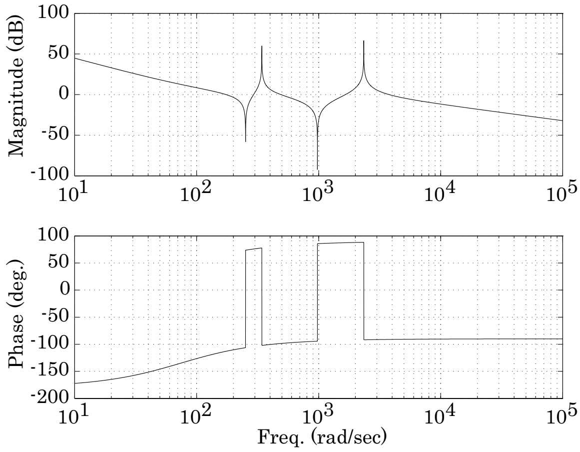

Figure 73: Bode plots of $G_l(s)$ for PI control system

As shown in Fig. 73, the PI speed control system has enough stability margin; while in order to recover some vibration performance, additional factors with negative slope and phase-lag are needed. However introducing these factors will simultaneously lead to phase margin loss. Namely, there exists a tradeoff between stability margin loss and vibration suppression strength in torsional system's PI speed control.

8.3 Fractional Order Low-pass Filter

In order to achieve a proper controller, which is neither conservative nor aggressive, redesigning the PI controller or applying other control methods can be options; while in this chapter, a fractional order low-pass filter $\frac{1}{(\tau s+1)^{\alpha}}$ is introduced (see Fig. 74). The tradeoff between stability margin loss and vibration suppression strength can be easily adjusted by choosing only one control parameter, fractional order α.

As shown in Fig. 75(a) and (b), a predictable and easy tradeoff between phase margin and vibration suppression strength can be achieved by choosing proper fractional order α. With fractional order low-pass filter, a clear-cut control design could be obtained. Parameter τ will give control system enough large band width for a fast time response. Here considering the frequency range of torsion vibration mode, τ is taken as 0.005(=1/200).

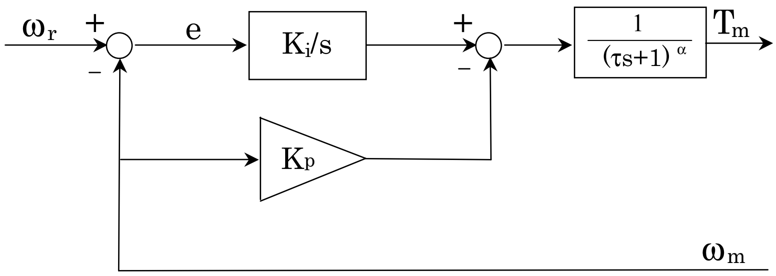

Figure 74: PI controller with fractional order low-pass filter

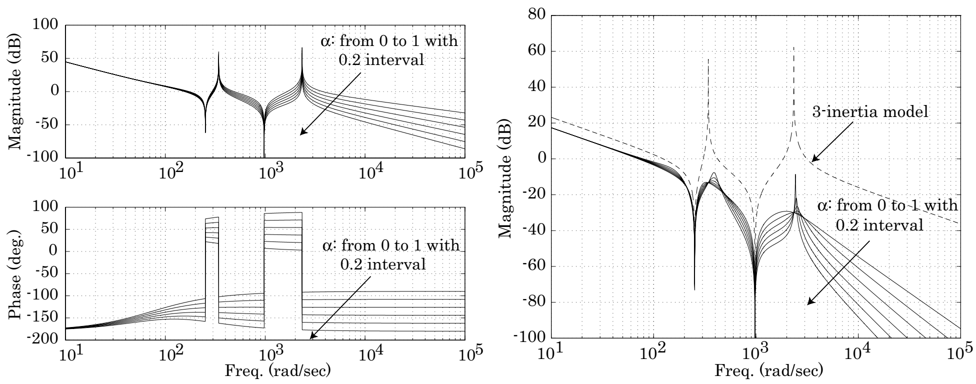

(a) $G_l(s)$: relative stability (b) Open-loop: vibration suppression

Figure 75: Bode plots with fractional order low-pass filter

8.4 Vibration Suppression with Parameter Variation

In torsional system, vibration occurs because kinetic energy, which is manifested as speeds of inertia (mass) elements, can be converted into elastic potential energy and back to kinetic energy [24]. The elastic potential energy is due to the deformation in spring-like elements, the long torsional shaft and the gears. For a rotation system like torsional system with the single degree of freedom θ. Kinetic energy stored in the inertia element is

$$KE = \frac{1}{2}J\dot{\theta}^2 \tag{179}$$

Elastic potential energy stored in the spring is

$$PE = \frac{1}{2}K_s\theta^2 \tag{180}$$

J is the moment of inertia of the flywheels and K_s is the torsional stiffness of the shaft. Larger J will store more kinetic energy; while for the same elastic potential energy, smaller K_s will lead to larger θ. Therefore, large load side inertia and thin shaft make vibration suppression of the torsional system more difficult.

In order to verify proposed FOC approach's superiority in vibration suppression, besides the gear backlash, other uncertainties, load inertia variation and shaft variation, are also introduced to experiments to further verify FOC approach's robustness. Experiments with large load inertia (5 load flywheels) and thin shaft (4mm diameter) will be carried out.

The Bode plots of $G_l(s)$ and open-loop gain are shown in Fig. 76 and Fig. 77 using three-inertia model. As mentioned in chapter 3, the dynamic of the shaft can be described more adequately by fractional order model, especially for thin shaft. However, practices show the conventional three-inertia model may be not enough, but can still provide good vision for control system design and analysis.

From the Bode plots, it can be seen the parameter variations mainly move torsional vibration mode to lower frequency region. This movement may lead to stability problem due to decreased phase margin around torsional vibration mode. Especially in thin shaft case (see Fig. 77), larger open-loop gain around the torsional vibration mode makes it easier to cause vibrations than in nominal case.

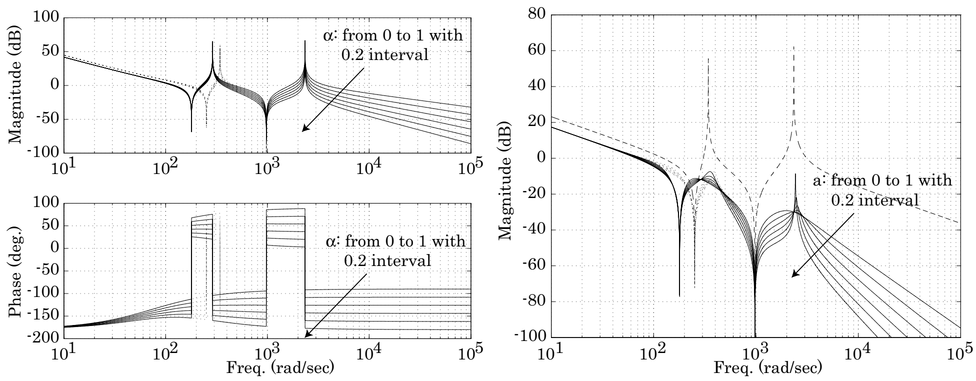

(a) $G_l(s)$: relative stability

(b) Open-loop: vibration suppression

Figure 76: Bode plots with load inertia variation (5 load flywheels): dashed line in (a) nominal case; (b) three-inertia model

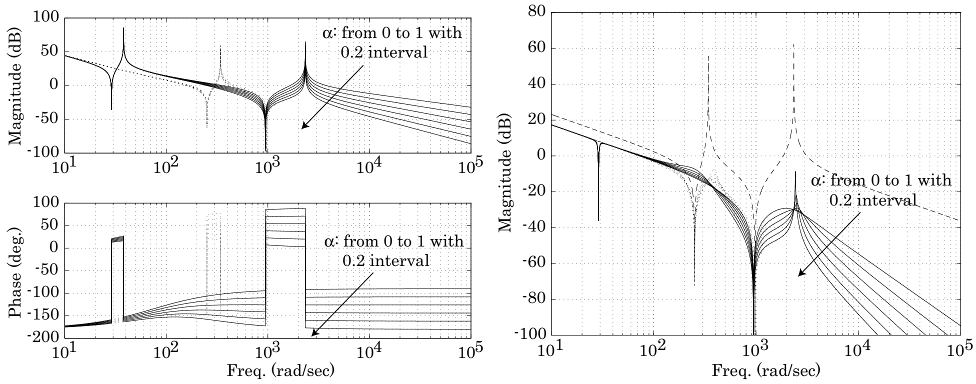

(a) $G_l(s)$: relative stability (b) Open-loop: vibration suppression

Figure 77: Bode plots with shaft variation (diameter 4mm): dashed line in (a) nominal case; (b) three-inertia model

As shown in the Figures of Bode plots, despite the existence of large parameter variations, the control system can still keep enough phase margin and better vibration suppression performance by choicing proper fractional order α of the low-pass filter. By introducing fractional order low-pass filter, the phase margin can be easily adjusted accurately to any desired value among integer order filters; while some vibration suppression performance can be recovered compared to using conventional integer order filters only.

8.5 Experimental Results

8.5.1 Nominal case with gear backlash

Experiments are carried out with sampling time T=0.001sec. The fractional order low-pass filters are realized by broken-line method, where approximation order $N = 2$ and approximation band is [200 10000]. Since the driving servomotor's input torque command T_m has a limitation of maximum $\pm 3.84\ Nm$, K_i is reduced to 30.6417 by trial-and-error.

Firstly, integer order PI speed control experiment is carried out. As shown in Fig. 78 the PI control system can achieve satisfactory time responses when backlash angle is adjusted to zero degree ($\delta = 0$); while persistent vibration occurs when gear backlash non-linearity exists (see $\delta = 0.6$ case). Obviously, PI control only can not provide enough strength for suppressing backlash vibration.

Figure 79 shows experimental results with different α order filters. Vibration occurred in

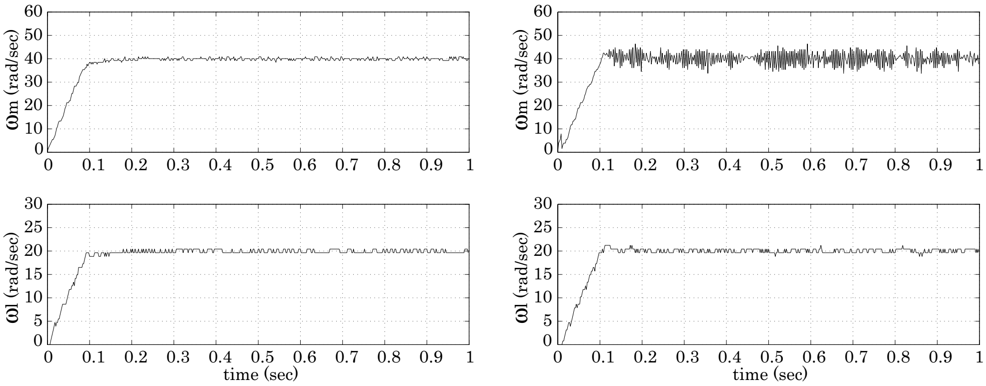

(a) $\delta = 0deg.$ (b) $\delta = 0.6deg.$

Figure 78: Time responses of integer order PI control system

PI-only control is effectively suppressed. Taking α as 0.4 gives the best time response. For other higher α order cases, their time responses are not such satisfied due to larger phase margin loss. FOC approach is effective to adjust the tradeoff between stability margin loss and vibration suppression strength, in which only one control parameter, fractional order α, is needed.

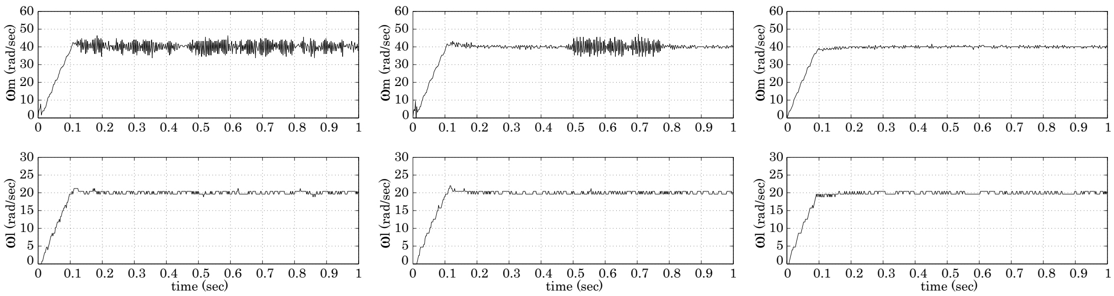

(a) PI-only (b) $\alpha = 0.2$ (c) $\alpha = 0.4$

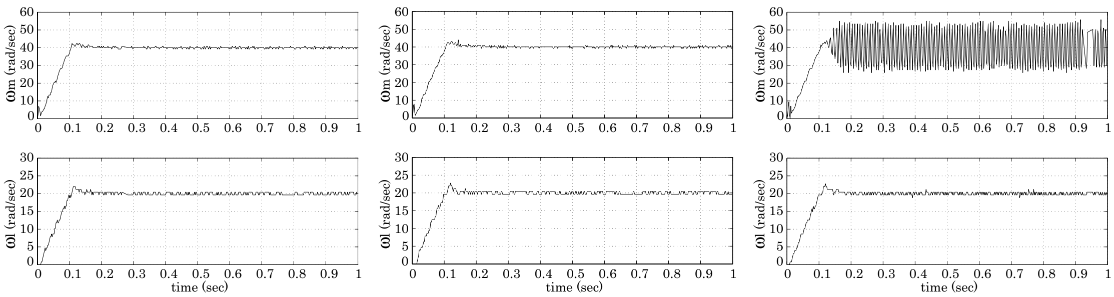

(d) $\alpha = 0.6$ (e) $\alpha = 0.8$ (f) $\alpha = 1.0$

Figure 79: Time responses with fractional order $\frac{1}{(\tau s+1)^{\alpha}}$ filters

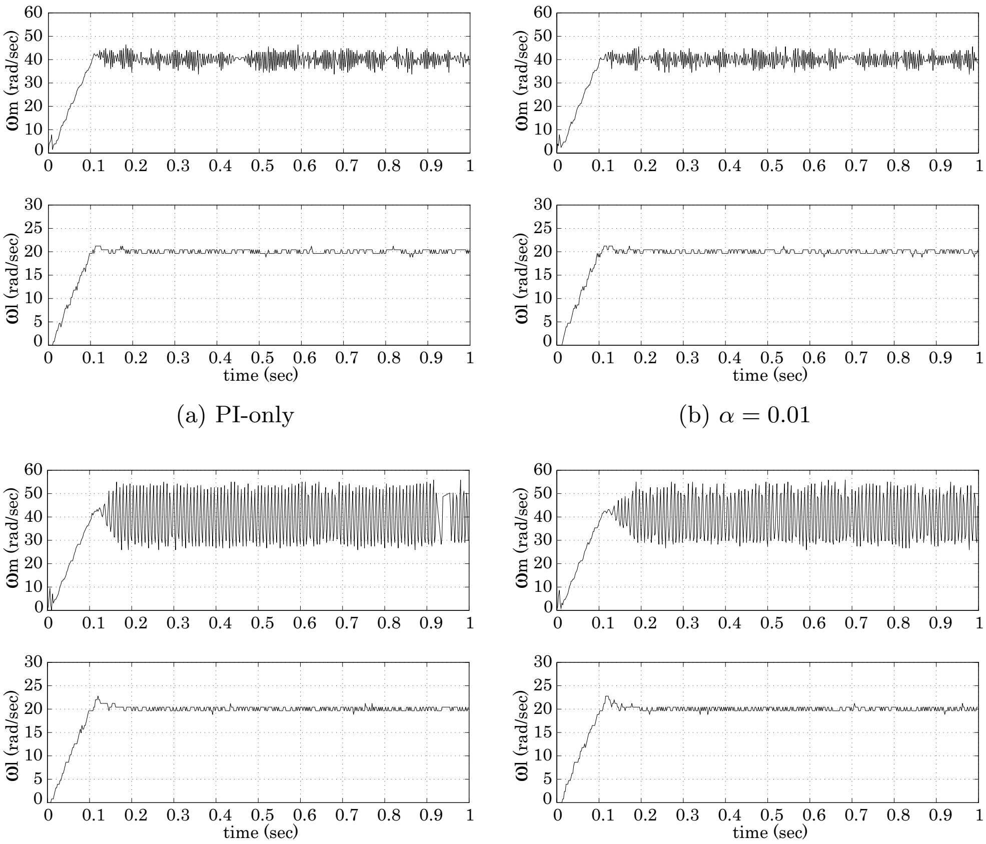

(a) PI-only (b) $\alpha = 0.01$

(c) $\alpha = 1.0$ (d) $\alpha = 0.99$

Figure 80: Continuity of time responses with different fractional order α

In order to verify whether the fractional order filter can give a continuous tradeoff tuning, the time responses of $\alpha = 0.01$ and $\alpha = 0.99$ cases are also experimented. As shown in Fig. 80, the results display a good continuity. Attention should be paid toward the reasons for vibrations in two cases. Poor vibration suppression performance causes vibration in $\alpha = 0.01$ case; while nearly zero phase margin in $\alpha = 0.99$ leads to much more severe vibration. Namely, the reason for the second case is its poor stability performance. A proper fractional order α can obtain a better tradeoff between these two extreme cases.

Figure. 81 shows experimental results with the 1st-order and 3rd-order approximations of broken-line method. Even taking 1st-order approximation can give a relatively good performance.

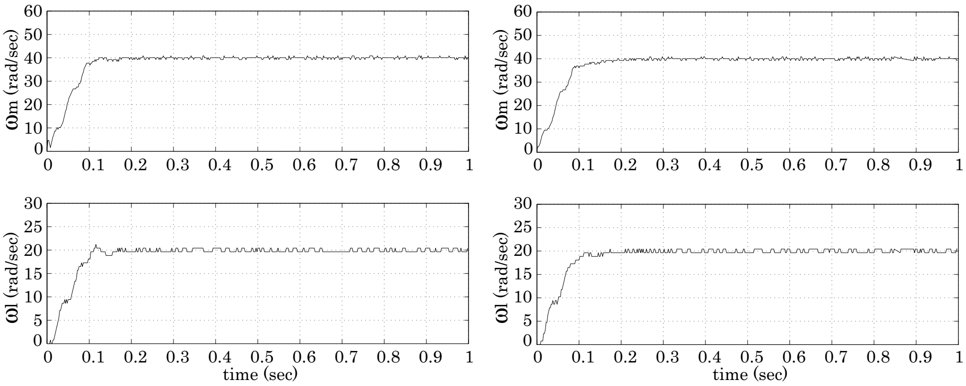

(a) 1st-order (b) 3rd-order

Figure 81: Time responses with different approximation order of $\frac{1}{(\tau s+1)^{0.4}}$ filter

8.5.2 Load inertia and shaft variations

Figure 82 shows that taking α as 0.4 and 0.6 can still have good vibration suppression performance. In Fig. 83 with shaft variation, small α, 0 and 0.2, is not enough to suppress backlash vibration; while large α, 0.8, will cause stability problem. Intermediate values, 0.4 and 0.6, give good tradeoff between these two cases.

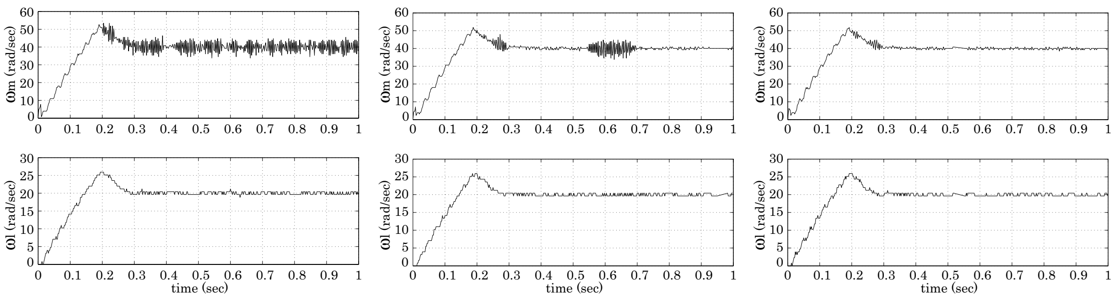

(a) PI-only (b) $\alpha = 0.2$ (c) $\alpha = 0.4$

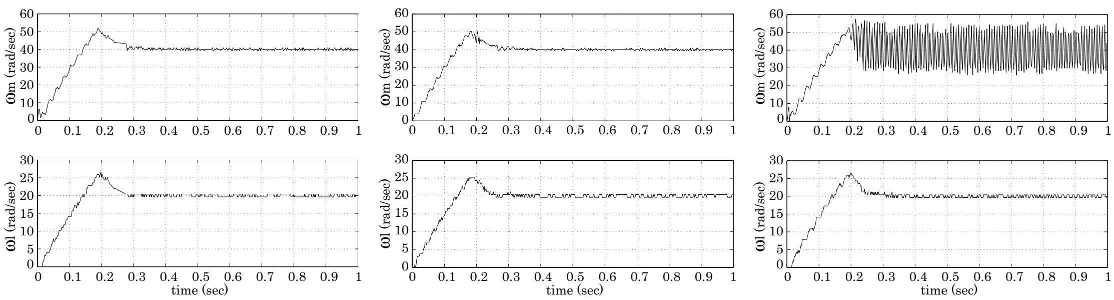

(d) $\alpha = 0.6$ (e) $\alpha = 0.8$ (f) $\alpha = 1.0$

Figure 82: Time responses with load inertia variation (5 load flywheels)

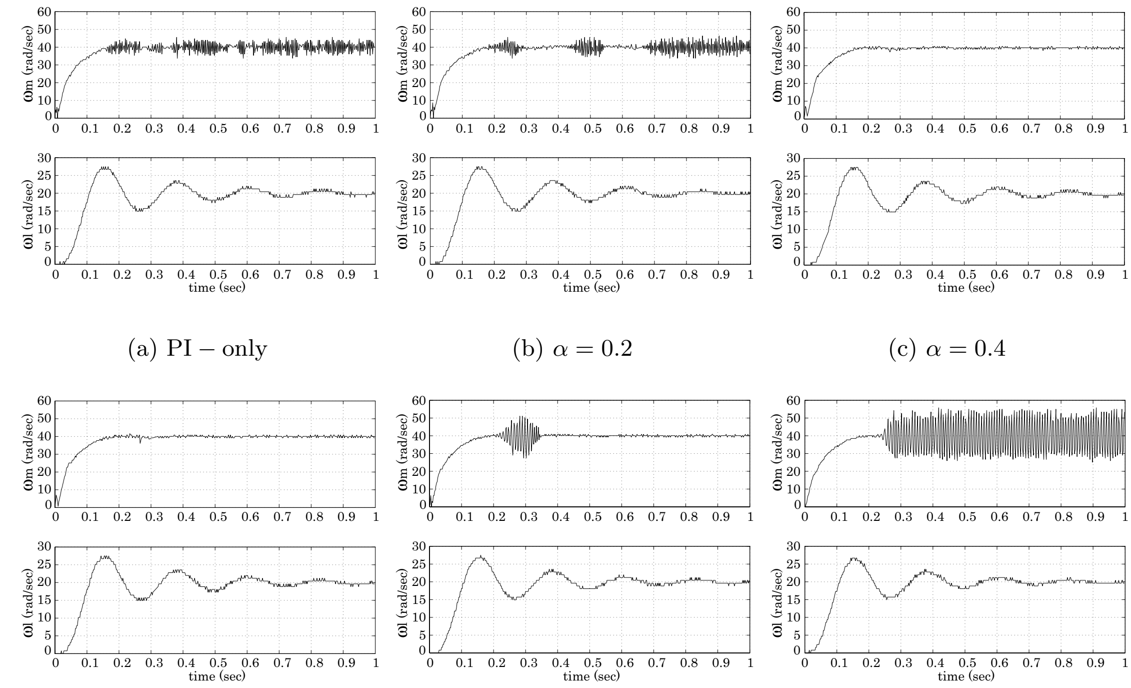

(a) PI − only (b) $\alpha = 0.2$ (c) $\alpha = 0.4$

(d) $\alpha = 0.6$ (e) $\alpha = 0.8$ (f) $\alpha = 1.0$

Figure 83: Time responses with shaft variation (diameter 4mm)

8.6 Summary

In this chapter, a conventional PI controller with fractional order low-pass filter $\frac{1}{(\tau s+1)^{\alpha}}$ is proposed to give a straightforward tradeoff adjustment between stability margin loss and vibration suppression strength. In oscillatory system control, this kind of tradeoff is a common problem. As shown in above theoretical analysis and experimental results, by introducing FOC concept, we can design control system in a clear-cut way since control system's frequency response can be easily adjusted to desired shape with few control parameters. Namely, the tuning knob can be reduced significantly compared to high-order transfer functions obtained by conventional IOC approaches.

At the same time, it can be seen using fractional order controller is a general method to tradeoff inconsistent control demands, which is not limited to the specific problem. "Effective & clear-cut design" can be achieved by expanding controller's order to fractional.

FOC is not an abstract concept, but a natural and powerful expansion of the well-developed IOC. Knowledge and design tools developed in IOC can still be made good use of in FOC research, as demonstrated in this paper.

For example, upgrading traditional PID controller by introducing fractional order factors, such as fractional order I^{α}, D^{β} controllers or fractional order filters, could give a more effective control of complex dynamic features. It is interesting to find that in the experiments the 1st-order approximation can also have a relative good performance (see Fig. 81(a)). This filter is actually a simple one order controller:

$$0.2091\frac{(s+3092.4949)}{(s+646.7270)} \tag{181}$$

The author does believe some well-designed IOC system might in fact be a unconscious approximation of FOC system. If this hypothesis can be established, FOC's advantages in control field would be further verified.

CHAPTER IX

FRACTIONAL ORDER DISTURBANCE OBSERVER

9.1 Conventional Disturbance Observer

The disturbance observer regards the difference between actual output and the output of nominal model as an equivalent disturbance applied to the nominal model. It estimates the equivalent disturbance and utilize this estimation as a compensation signal. The disturbance observer (DOB) concept was proposed by Ohnishi in 1987 [43]. Umeno and Hori refined the framework of disturbance observer theory based on the design of TDOF (Two Degree Of Freedom) servo controllers and the factorization approach [44]. It is now a common practice to use DOB in many high precision motion control systems.

Disturbance observers offer several attractive features. In the absence of large model errors, they allow independent tuning of disturbance rejection characteristics and command following characteristics. Further more, compared to integral action, disturbance observers allow more flexibility via the selection of the order (relative degree) and bandwidth of low-pass filtering (the cut-off frequency); this filtering is frequently referred to as disturbance observer's Q-filter.

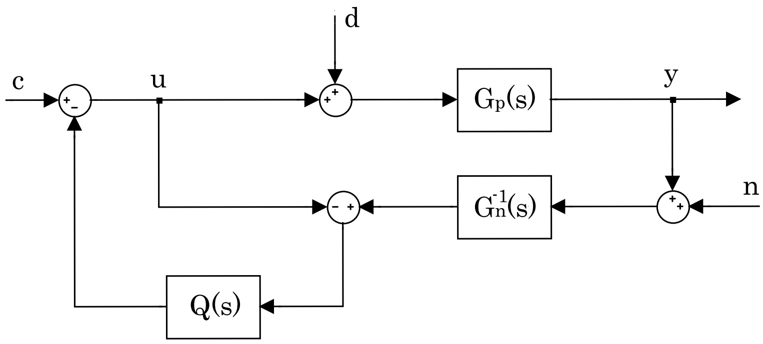

Figure 84: Conventional form of disturbance observer

In conventional disturbance observer, the basic idea is to use a nominal inverse model of the plant to estimate the disturbance (see Fig. 84). It will be mentioned later in this chapter that this disturbance observer configuration is actually another form of loop-shaping to add more attenuation in the lower frequency range at the cost of the reduced stability margin. However, using disturbance observer structure allows simple and intuitive tuning of disturbance rejection characteristics. This explains why disturbance observer is more welcome by the control practitioners.

In this chapter, firstly the conventional disturbance observer is applied to the robust control of the experimental torsional system. As shown in Fig. 85, the inverse plant model for disturbance observer is Js, where J equals the sum of J_m, J_g and J_l. In this simple inverse model, the three masses of driving motor, gear and load are considered to be connect with a rigid shaft that can be described as a single mass J. The Q-filter is a low-pass filter to restrict the effective bandwidth of the disturbance observer. For simplicity of the discussion, the $Q-$filter is assumed to be in following form:

$$Q(s) = \frac{1}{(\tau s + 1)^n} \tag{182}$$

where τ is cut-off frequency and n is the relative degree of Q-filter.

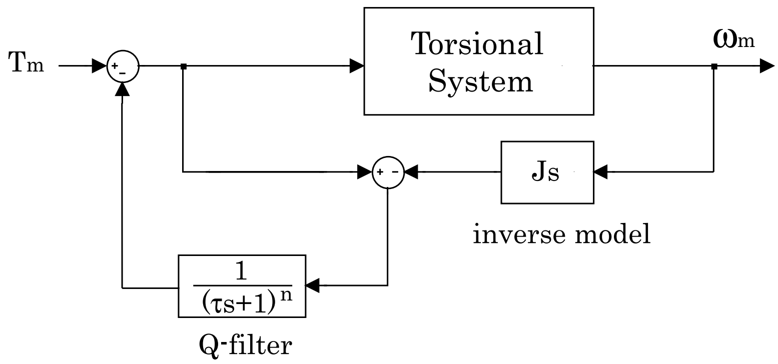

Figure 85: Conventional disturbance observer for the robust control of experimental torsional system

The disturbance observer is applied to estimate disturbance torque $\hat{T}_d$, which is generated due to unmodeled dynamics in single inertia model Js. Considering the frequency range of torsion vibration mode, τ is taken as 0.005(=1/200). By choosing different relative degree n, the control system's frequency responses can be adjusted. As shown in Fig. 86, n=1 has the best vibration suppression performance. The three-inertia model is used as for approximating actual torsional system in Fig. 87.

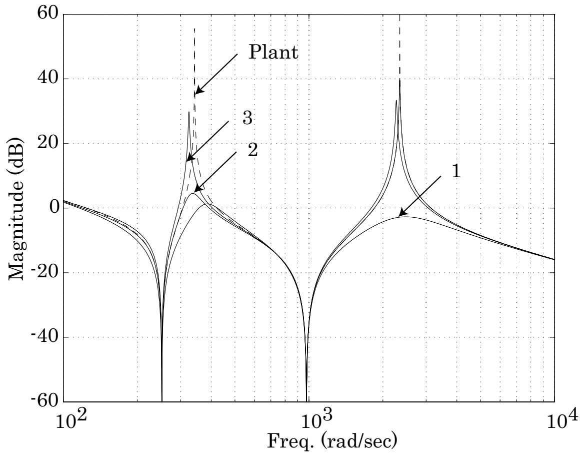

Figure 86: Open-loop gain plot with different integer order n

Simulation results show PI speed controller with disturbance observer (n=1) can give a good control performance in nominal case, where backlash angle $\delta = 0.6deg$ and and maximum torque limitation is $\pm 3.84Nm$. In the simulation, gear backlash is described using deadzone factor and elastic factor, which is far from adequate due to gear backlash's complex dynamic features, as shown in section 7.4. Whether disturbance observer with the 1st-order Q-filter can suppress backlash vibration effectively or not should be verified by experiments.

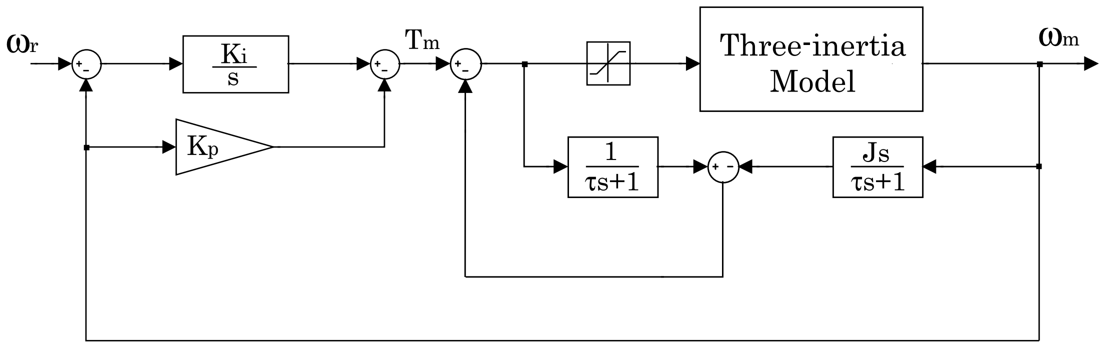

Figure 87: Block diagram for simulation with three-inertia model

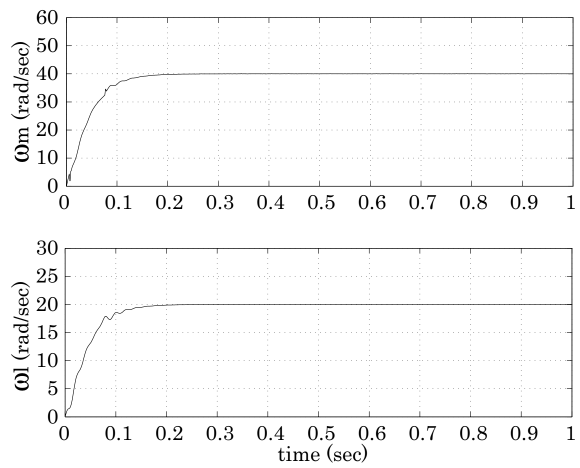

Figure 88: Time responses in simulation (n=1)

9.2 Novel Fractional Order Q-Filter

An equivalent block diagram for the disturbance observer is shown in Fig. 89. From the figure, transfer functions from command, disturbance, and noise to output are

$$G_{CY}(s) = \frac{Y(s)}{C(s)} = \frac{G_p(s)G_n(s)}{G_n(s) + Q(s)(G_p(s) - G_n(s))} \tag{183}$$

$$G_{DY}(s) = \frac{Y(s)}{D(s)} = \frac{G_p(s)G_n(s)(1 - Q(s))}{G_n(s) + Q(s)(G_p(s) - G_n(s))} \tag{184}$$

$$G_{NY}(s) = \frac{Y(s)}{N(s)} = \frac{G_p(s)Q(s)}{G_n(s) + Q(s)(G_p(s) - G_n(s))} \tag{185}$$

The behaviors of the above equations as $Q \to 1$ and $Q \to 0$ show why Q is chosen as a low-pass filter. As $Q \to 1$ at low frequencies, $G_{CY}(s) \to G_n(s)$ and $G_{DY}(s) \to 0$. And at high frequencies, $Q \to 0$ leads to $G_{NY} \to 0$.

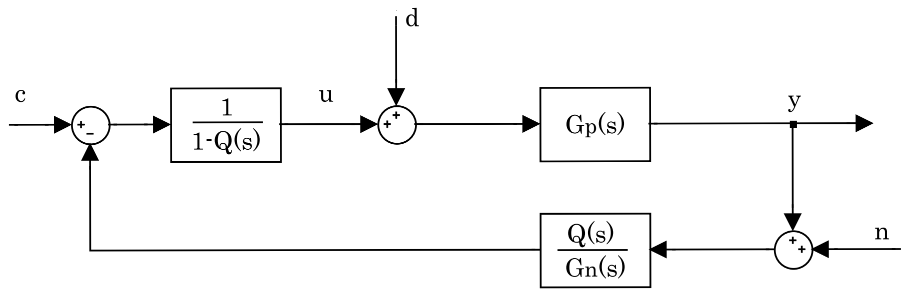

Figure 89: Equivalent diagram of the conventional disturbance observer

The key design issue for disturbance observer is choosing $Q(s)$ to provide a good tradeoff between disturbance rejection performance versus stability robustness and noise sensitivity. The selection of $Q-$filter's parameters are limited by unmodeled dynamics. Consider these uncertainties as a multiplicative perturbation of the nominal system gives

$$G_p(s) = G_n(s)(1 + \Delta(s)) \tag{186}$$

From Fig. 89, the open-loop transfer function for the disturbance observer system, in the absence of unmodeled dynamics, is

$$L(s) = \frac{Q(s)}{1 - Q(s)} \tag{187}$$

This shows the sensitivity function $S(s)$ and the complimentary sensitivity function $T(s)$ [46]. For the disturbance observer loop in Fig. 89, $T(s)$ equals to $Q(s)$ and $S(s)$ equals to $1-Q(s)$. Therefore, for the multiplicative uncertainty, the robust stability of the inner loop formed by the disturbance is assured [27]:

$$\| T(j\omega)\Delta(j\omega) \|_\infty \leq 1 \tag{188}$$

In above chapters, theoretical analysis and experimental results show by taking fractional order, control system's frequency responses can be effectively adjusted. FOC may also be applied in disturbance observer. A fractional order Q-filter was proposed by Chen with simple theoretical analysis as the possibility of better tradeoff between phase margin loss and vibration suppression strength [45].

In this chapter, the fractional version of Q-filter and its properties will be further exploited with robust control analysis and experimental verification. The fractional order Q-filter is the Q-filter whose relative degree can be any real number, not only integers:

$$Q(s) = \frac{1}{(\tau s + 1)^\alpha} \tag{189}$$

$T(s)$ and $S(s)$, actually $Q(s)$ and $1 - Q(s)$, with fractional relative degree α are shown in Fig. 90. It can be seen with fractional α the frequency responses of $T(s)$ and $S(s)$ are rightly between conventional integer order ones.

For clearness, the gain plots of fractional order $Q-$filter and the time delay uncertainty:

$$\Delta(s) = e^{-sT_d} - 1 \tag{190}$$

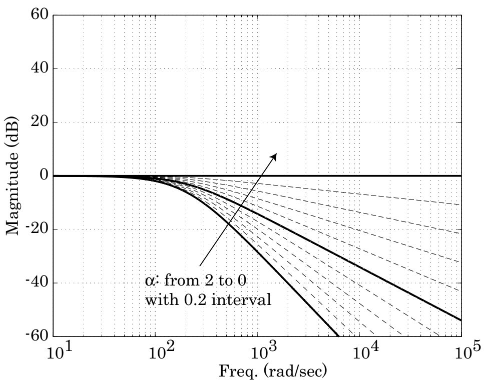

(a) Complimentary sensitivity function $T(s):\ Q(s)$

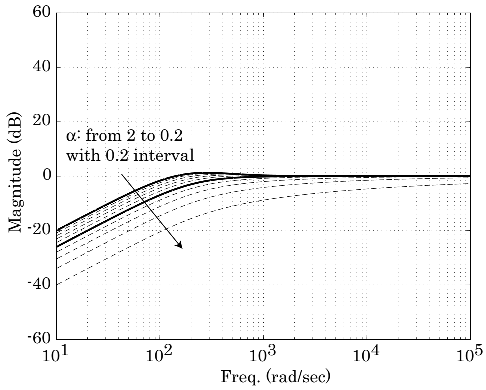

(b) Sensitivity function $S(s):\ 1 - Q(s)$

Figure 90: Effect of taking fractional order filter on inner disturbance observer loop

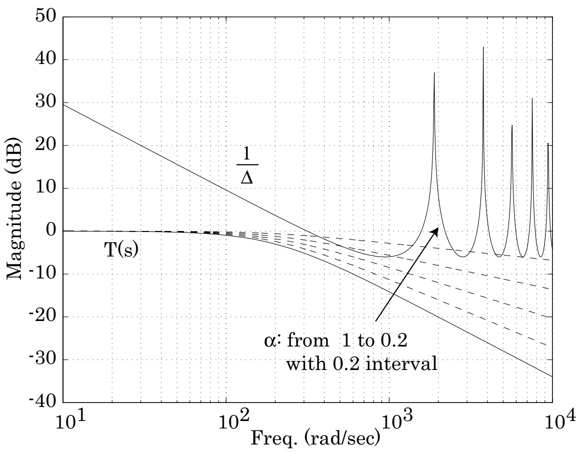

Figure 91: Fractional order $Q-$filter with time delay uncertainty

in section 4.4 is shown again in Fig. 91. Obviously, by taking proper fractional order relative degree α, some disturbance rejection performance can be easily recovered; while the robust stability criteria is still satisfied.

For an application, disturbance observer with fractional order Q-filter is used in the robust control of the torsional system. In torsional system control, suppressing torsional vibration and backlash vibration with parameter variations is one of central problems. From open-loop Bode plot, Fig. 92, it can be seen that around backlash vibration mode, there is enough phase margin; while the small phase margin around torsional vibration mode may cause stability problem.

On the robustness aspect, control system with small fractional order filter tends to be bad robust stability, but could give a better backlash vibration suppression performance due to their smaller gain characteristics (see Fig. 91 and Fig. 92). Namely, a tradeoff between robust stability loss and backlash vibration suppression strength exists in the disturbance observer approach.

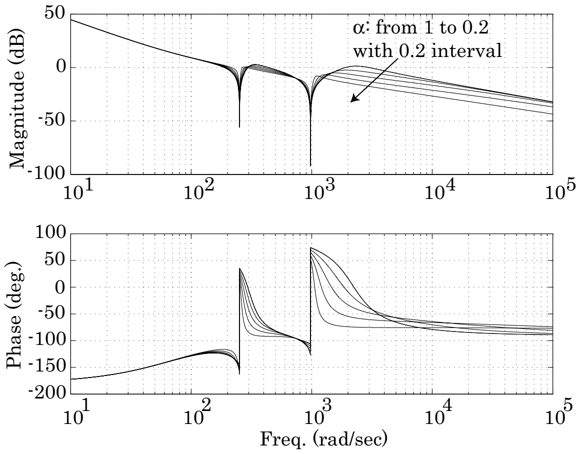

Figure 92: Open-loop Bode plots with different α

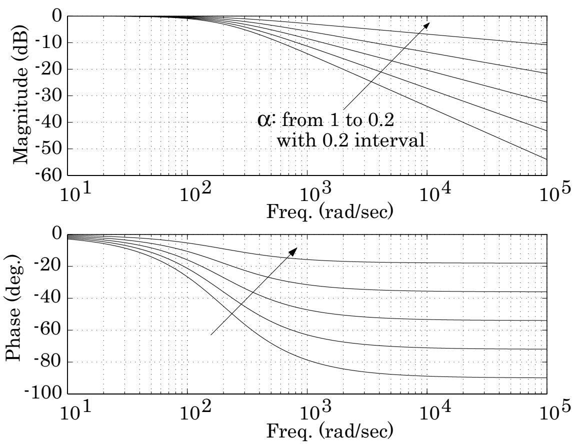

Figure 93: Bode plots of fractional order Q-filter $\frac{1}{(\tau s+1)^{\alpha}}$

For conventional disturbance observer, the possibility of better tradeoff is restricted since only integral order n can be chosen. As mentioned in above section, taking n as 1, the smallest value for n, gives the best vibration suppression performance for conventional disturbance observer. To further improve vibration suppression performance while keep enough robust stability margin, introducing Q-filter, whose order is between 0 and 1, is actually a natural choice. The Bode plots of the fractional order Q-filter are shown in

Fig. 93. It can seen a clear-cut design of "in-between" frequency responses is achieved by only adjusting the fractional order α. A proper selected fractional order α can easily recover some vibration suppression strength while keep enough robust stability margin.

9.3 Comparative Experiments

9.3.1 Conventional disturbance observer

Experiments are carried out with sampling time T=0.001sec. The fractional order low-pass filters are realized by broken-line method, where $N = 2$ and approximation band is [200 10000].

Firstly, speed control experiment with integer order Q-filter is carried out. As shown in Fig. 94, the control system can achieve satisfactory response when backlash angle is adjusted to zero degree (δ=0). With the existence of gear backlash non-linearity, persistent vibration occurs (see δ=0.6 case). Fig. 95 shows that compared with PI-only control, introducing disturbance observer can give better vibration suppression performance. However, this performance improvement is not enough to suppress effectively the vibration caused by gear backlash.

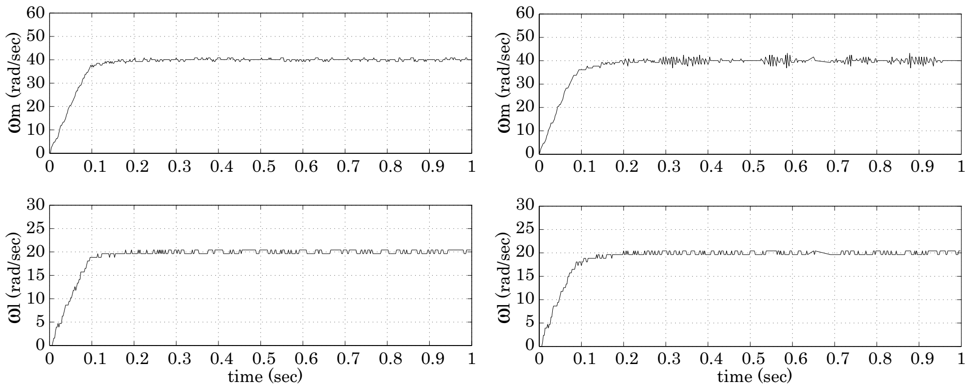

(a) $\delta = 0$ (b) $\delta = 0.6$

Figure 94: Time responses with integer order Q-filter (n=1)

For higher order n, like n=2 and n=3, the vibration suppression performance is actually deteriorated, while the control system still keeps stable (see Fig. 96). This experimental result verifies that a tradeoff between robust stability and vibration suppression strength exists and can be adjusted by different order n of the Q-filter.

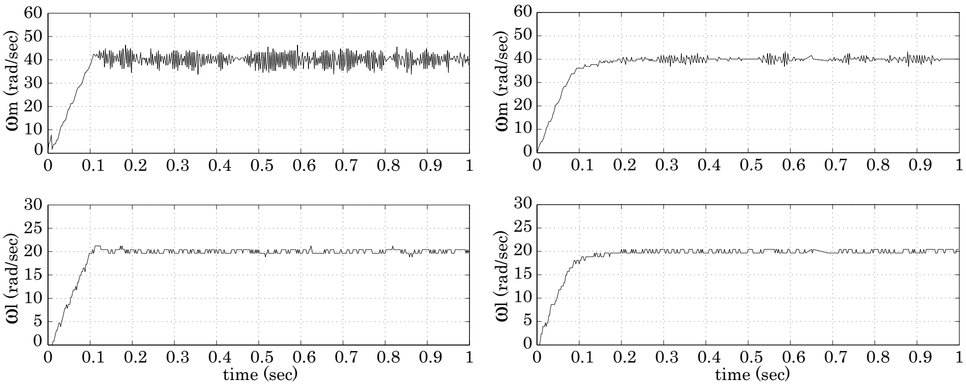

(a) PI-only

(b) PI+DOB (n=1)

Figure 95: Comparison of PI-only control and PI+DOB control

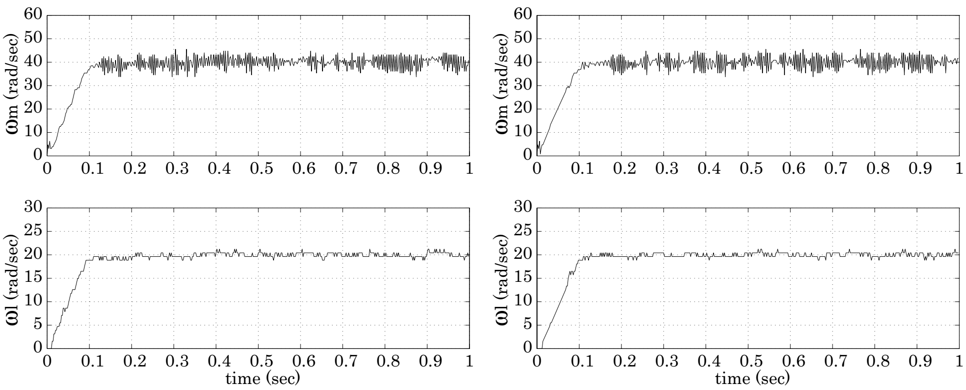

(a) $n = 2$

(b) $n = 3$

Figure 96: Time responses with integer order Q-filter ($n = 2, 3$)

9.3.2 DOB with fractional order Q-filter

Figure 97 shows the experimental results with different α for fractional order Q-filter $\frac{1}{(\tau s+1)^{\alpha}}$. By taking α as 0.8, the vibration caused by gear backlash is effectively suppressed and the best time response is achieved. The response of 0.8 order Q-filter has nearly same time response where the gear backlash does not exist (compare Fig. 94(a) and Fig. 97(b)).

Higher α, for example 1.0, cannot suppression backlash vibration while the control system is still be stable. In the time response of $\alpha = 0.6$ case, even backlash vibration is suppressed, the time responses reveal it's relative poor stability performance. For small α like 0.4, the fractional order Q-filter actually instablizes the control system. In Fig. 98, it

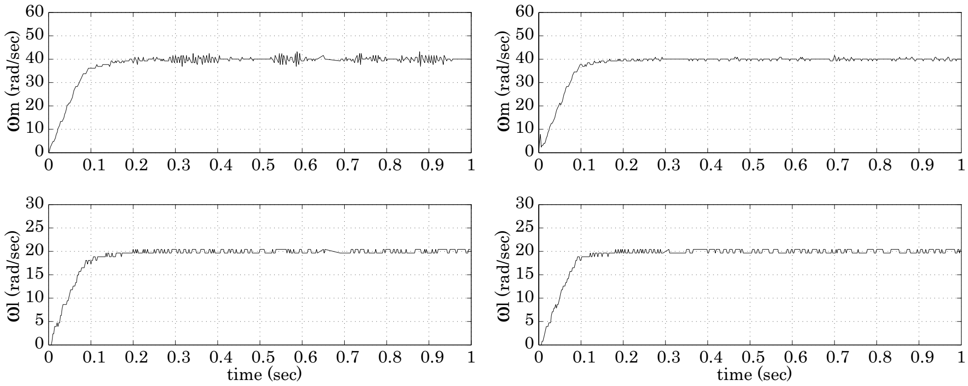

(a) $\alpha = 1.0$ (b) $\alpha = 0.8$

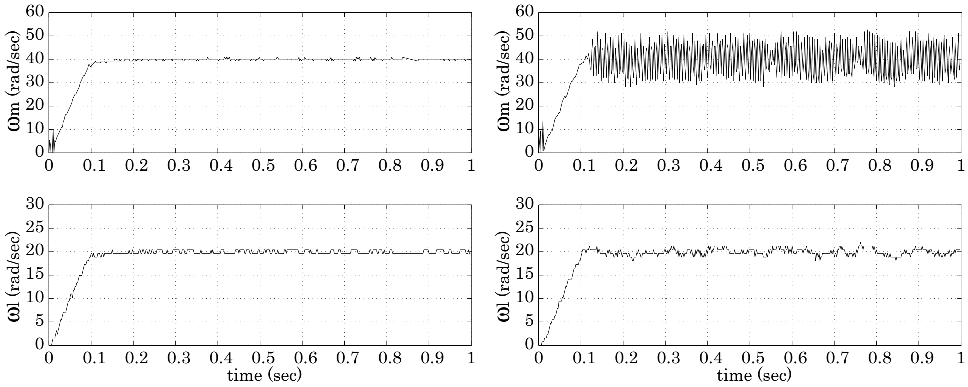

(c) $\alpha = 0.6$ (d) $\alpha = 0.4$

Figure 97: Time responses with different fractional order α

can be seen clearly that the existence of gear backlash and larger gain of 0.4 order Q-filter give bad robust stability performance for the inner disturbance observer loop.

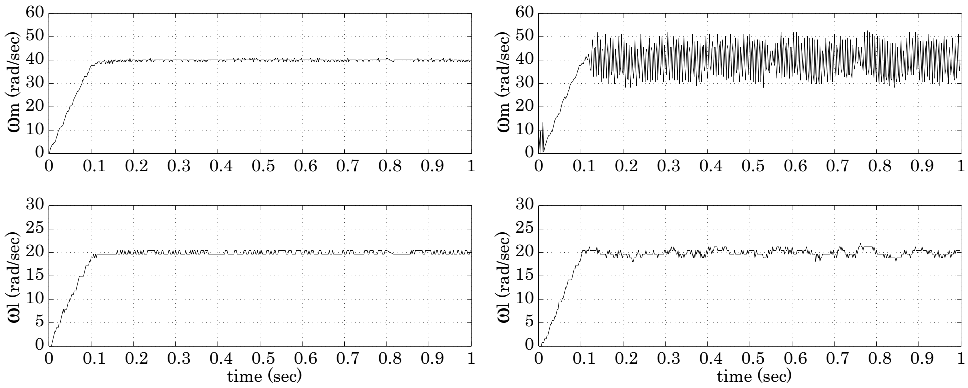

(a) without backlash (b) with backlash

Figure 98: Time responses with 0.4 order Q-filter

9.3.3 Robustness against parameter variations

Fig. 99 and Fig. 100 show the experimental results with load inertia and shaft elasticity variations. As same as in the above nominal case, control system with integer order $Q-$filter, i.e. $\alpha = 1,\ 2,\ 3$, can not suppress the backlash vibration. Too strong vibration suppression strength of $\alpha = 0.6$ case actually leads to robust stability problem. Taking α as 0.8 gives good performance in both nominal and parameter variation cases.

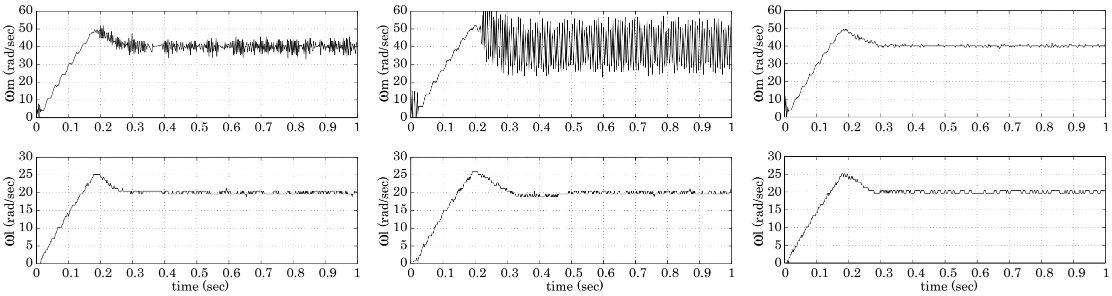

(a) PI − only (b) $\alpha = 0.6$ (c) $\alpha = 0.8$

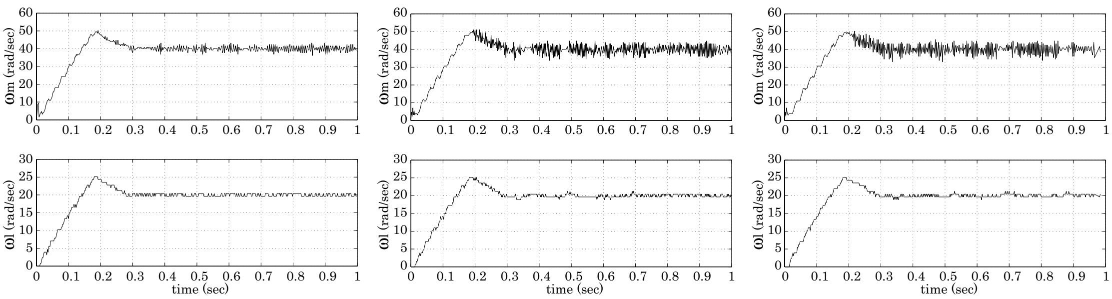

(d) $\alpha = 1.0$ (e) $\alpha = 2.0$ (f) $\alpha = 3.0$

Figure 99: Time responses with load variation (5 flywheels)

9.4 Summary

In this chapter, a fractional order Q-filter of disturbance observer, $\frac{1}{(\tau s+1)^{\alpha}}$, was introduced to substitute the integer order Q-filter $\frac{1}{(\tau s+1)^{n}}$ used in conventional disturbance observer for the speed control of torsional system. The theoretical analysis and experimental results show that changing Q-filter's order fractionally could give more possibility and an effective way to obtain better tradeoff between control system's robust stability and vibration suppression performance.

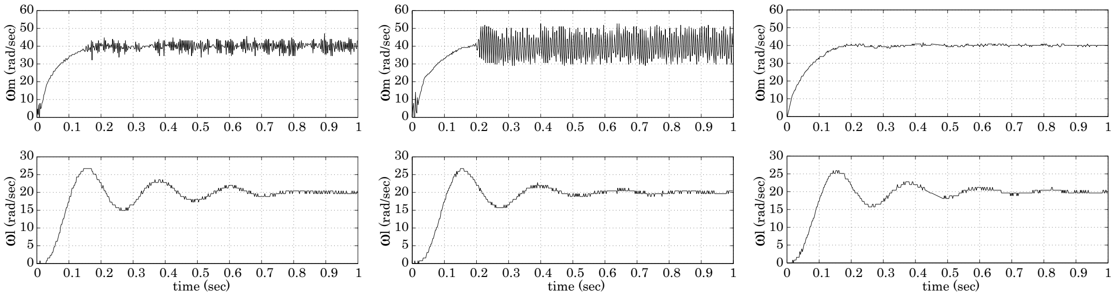

(a) PI − only (b) $\alpha = 0.6$ (c) $\alpha = 0.8$

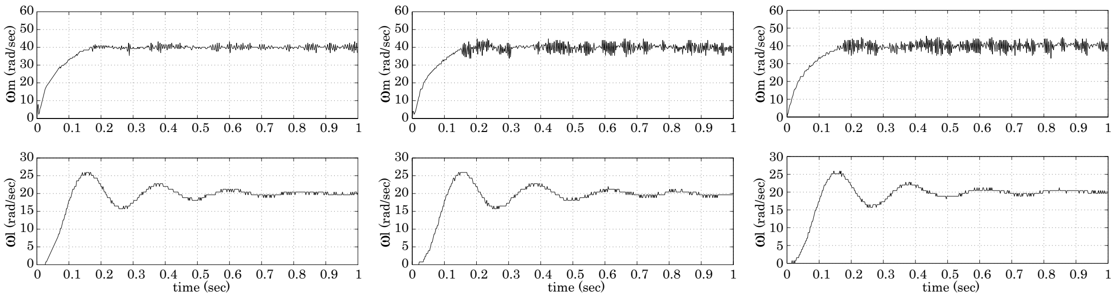

(d) $\alpha = 1.0$ (e) $\alpha = 2.0$ (f) $\alpha = 3.0$

Figure 100: Time responses with shaft variation (4mm diameter)

It can be seen introducing fractional order components is actually a nature thinking. When taking integer order controller only can not meet control demand, usually too aggressive or too conservative, further adjustment by letting control order be fractional could be a good choice. As the control order has much bigger influence on control performance than coefficients, FOC approach could give a clear-cut and effective control design with less control parameters.

This chapter contributes to expand control application field for FOC research to one of popular control practices, the disturbance observer. The author believes there are lots of existing control practices whose performance could be easily upgraded through FOC approach.

CHAPTER X

CONCLUSIONS AND FUTURE WORKS

10.1 Position of FOC

- **Theoretical position:** FOC opened a new dimension for control theory. The highly developed control theory based on integer order differential equations shows quite different characteristics when it is expanded into fractional order field. At the same time, FOC is actually a nice generalization of IOC theory. This generalization gives huge space for researchers to see conventional IOC theory in a fresh light and find new and interesting things.

- **Practical advantages:** From practice viewpoint, the ideal fractional order controllers can only be realized by proper approximation with finite differential or difference equations. Namely, "design by FOC and realize by IOC" are inevitably. The practical advantages for FOC is to provide more flexibility and insight in control design and thus give a clear-cut approach for designing robust control system. The author does believe some well-designed IOC system might in fact be a unconscious approximation of FOC system.

10.2 Unfamiliar but Natural Choice

- **Modeling and identification:** The dynamic features of "real" systems can be described more adequately by fractional order models. Especially for light materials and flexible structures, not only damping, but also other variety of physical phenomena such as visco-elasticity and anomalous relaxation should be taken into account. This demand naturally needs fractional order models, which is a hopeful tool for modeling complex dynamic features.

- **Control design:** Control design is a kind of tradeoff between different prescribed control demands, which are usually contradicted. Good design means a better method to control same plant that can satisfy these contradicted demands with lower cost in both design and realization. By introducing FOC, control system's characteristics, both in time domain and frequency domain, can be further and effectively adjusted. Therefore, a better tradeoff could be obtained compared to conventional IOC approaches.

10.3 Effective and Clear-cut Control Design

- **Powerful s^{α} operator:** As emphasized in above chapters, changing the order of Laplace operator s order significantly affects control system's characteristics. Especially, in frequency domain, this effect is straightforward. Fractional order controllers are able to realize complicated frequency response easily with less control parameters, usually fractional orders only. Therefore, the tuning knob can be reduced significantly compared to high-order transfer functions designed by conventional IOC approaches.

- **Two-stage design approach:** FOC is a generalization of conventional IOC control. FOC plays an "interpolation" role among IOC systems. As to real applications, fractional order controllers are realized by conventional integer order controllers after proper approximation. Therefore, the highly developed IOC theory should be made the most of. The two-stage design approach used in this dissertation rightly satisfies this reasonable conclusion. The FOC applications in chapter 7, chapter 8 and chapter 9 show the clear-cutness and effectiveness of the two-stage design in practical applications, in which IOC design method gives a good sense of direction and novel FOC design method further improves control performance.

10.4 Realization by Proper Approximation

- **Various approaches:** Several realization methods were proposed for the realization of fractional order controllers. Since most controllers are implemented on digital computers, discretization of fractional order controllers is more concerned. Short Memory Principle, Sampling Time Scaling, Tustin Taylor Expansion and Lagrange

Interpolation Function can be applied to direct discretization. Since the broken-line method approximates fractional order controllers in frequency domain firstly, further discretization is needed.

- **Reasonable approximation:** The experimental results in chapter 7, chapter 8 and chapter 9 verify the reliability of fractional order controller's realization. In direct discretization methods, the Short Memory Principle gives the best performance with simple approximation algorithm. The broken-line method provides more flexibility in design of fractional order controllers with satisfied approximate accuracy. The order of approximation, which means how good the approximation is needed, should be decided by the demand of specific control problem, as is true in the discretization of conventional integer order controllers.

10.5 Future Works

- **Identification and modeling:** Identification and modeling of flexible structures using fractional order models will provide more insight and more reliable basis for control design. Especially for a structure with light materials and fast motions, fractional order models could give an effective description of the complex dynamic features. And the FOC systems designed using fractional order models should give a better control performance, such as vibration suppression, better robustness and so on.

- **Systematic design method:** The systematic design method is still an open problem for FOC research. The optimal control methods, such as H_2 and H_∞ can be expanded to FOC control design. However, the optimization will become quite complicated. Genetic algorithm can be a solution to reduce the complexity of optimization. For a clear-cut and effective FOC design, making the most of FOC's advantages over IOC is crucial.

  And for applying FOC in MIMO system, using transfer function matrix mentioned in section 3.1 should be an interesting research field.

- **Control design using $s^{0.5}$:** The even orders of $s^{0.5}$, $(s^{0.5})^0$, $(s^{0.5})^2$, $\ldots$, $(s^{0.5})^{2n}$, are actually integer order s operator, s^0, s^1, $\ldots$, s^n. And $(j\omega)^{0.5} = \omega^{0.5}\angle\frac{\pi}{4}$. Namely, introducing integer order $s^{0.5}$ operator can be considered to be able to "split" conventional IOC system into half. The stability of $R(s^{0.5})$ system can also be easily determined (see section 4.2). Tools not only in frequency domain but also in time domain such as root-locus technique can be applied. Some interesting results should be achieved in this FOC research direction.

- **Fractional order z^α operator:** From FOC viewpoint, some modern digital control techniques, such as multi-rate sampling control, can be considered as trying to realize or approximate fractional order z^α operator. For example, $z^{-0.5}$ means the value of input between latest two sampled inputs. Generalizing present digital control techniques based on FOC concept should be a quite challenging and meaningful research.

- **Comparison with popular IOC methods:** As mentioned above, FOC is actually a nature choice. Especially in frequency domain, it is easy to understand that there is no reason why only integer order s can be taken. The author strongly believes that conventional high-order controllers designed by popular IOC methods such as H_2 and H_∞ might actually be unconscious approximations of fractional order controllers. Review of conventional IOC methods from novel FOC viewpoint should be fruitful and beneficial for the development of both IOC and FOC theories.

- **Expansion of application field:** In this dissertation, torsional system is used as the testing bench, whose control was one of benchmark problems for motion control. The theoretical analysis and experimental results show the hopeful aspect for applying FOC in motion control. Actually, due to the non-linearities, demands for robustness and other special control performances in motion control problems, FOC could be a general and effective approach with "in-between" characteristics. Expansion of FOC application in the control of harddisk, robot, electrical vehicle, wheelchair, etc, is important for absorbing more interest and attention from academic communities and also should be helpful for the future development of FOC research.

Finally, the author would like to end this dissertation with the following expressive quotation:

"... all systems need a fractional time derivative in the equations that describe them ... systems have memory of all earlier events. It is necessary to include this record of earlier events to predict the future ...

The conclusion is obvious and unavoidable: Dead matter has memory. Expressed differently, we may say that nature works with fractional time derivatives."– S. Westerlund, Dead matter has memory! *Physics Scripta*, Vol. 43, 1991, pp. 174-179

With fractional order calculus and control, we may be able to extend a lot of new things ...

APPENDIX A

EXPERIMENTAL TORSIONAL SYSTEM

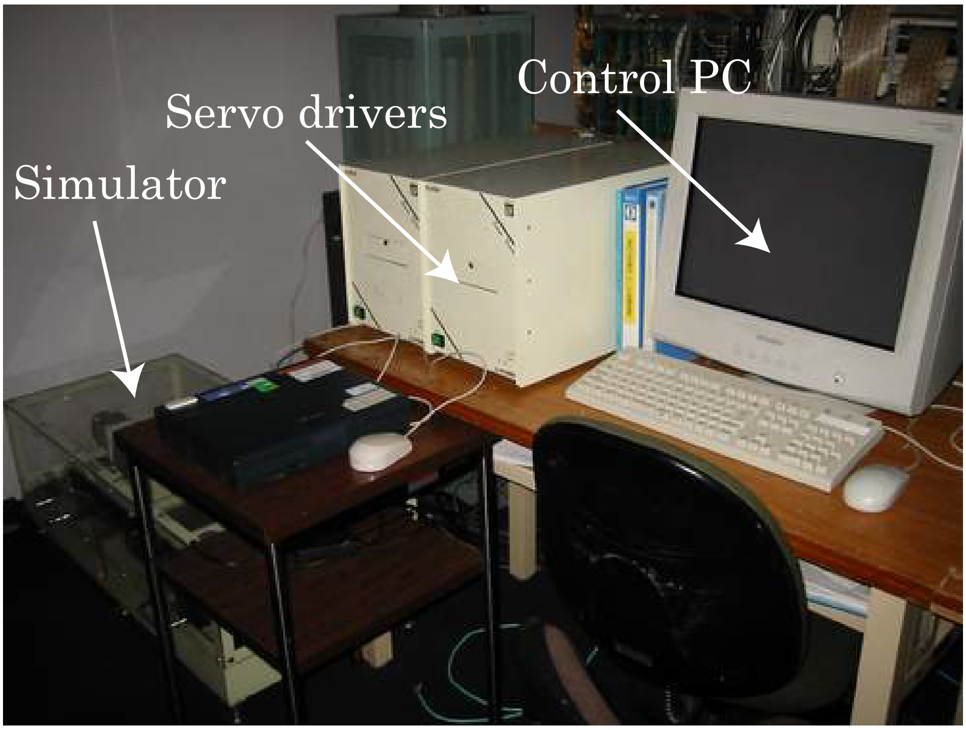

(a) Experimental environment

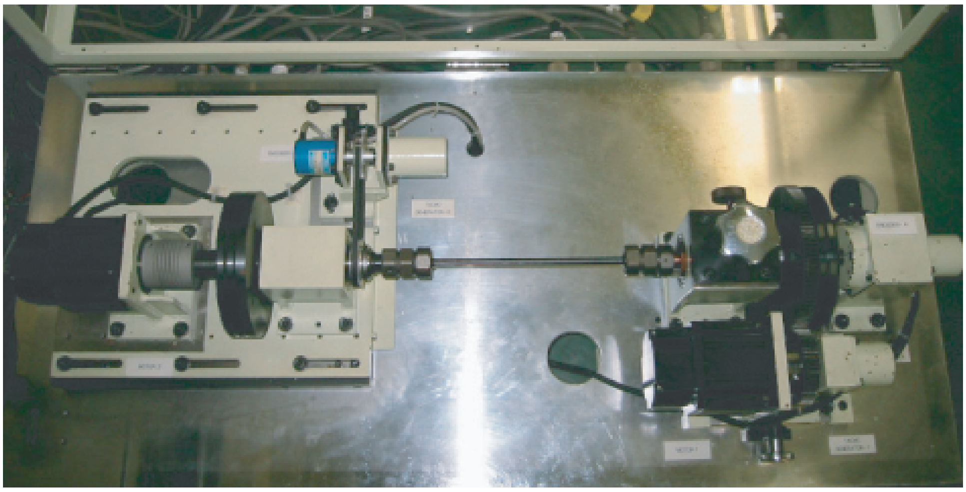

(b) Servo simulator

Figure 101: Photographs for the experimental torsional system

A.1 Servo Simulator

Servo simulator's setup is shown in Fig. 102. A long torsional shaft connects driving side and load side. Driving force is transmitted from driving servomotor to the shaft through gears whose reduction ratio N_g is 2. Some parts are are changeable, such as the number of flywheels in driving side and load side, shaft with different diameter and gears' backlash angle. Namely, parameters, J_g and J_l the inertias of gear (driving side) and load side, K_s the elastic coefficient of the torsional shaft and δ the gear backlash angle, can be adjusted for specific experiment (see Fig. 103). The encoders and tacho-generators are used as position and rotation speed sensors.

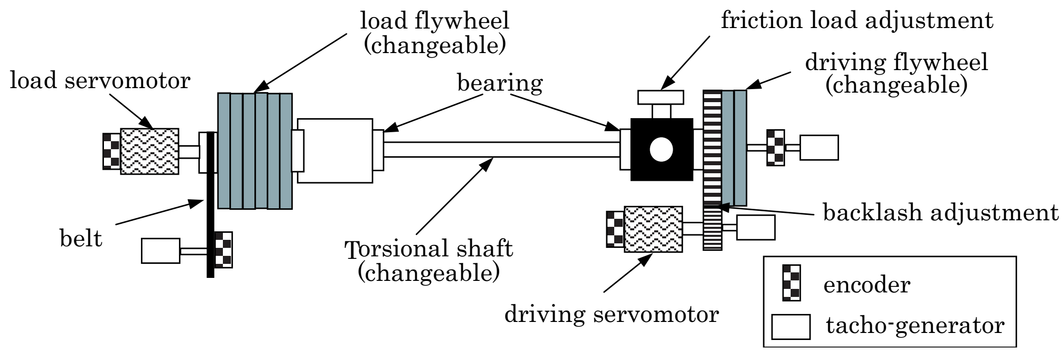

Figure 102: Experimental setup of servo simulator

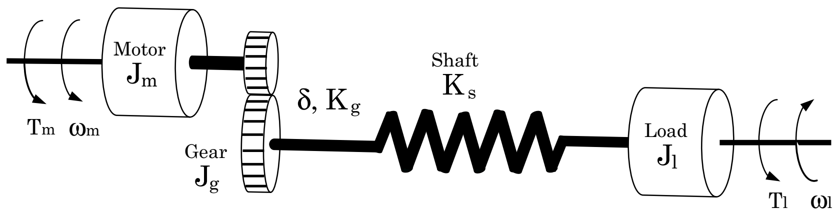

Figure 103: Three-inertia model for the servo simulator

Driving flywheel J_{g1}	$3.6573 \times 10^{-3}(Kg \cdot m^2)$ (each)
Load flywheel J_{l1}	$3.7878 \times 10^{-3}(Kg \cdot m^2)$ (each)
Drive side basic J_{l0}	$6.1342 \times 10^{-3}(Kg \cdot m^2)$
Drive servomotor J_{m0}	$6.5338 \times 10^{-4}(Kg \cdot m^2)$
Load side basic J_{l0}	$4.1062 \times 10^{-3}(Kg \cdot m^2)$ (including load servomotor)

Table 6: Inertias of flywheels and motors in driving side and load side

Shaft: 4mm	$2.4504(Nm/rad)$
Shaft: 8mm	$3.9207 \times 10^1(Nm/rad)$
Shaft: 12mm	$1.9849 \times 10^2(Nm/rad)$
Shaft: 16mm	$6.2731 \times 10^2(Nm/rad)$
Shaft: 20mm	$1.5315 \times 10^3(Nm/rad)$
Gear	$3000(Nm/rad)$

Table 7: Shaft and gear elastic coefficients K_{s0} and K_g

Size	$1070(mm) \times 375(mm) \times 500(mm)$
Weight	$150(Kg)$
Servomotor (Drive & Load)	$500W$ Brushless DC motor (MHI-AM500HEX) rated torque: $1.6(Nm)$ rated speed: $3000(rpm)$ maximum torque: $3.84(Nm)$ built-in encoder: $2000(pulse/rev)$
Torsional shaft (five)	diameter: $4, 8, 12, 16, 20(mm)$ Length: $200(mm)$
Drive flywheel (two)	diameter: $150(mm)$ thickness: $10(mm)$
Load flywheel (five)	diameter: $150(mm)$ thickness: $10(mm)$

Table 8: Servo simulator's specifications

The parameters and servo simulator's specifications are listed in Table. 6, Table. 7 and Table. 8. The maximum torque for driving servomotor is $\pm 3.84NM$. Namely, an output torque saturation exists in the servo simulator. Due to the severe noise in tacho-generator's output signal, the encodes are used as speed sensors by calculating changing ration of rotation angle in one sampling time. The encoders' count evaluation is set to be quad edge evaluation. Therefore, when sampling time is $0.001sec$, the coarse quantization for rotation speed is

$$\pm \frac{2\pi}{4 \times 2000 \times 0.001} = \pm 0.7854(rad/sec) \tag{191}$$

Considering gear's reduction ratio N_g, the inertias of driving servomotor J_m, gear (including driving flywheels) J_g and load side J_l can be calculated by following equations (see Fig. 103, Table. 6 and Table. 7):

$$\begin{aligned} J_m &= J_{m0} \\ J_g &= (J_{g0} + mJ_{g1})/N_g^2 \end{aligned}$$

$$
\begin{aligned}
J_l &= (J_{l0} + nJ_{l1})/N_g^2 \\
K_s &= K_{s0}
\end{aligned} \tag{192}
$$

In nominal setup, the numbers of driving flywheels m and load flywheels n are both 2. Namely, the system parameters are:

Servomotor inertia J_m	$0.0007(Kgm^2)$
Driving gear inertia J_g	$0.0034(Kgm^2)$
Load inertia J_l	$0.0029(Kgm^2)$
Shaft elastic coefficient K_s	$198.4900(Nm/rad)$
Gear elastic coefficient K_g	$3000(Nm/rad)$

Table 9: Parameter setting of nominal setup

A.2 Digital Control System

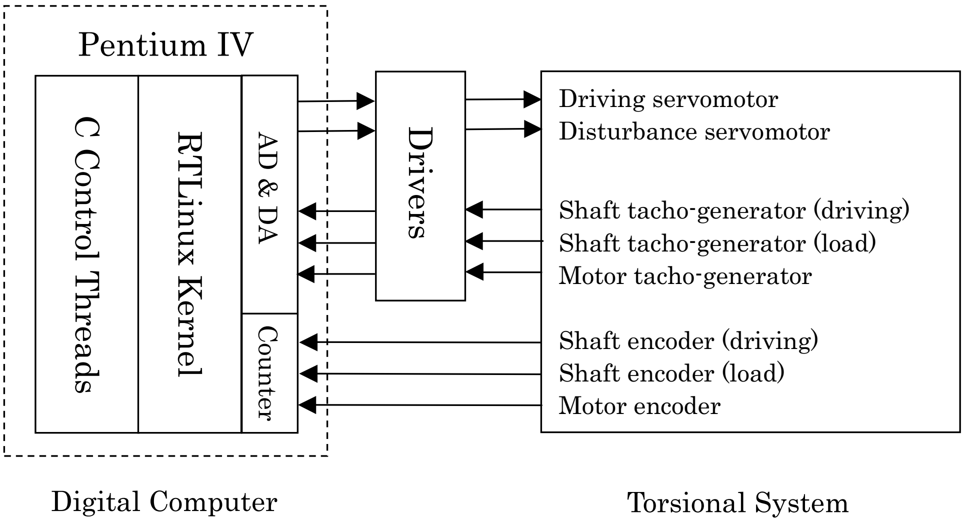

Figure 104: Digital control system of the experimental torsional system

As shown in Fig. 101(a) and Fig. 104, the experimental torsional system is controlled by a PC with 1.6GHz Pentium IV CPU and 512M memory. Realtime operating system RTLinux^{TM} distributed by Finite State Machine Labs, Inc. is used to guarantee the timing correctness of all hard realtime tasks [47]. The kernel version for RTLinux is 2.4.4.

Control programs are written in RTLinux C threads which can be executed with strict timing requirement of control sampling time. The torque commands are calculated by the digital computer and sent to the two servo drivers. A 12-bit analogue input/output board with 4 output DA channels and 8 input AD channels is used to convert digital torque commands to analogue signals and analogue output voltage of tacho-generators to digital signals, while the pulse output signals of encoders are counted by a 4-channel 24-bit encoder pulse counter board.

As shown in Fig. 105, the control algorithm is written in the while(1) loop of a thread named void *ctrl_thread(void *arg). The start/stop command for the control thread is sent from foc.app through FIFO_CMD channel. The handler int my_handler(unsigned int fifo) is used to receive start/stop command from foc.app, create/cancel control thread ctrl_thread() and set sampling time for the while(1) loop in the thread. Torque command is calculated in ctrl_thread() and sent to servo drivers. Finally, experimental data, executive time t, reference value ref, rotation speeds ω_m, ω_g and ω_l, and driving servomotor torque command T_m are transfered to foc.app through FIFO_DATA channel and saved in data files.

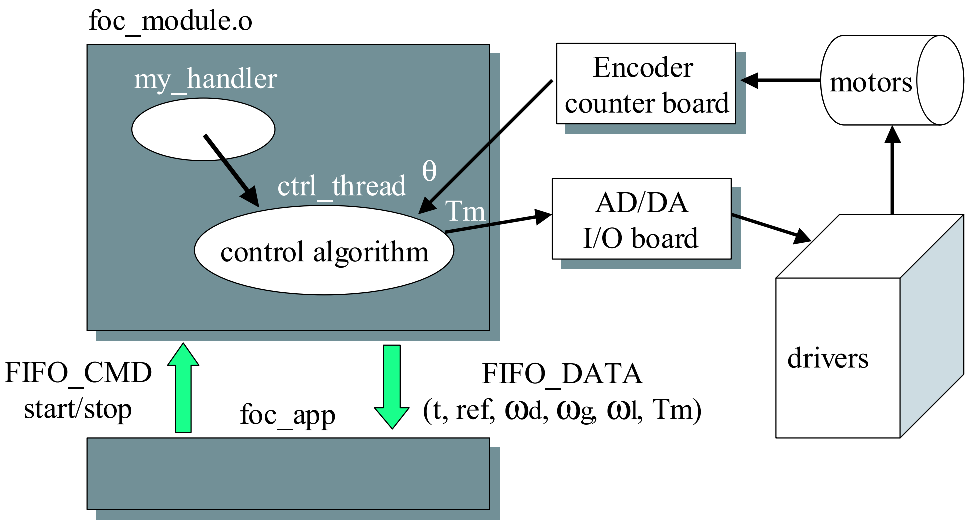

Figure 105: Conceptual diagram for RTLinux control program

APPENDIX B

COEFFICIENT DIAGRAM METHOD

B.1 Coefficient Diagram

For a characteristic polynomial:

$$P(s) = \sum_{i=0}^{n} a_i s^i = a_n s^n + ... + a_1 s + a_0 \tag{193}$$

Stability index γ_i, equivalent time constant τ, and stability limit γ_i^* are defined as follows:

$$\begin{aligned} \gamma_i &= a_i^2/(a_{i+1}a_{i-1}),\ i = 1,\ ...,\ (n-1) & (194) \\ \tau &= a_1/a_0 & (195) \\ \gamma_i^* &= 1/\gamma_{i+1} + 1/\gamma_{i-1},\ \gamma_n^* = \gamma_0^* = \infty & (196) \end{aligned}$$

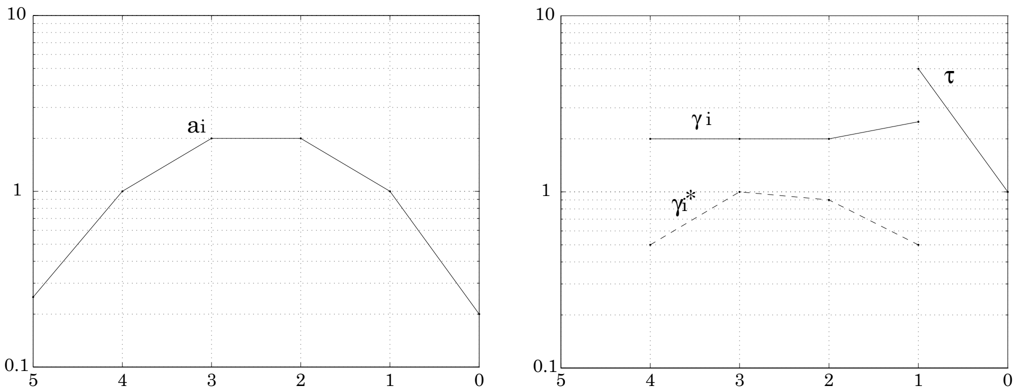

(a) a_i versus i

(b) γ_i, γ_i^*, τ versus i

Figure 106: Example of the coefficient diagram

For an example, when the characteristic polynomial is expressed as

$$P(s) = 0.25s^5 + s^4 + 2s^3 + 2s^2 + s + 0.2 \tag{197}$$

then

$$a_i = [0.25\ 1\ 2\ 2\ 1\ 0.2] \tag{198}$$

$$\gamma_i = [2\ 2\ 2\ 2.5] \tag{199}$$

$$\tau = 5 \tag{200}$$

$$\gamma_i^* = [0.5\ 1\ 0.9\ 0.5] \tag{201}$$

The coefficient diagram is shown in Fig. 106, where coefficient a_i is read in Fig. 106(a) and stability index γ_i, stability limit γ_i^*, equivalent time constant τ are read in Fig. 106(b). The τ is expressed by a line connecting 1 to τ. As shown in Fig. 107, if the a_i curve is left-end down, the equivalent time constant τ is small and response is fast. The equivalent time constant τ specifies the response speed.

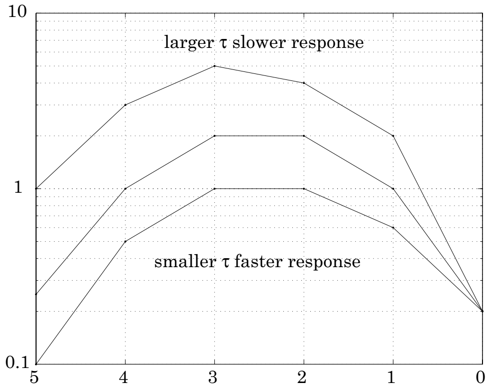

Figure 107: Effect of equivalent time constant τ

B.2 Stability Condition

Based on the sufficient condition for stability and instability proposed by Lipatov, the stability condition for Coefficient Diagram Method (CDM) can be decided. The sufficient condition for stability is given as:

$$\gamma_i > \gamma_i^*, \text{ for all } i = 1, ..., (n-2) \tag{202}$$

The sufficient condition for instability is given as:

$$\gamma_{i+1}\gamma_i \leq 1, \text{ for some } i = 1, ..., (n-2) \tag{203}$$

The stability index γ_i can be rewritten as:

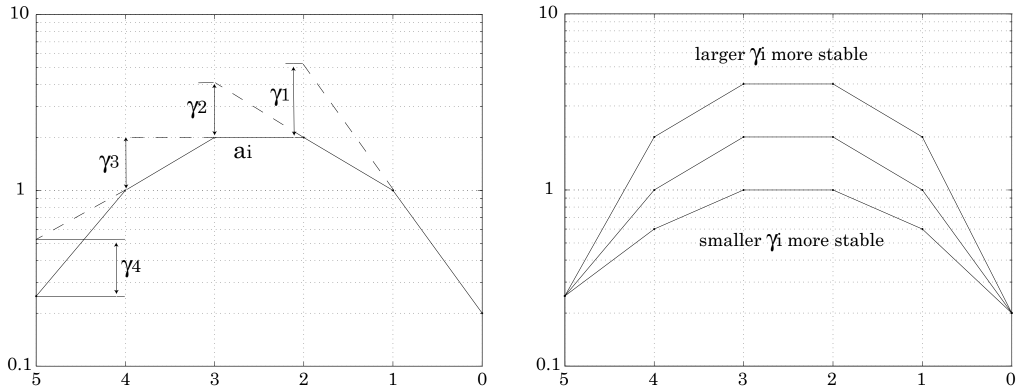

(a) graphically expressed γ_i (b) Changing of a_i curve's curtature

Figure 108: Effect of stability index γ_i

$$log_{10}\gamma_i = log_{10}\left[a_i^2/(a_{i+1}a_{i-1})\right] = (log_{10}a_i - log_{10}a_{i-1}) - (log_{10}a_{i+1} - log_{10}a_i) \tag{204}$$

Therefore, γ_i can be graphically obtained (see Fig. 108(a)). If the curvature of the a_i curve becomes larger, the system becomes more stable due to the larger stability index γ_i (see Fig. 108(b)). Namely, control system's stability can be determined graphically from coefficient diagram.

B.3 Standard Form

The recommended standard form for CDM is

$$\gamma_1 = 2.5,\ \gamma_2 \sim \gamma_{n-1} = 2 \tag{205}$$

When $a_0 = 0.4$ and $\tau = 2.5$ are chosen, the characteristic polynomial $P(s)$ is obtained in following form:

$$\begin{aligned} P(s) &= 2^{-\frac{(n-2)(n-1)}{s}} s^n + \ldots \\ &+ 2^{-10}s^6 + 2^{-6}s^5 + 2^{-3}s^4 + 0.5s^3 + s^2 + s + 0.4 \end{aligned} \tag{206}$$

The so-called canonical transfer functions are helpful to clarify the characteristics of $P(s)$. The system type 1 close-loop canonical transfer function is in following form:

$$T_1(s) = a_0/(a_n s^n + \ldots + a_1 s + a_0) \tag{207}$$

and for system type 2:

$$T_2(s) = (a_1 s + a_0)/(a_n s^n + \ldots + a_1 s + a_0) \tag{208}$$

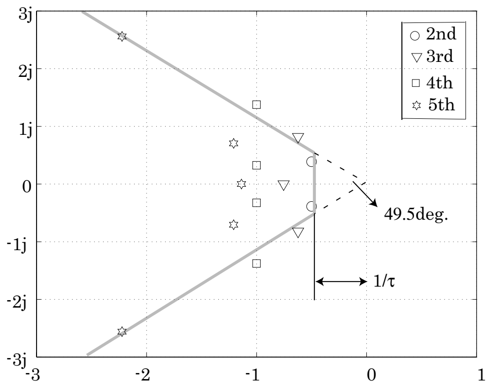

Figure 109: Pole location of CDM standard form

The standard form has favorable characteristics as listed below:

1. For system type 1, overshoot is almost zero. For system type 2, necessary overshoot of about 40% is realized [48].

2. Among the system with same equivalent time constant τ, the standard form has the shortest settling time. The settling time is about 2.5$\sim$3τ.

3. The lower order poles are aligned on a vertical line. The higher order poles are located within a sector 49.5 degrees from the negative real axis, and their damping coefficient ξ is larger than 0.65 (see Fig. 109).

B.4 Recent Development

The standard form was emphasized at the early stage of CDM, in which robustness was not guaranteed. The choice of $\gamma_1 = 2.5,\ \gamma_2 = \gamma_3 = 2$ is recommended due to stability and response requirement, but it is not necessary to make $\gamma_4 \sim \gamma_{n-1}$ equal to 2. The condition can be relaxed as

$$\gamma_i > 1.5\gamma_i^* \tag{209}$$

With such freedom, control design using CDM can integrate robustness in the characteristic polynomial design with a small sacrifice of stability and response. Namely, the essence of CDM lies in the proper selection of stability indices γ_i in a manner that both robustness and stability are guaranteed as shown in section 8.1.

Therefore, control system's stability, response and robustness can be graphically expressed in the diagrams of CDM. This advantage is the source for the effectiveness of CDM design. The recent development of CDM can be found in Ref. [48] and Ref. [49], in which a systematic approach for guarantee of robustness in CDM design is discussed in detail.

APPENDIX C

LIST OF PUBLICATIONS

C.1 Journals

1. Chengbin Ma, Yasumasa Fujii and Kenji Yamaji: "China's electric power sector's options considering its environmental impacts", *Environmental Economics and Policy Studies*, Vol. 5, pp. 319-340, Springer-Verlag 2002 (2002)

2. Chengbin Ma, Yoichi Hori: "Backlash Vibration Suppression Control of Torsional System by Novel Fractional Order PID^k Controller", *IEEJ Transactions on Industry Applications*, Vol. 124, No. 3, pp. 312-317 (2004)

3. Chengbin Ma, Yoichi Hori: "The Time-Scaled Trapezoidal Rule for Discrete Fractional Order Controllers", *Nonlinear Dynamics*, Kluwer Academic Publishers (Accepted)

4. Chengbin Ma, Yoichi Hori: "Time-domain Evaluation of Fractional Order Controllers' Direct Discretization Methods", *IEEJ Transactions on Industry Applications* (will be published in August, 2004)

C.2 International conferences

1. Chengbin Ma, Yoichi Hori: "Geometric Interpretation of Discrete Fractional Order Controllers based on Sampling Time Sampling Property and Experimental Verification of Fractional $1/s^\alpha$ Systems' Robustness", ASME Design Engineering Technical Conferences & Computers and Information In Engineering Conference, September 2-6, 2003, Chicago, Illinois, USA

2. Chengbin Ma, Yoichi Hori: "Backlash Vibration Suppression Based on The Fractional Order Q-Filter of Disturbance Observer", The 8th IEEE International Workshop on Advanced Motion Control, March 25-28, 2004, Kawasaki, Japan

3. Chengbin Ma, Yoichi Hori: "The Application of Fractional Order Control to Backlash Vibration Suppression", American Control Conference, June 30-July 2, 2004, Boston, Massachusetts, USA (Accepted)

4. Chengbin Ma, Yoichi Hori: "Tradeoff Adjustment of Fractional Order Low-pass Filter for Vibration Suppression Control of Torsional System", The 1st IFAC Workshop on Fractional Differentiation and its Applications, July 19-20, 2004, Bordeaux, France (Accepted)

5. Chengbin Ma, Yoichi Hori: "An Introduction of Fractional Order Control and Its Applications in Motion Control", International session, The 23nd Chinese Control Conference, August 10-13, 2004, Wuxi, China (Accepted)

6. Chengbin Ma, Yoichi Hori: "The application of Fractional Order $PI^{\alpha}D$ Controller for Robust Two-inertia Speed Control", The 4th International Power Electronics and Motion Control Conference, August 14-16, 2004, Xi'an, China (Accepted)

C.3 Domestic conferences

1. Chengbin Ma, Yoichi Hori: "Experimental evaluation of torsional system's vibration suppression control performance by discrete fractional order controller", Papers of Technical Meeting on Industrial Instrumentation and Control, IEE Japan, pp. 39-44, March 13, 2003, Tokyo, Japan

2. Chengbin Ma, Yoichi Hori: "Design of Robust Fractional Order $PI^{\alpha}D$ Speed Control for Two-inertia System", Japan Industry Applications Society Conference, August 26-28, 2003, Tokyo, Japan

C.4 Others

1. Chengbin Ma, Yoichi Hori: "Fractional Order Motion Control", The 6th University of Tokyo-Seoul National University Joint Seminar on Electrical Engineering, November 21, 2003, Seoul, Korea

REFERENCES

[1] K. B. Oldham and J. Spanier: The Fractional Calculus, Academic Press, New York and London (1974)

[2] A. Tustin and et. al: "The design of Systems for Automatic Control of the Position of Massive Objects", *Proc., IEE*, Vol. 105-C, No. 1, pp. 1-57 (1958)

[3] S. Manabe: "The Non-integer Integral and its Application to Control Systems", *J. IEE Japan*, Vol. 80, No. 860, pp. 589-597. (1960) (in Japanese)

[4] S. Manabe: "The System Design by the Use of Non-integer Integrals and Transport Delay", *J. IEE Japan*, Vol. 81, No. 878, pp. 1803-1812. (1962) (in Japanese)

[5] S. Manabe: "The System Design by the Use of a Model Consisting of a Saturation and Non-integer Integrals", *J. IEE Japan*, Vol. 82, No. 890, pp. 1731-1740. (1962) (in Japanese)

[6] M. Axtelland M. E. Bise: "Fractional Calculus Applications in Control Systems", Proc., the IEEE 1990 Nat. Aerospace and Electronics Conference, New York, USA, pp. 563-566 (1990)

[7] I. Podlubny: Fractional Differential Equations, Vol. 198, Mathematics in Science and Engineering, New York and Tokyo, Academic Press (1999)

[8] B. M. Vinagre, V. Feliú and J. J. Feliú: "Frequency Domain Identification of a Flexible Structure with Piezoelectric Actuators Using Irrational Transfer Function", Proc., the 37th IEEE Conference on Decision & Control, Tampa, Florida, USA, pp. 1278-1280 (1998)

[9] J. A. Tenreiro Machado: " Theory Analysis and Design of Fractional-Order Digital Control Systems", *Journal Systems Analysis Modeling Simulation*, Vol. 27, pp. 107-122 (1997)

[10] A. Oustaloup, J. Sabatier and X. Moreau: "From Fractal Robustness to the CRONE Approach", *The European Series in Applied and Industrial Mathematics*, Vol. 5, pp. 177-192 (1998)

[11] I. Petras and B. M. Vinagre: "Practical Application of Digital Fractional-order Controller to Temperature Control", *Proc. Acta Montanistica Slovaca*, Kosice (2001)

[12] A. Oustaloup, X. Moreau and M. Nouillant: "The CRONE Suspension", *Control Eng. Practice*, Vol. 4, No. 8, pp. 1101-1108 (1996)

[13] A. Oustaloup, B. Mathieu and P. Lanusse: "The CRONE Control of Resonant Plants: Application to a Flexible Transmission", *European Journal of Control*, Vol. 1, pp. 113-121 (1995)

[14] P. Lanusse, V. Pommier and A. Oustaloup: "Fractional Control-System Design for a Hydraulic Actuator", Proc. of the 1st IFAC conference on Mechatronics systems, Darmstadt, Germany (2000)

[15] D. Matignon: "Stability Properties for Generalized Fractional Differential Systems", *The European Series in Applied and Industrial Mathematics*, Vol. 5, pp. 145-158 (1998)

[16] D. Matignon and B. d'Andréa-Novel: "Some Results on Controllability and Observability of Finite-dimensional Fractional Differential Systems", Proc. of Computational Engineering in Systems and Application multiconference, Vol. 2, pp. 952-956, Lille, France (1996)

[17] http://www.me.uic.edu/detc2003/: the official website for International Design Engineering Technical Conferences & Computers and Information in Engineering Conference, Chicago, Illinois, September 2-6, 2003

[18] http://www.lap.u-bordeaux1.fr/fda04/General_Information.html: the official website for the 1st IFAC Workshop on Fractional Differentiation and its Applications, Bordeaux, France, July 19-21, 2004

[19] I. Podlubny: "Fractional-order Systems and $\mathrm{PI}^{\lambda}\mathrm{D}^{\mu}$ Controller", *IEEE Transaction on Automatic Control*, Vol. 44, No 1, pp. 208-214 (1999)

[20] L. Dorcak, I. Petras, I. Kostial: "The Modelling and Analysis of Fractional-order Regulated Systems in the State Space", Proc. of the 1st International Carpatian Control Conference, pp. 185-188, Podbanske, Slovak Republic (2000)

[21] I. Petras: "Control of Fractional-order Chua's System", Preprint for J. Electrical Engineering

[22] I. Petras, B. M. Vinagre, L. Dorcak and V. Feliú: "Fractional Digital Control of a Heat Solid: Experimental Results", Proc. of the 3rd International Carpatian Control Conference, pp. 365-370, Malenovice, Czech Republic (2002)

[23] S. Manabe: "A Suggestion of Fractional-order Controller for Flexible Spacecraft Attitude Control", *Nonlinear Dynamics*, Vol. 29, pp. 251-268 (2002)

[24] C. W. de Silva: Vibration-Fundamentals and Practice, CRC press, London and New York (2000)

[25] L. L. Ludovic, A. Oustaloup, J. C. Trigeassou and F. Levron: "Frequency Identification by Non-Integer Model". Proc. of IFAC System Structure and Control Conference, Nantes, France (1998)

[26] I. Petras, Y. Q. Chen and B. M. Vinagre: "A Robust Stability Test Procedure For A Class of Uncertain LTI Fractional Order System", Proc. of the 3rd International Carpatian Control Conference, pp. 247-252, Malenovice, Czech Republic (2002)

[27] K. Zhou and J. C. Doyle: "Essentials of Robust Control", Prentice-Hall Press, New Jersey (1998)

[28] I. Petras: "The Fractional Order Controllers: Methods for Their Synthesis and Application", *J. Electrical Engineering*, Vol. 50, No. 9-10, pp. 284-288 (1999)

[29] I. Petras: "Design of Fractional-order Controllers via H_∞ Norm Minimisation", Proc. of IFAC Control Systems Design Conference, pp. 445-448, Bratislava, Slovak Repulic (2000)

[30] D. Valério and J. S. Costa: "Non-Integer Order Control of A Flexible Robot", Preprint for the 1st IFAC Workshop on Fractional Differentiation and its Applications, Bordeaux, France (2004)

[31] I. Podlubny: "Geometric and Physical Interpretation of Fractional Integration and Fractional Differentiation", *Fractional Calculus and Applied Analysis*, Vol. 5, No. 4, pp. 367-386 (2002)

[32] K. J. Åström and B. Wittenmark: Adaptive Control, Addison-Wesley Press, Reading, Mssachusetts · Menlo Park, California · New York · Don Mills, Ontario · Workingham, England · Amsterdam · Bonn · Sydney · Sigapore · Tokyo · Madrid · San Juan (1998)

[33] A. Oustaloup, F. Levron, and F. M. Nanot: "Frequency-Band Complex Noninteger Differentiator: Characterization and Synthesis", *IEEE Transactions on Circuits and Systems-I: Fundamental Theory and Applications*, Vol. 47, No. 1, pp. 25-39 (2000)

[34] J. A. Tenreiro Machado: "Discrete-Time Fractional-Order Controllers", *Fractional Calculus & Applied Analysis*, Vol. 4, No. 1, pp. 47-66 (2001)

[35] C. Hwang, J. Leu and S. Tsay: "A Note on Time-Domain Simulation of Feedback Fractional-Order Systems", *IEEE Transactions on Automatic Control*, Vol. 47, No. 4, pp. 625-631 (2002)

[36] M. Nordin and P. O. Gutman: "Controlling mechanical systems with backlash − a survey", *Automatica*, Vol. 38, pp. 1633-1649 (2002)

[37] S. Manabe: "Controller Design of Two-Mass Resonant System by Coefficient Diagram Method", *T. IEE Japan*, Vol. 118-D, No. 1, pp. 58-66 (1998) (in Japanese)

[38] Y. Hori: "Control of 2-Inertia System only by a PID Controller", *T. IEE Japan*, Vol. 112-D, No. 5, pp. 499-500 (1995) (in Japanese)

[39] Y. Hori: "Vibration Suppression and Disturbance Rejection Control on Torsional Systems", Proc. of IFAC Workshop on Motion Control, pp. 41-50, Munich, Germany (1995)

[40] Y.Hori: "A Review of Torsional Vibration Control Methods and a Proposal of Disturbance Observer-based New Techniques", Proc. of the 13th IFAC World Congress, San Francisco, USA (1996)

[41] Y. Hori, H. Sawada and Y. Chun: "Slow Resonance Ratio Control for Vibration Suppression and Disturbance Rejection in Torsional System", *IEEE Trans. on Industrial Electronics*, Vol. 46, No. 1, pp. 162-168 (1999)

[42] H. Kobayashi, Y. Nakayama and K. Fujikawa: "Speed Control of Multi-inertia System only by a PID Controller", *T. IEE Japan*, Vol. 122-D, No. 3, pp. 260-265 (2002) (in Japanese)

[43] K. Onishi: "A New Method for Mechatronics", *T. IEE Japan*, Vol. 107-D, pp. 77-88, (1987) (in Japanese)

[44] T. Umeno and Y. Hori: "Robust Speed Control of DC Servomotors using Modern Two-Degrees-of-Freedom Controller Design", *IEEE Transactions on Industrial Electronic*, Vol. 38, No. 5, pp. 363-368 (1991)

[45] Y. Chen, B. M. Vinagre and I. Podlunbny: "On Fractional Order Disturbance Observer", Proc. of the 19th Biennial Conference on Mechanical Vibration and Noise, ASME Design Engineering Technical Conferences & Computers and Information in Engineering Conference, Chicago, Illinois, USA (2003)

[46] C. J. Kempf and S. Kobayashi: "IEEE Transactions on Control Systems Technology", Vol. 7, No. 5, pp. 513-526 (1999)

[47] http://www.fsmlabs.com: the official website for FSMLabs, Inc., creators of RTLinux

[48] S. Manabe: "Coeficient Diagram Method", Porc. of the 14th IFAC Symposium on Automatic Control in Aerospace, pp. 199-210, Seoul, Korea (1998)

[49] S. Manabe: "Classical Control and Coeficient Diagram Method for Motion Control", Proc. of Motion Engineering Symposium, session G1, pp. 1-13, Makuhari, Japan (2002) (Japanese)